AD NUMBER
AD383410
CLASSIFICATION CHANGES
TO: **UNCLASSIFIED**
FROM: **CONFIDENTIAL**
LIMITATION CHANGES
TO: **Approved for public release; distribution is unlimited.**
FROM: **Distribution authorized to U.S. Gov't. agencies and their contractors; Administrative/Operational Use; AUG 1967. Other requests shall be referred to Air Force Rocket Propulsion Lab., Edwards AFB, CA.**
AUTHORITY
AFRPL ltr 5 Feb 1986 ; AFRPL ltr 5 Feb 1986

AD 383 410

AUTHORITY:
AFRPL ltr 5Feb 86

SECURITY MARKING

The classified or limited status of this report applies to each page, unless otherwise marked.
Separate page printouts MUST be marked accordingly.

THIS DOCUMENT CONTAINS INFORMATION AFFECTING THE NATIONAL DEFENSE OF THE UNITED STATES WITHIN THE MEANING OF THE ESPIONAGE LAWS, TITLE 18, U.S.C., SECTIONS 793 AND 794. THE TRANSMISSION OR THE REVELATION OF ITS CONTENTS IN ANY MANNER TO AN UNAUTHORIZED PERSON IS PROHIBITED BY LAW.

NOTICE: When government or other drawings, specifications or other data are used for any purpose other than in connection with a definitely related government procurement operation, the U. S. Government thereby incurs no responsibility, nor any obligation whatsoever; and the fact that the Government may have formulated, furnished, or in any way supplied the said drawings, specifications, or other data is not to be regarded by implication or otherwise as in any manner licensing the holder or any other person or corporation, or conveying any rights or permission to manufacture, use or sell any patented invention that may in any way be related thereto.

AFRPL-TR-67-208, PART I

(Unclassified)

HEAT TRANSFER STUDY OF MHF-5 AND MMH

Donald C. Rousar
Norman E. Van Huff
Roger E. Anderson
Arnold Fink
Aerojet-General Corporation

TECHNICAL REPORT AFRPL-TR-67-208, PART I

August 1967

Prepared for

AIR FORCE ROCKET PROPULSION LABORATORY
Edwards Air Force Base California

1068

NOTICES

When US Government drawings, specifications, or other data are used for any purpose other than a definitely related government procurement operation, the government thereby incurs no responsibility nor any obligation whatsoever, and the fact that the government may have formulated, furnished, or in any way supplied the said drawings, specifications, or other data is not to be regarded by implication or otherwise, as in any manner licensing the holder or any other person or corporation, or conveying any rights or permission to manufacture, use, or sell any patented invention that may in any way be related thereto.

AFRPL-TR-67-208, Part I

(Unclassified)

HEAT TRANSFER STUDY OF MHF-5 AND MMH

Donald C Rousar
Norman E Van Huff
Roger E Anderson
Arnold Fink

FOREWORD

This is the final technical report for Contract AF 04(611)-11607, Heat Transfer Study of MMH and MHF-5. The work reported herein was performed during the period 1 July 1966 to 31 May 1967. The Air Force Project Engineer was Captain William H. Summers, RPCL.

The Heat Transfer Study of MMH and MHF-5 was conducted by the Engineering Division of Liquid Rocket Operations, Aerojet-General Corporation, Sacramento, California. The testing was done at the Research Physics Laboratory.

Contributors to this program, in addition to those noted on the title page, include the following Aerojet personnel:

R. F. Bechtold
N. B. Davidson
Y. W. Louie
P. M. Loyd
S. D. Mercer
J. E. Nelson
R. J. Pruett
J. R. Selby
E. A. Witt

Classified information has been extracted from the asterisked documents listed under References (in the text and in Appendix A and B).

This technical report has been reviewed and is approved.

W. H. EBELKE, Colonel, USAF
Chief, Propellant Division
Air Force Rocket Propulsion Laboratory

AFRPL-TR-67-208

Unclassified Abstract

This report presents the results of an experimental investigation of the heat transfer characteristics of MHF-5 and MMH at subcritical and supercritical pressures. Fifty-five heat transfer tests were conducted with electrically heated 347 stainless steel and Inconel 718 tubes within the following ranges of conditions: 250 to 3960 psia pressure, 17.7 to 205 ft/sec velocity, -42 to 308°F bulk temperature, and heat fluxes up to 49.6 Btu/in.^{2} sec. At subcritical pressures, the burnout heat flux of MHF-5 and MMH correlated with the product of velocity and subcooling. A reduction in burnout heat flux, attributed to viscous effects, was observed with MHF-5 and MMH at low bulk temperatures. This behavior was noted in previous investigations with other propellants and a fairly general correlation for predicting this phenomenon was established. An unusual and pronounced effect of pressure on MHF-5 burnout heat flux was observed and empirically correlated. Burnout-like conditions were observed with both propellants at supercritical pressures. It was found that the heat flux at which this condition developed, termed the ultimate heat flux, could be predicted reasonably well with conventional forced convection expressions in conjunction with a maximum wall temperature of 700°F. Significant carbonaceous deposits formed in the supercritical pressure test sections and evidence of carburization and intergranular penetration by carbon were found. Chemical analysis results showed that no significant decomposition of the MHF-5 and MMH occurred during testing. In addition, the electrical resistivity of 347 stainless steel and Inconel 718 tubing was measured, and physical properties data for MHF-5 and MMH found in the literature were extrapolated to high pressures and temperatures.

TABLE OF CONTENTS

LIST OF TABLES

LIST OF ILLUSTRATIONS

LIST OF ILLUSTRATIONS (cont.)

LIST OF ILLUSTRATIONS (cont.)

NOMENCLATURE

A,B	= Correlation constants
C	= 0.000948 $\frac{\text{Btu/sec}}{\text{Watt}}$
C_p	= Specific heat, Btu/lb_m °F
d	= equivalent diameter, in.
ΔE	= Voltage drop across test section, volts
$F_{L/D}$	= Thermal entrance correction factor
F_p	= Pressure correction factor
F_T	= Bulk temperature correction factor
g_c	= Gravitational constant = 32.2 lb_m ft/$sec^2 lb_f$
h	= Heat transfer coefficient, Btu/sec $in.^2$ °F
I	= Current, amps
ID	= Test section inside diameter, in.
J	= 778 ft-lb_f/Btu
k	= Thermal conductivity, Btu/hr ft°F
L	= Test section heated length, in.
L/D	= Length to diameter ratio
Nu	= Nusselt Number = (hd/k) (3600) (12)
OD	= Test section outside diameter, in.
P	= Pressure, psia
P_{cr}	= Critical pressure, psia
P_r	= Prandtl Number = (3600 μCp)/k
Q_{in}	= Electrical energy input to the fluid, Btu/sec
Q_{out}	= Indicated output sensible energy, Btu/sec
R_e	= Reynolds Number = (Vdρ)/12μ
r	= radius, in.
T	= Temperature, °F
T_{cr}	= Critical Temperature, °F
T_{sat}	= Saturation temperature, °F
ΔTo	= Bulk temperature rise observed before application of test section power, °F
ΔT_{sub}	= subcooling = $T_{sat} - T_b$, °F

NOMENCLATURE (cont.)

V	= Velocity, ft/sec
$\dot{W}$	= Flow rate, lb_m/sec
X	= Distance from test section outlet, in.
ϕ	= Heat flux, Btu/in.^{2}sec
ϕ_{Bo}	= Burnout heat flux, Btu/in.^{2}sec
ϕ_{ult}	= Ultimate heat flux, Btu/in.^{2}sec
ρ	= Density, lb_m/ft^3
ρ_e	= Electrical resistivity, ohm in.
μ	= Viscosity, lb_m/ft sec
$\dot{w}$	= Flow rate, lb/sec

SUBSCRIPTS

ave	- indicates average between test section inlet and outlet
b	- refers to bulk conditions
i	- refers to inside tube wall conditions
in	- refers to inlet conditions
out	- refers to outlet conditions

I. INTRODUCTION

A. PROGRAM OBJECTIVE

(U) The purpose of this program was to measure the heat transfer characteristics of MHF-5 and MMH--these two propellants representing members of the hydrazine-type fuels considered for prepackaged and storable rocket applications. The program was oriented toward obtaining the information a thermal analyst requires to design regeneratively cooled thrust chambers, including burnout heat flux limits at subcritical pressures, ultimate heat flux limits at supercritical pressures, heat transfer coefficients, physical and transport properties, decomposition tendencies and material compatibility. A definite effort was made to concentrate on those ranges of pressures, coolant velocities, bulk temperatures and the materials that would be expected in future regeneratively cooled chambers.

B. DATA CORRELATION

(U) Correlating methods, including graphical representations and empirical equations that represent the data have been emphasized. Several of the equations follow closely the recommendations that were made by Van Huff and Rousar in Reference 1 which includes additional thermal information for 22 propellants as well as a timely bibliography summarizing the work that has been done in this field. It also considers other practical problems such as coolant passage geometry and asymmetric heating which were not examined in this particular program. Thus, the combination of Reference 1 and this report provides a thorough summary of the information available to design regeneratively cooled thrust chambers with MHF-5, MMH and other hydrazine type fuels.

C. PROGRAM PHASING

(U) The program consisted of three phases.

I, C, Program Phasing (cont.)

Phase 1: An analytical effort in which the available physical and transport properties for MHF-5 and MMH were extrapolated to the pressures and temperatures attained in the experimental program.

Phase 2: An experimental effort in which the forced convection characteristics of MHF-5 were measured over the following ranges of conditions:

Pressure:	250 to 3900 psia
Bulk Temperature:	-38 to 308°F
Velocities:	17.7 to 205 ft/sec
Heat Fluxes:	Up to 49.6 Btu/in.^{2} sec
Materials:	347 Stainless Steel and Inconel 718

A total of 38 tests was run; 35 producing burnout and ultimate heat flux information.

Phase 3: An experimental effort in which the forced convection characteristics of MMH were measured over the following ranges of conditions:

Pressure:	490 to 3960 psia
Bulk Temperature:	-42 to 305°F
Velocities:	48 to 160 ft/sec
Heat Fluxes:	Up to 28.7 Btu/in.^{2} sec
Materials:	347 Stainless Steel and Inconel 718

A total of 17 tests was run; all of these produced burnout and ultimate heat flux information.

D. REPORT ORGANIZATION

(U) This report is separated into six major sections plus three appendices. The conclusions and recommendations that follow the introduction present the recommended correlating equations plus important experimental observations. The AGC high pressure heat transfer loop and the testing

I, D, Report Organization (cont.)

procedures are discussed in Section III. Section IV presents a summary of the physical properties work, chemical analysis results are given in Section V, and data reduction methods are discussed in Section VI. Detailed examination of the test results are included in Section VII. These have been separated into the subcritical pressure results which were generally consistent with previous studies and the supercritical pressure results which were complicated by an extraordinarily wide variety of behavior. Possible causes for the peculiar behavior are postulated. The design section, Section VIII, presents comparisons of several coolants under conditions representative of regeneratively cooled thrust chambers. This includes recommendations for extrapolating the data to other fuels of the hydrazine family. Appendices A and B include the MHF-5 and MMH properties; Appendix C is a tabulation of all the test data.

II. CONCLUSIONS AND RECOMMENDATIONS

(U) The conclusions and recommendations listed below represent a condensation and interpretation of a great deal of experimental data. Sometimes it was not possible to correlate the data completely with the semi-empirical expressions listed below. In those cases, an approach which would be considered a conservative one has been recommended. It is felt that the recommendations represent valid design tools within the present state-of-the-art; however, they obviously should be reconsidered as new information becomes available. For this reason, all of the experimental data have been tabulated in Appendix C.

(U) 1. Forced convection heat transfer with MHF-5 and MMH is adequately described by the Hines Correlation

$$Nu_b = 0.005\ Re_b^{0.95}\ Pr_b^{0.4}$$

II, Conclusions and Recommendations (cont.)

This expression is recommended for design calculations at subcritical pressures when the wall temperature is less than the saturation temperature and at supercritical pressures when the wall temperature is less than 700°F.

(U) 2. Heat transfer coefficients significantly higher than given by the Hines Correlation were measured at low bulk temperatures with both propellants at subcritical and supercritical pressures. These high coefficients were due to thermal entrance effects and were correlated with a modified form of the Hines Correlation.

$$Nu_b = 0.005\ Re_b^{0.95}\ Pr_b^{0.4}\ (F_{L/D})$$

where: $$F_{L/D} = 1.0 + \frac{0.018\ Pr}{(L/D)^{1/2}}$$

for: $$L/D \leq 10\ ,\ 3.8 \leq P_r \leq 141.3$$

(U) 3. Normal nucleate boiling was observed with MHF-5 and MMH at subcritical pressures and at wall temperatures slightly greater than the saturation temperature. Steady-state film boiling was also observed with MMH. The burnout heat flux, that is the heat flux where a transition from nucleate boiling to film boiling occurred, correlates with the product of velocity and subcooling. Additional factors influencing the burnout heat flux of these propellants are:

a. Low bulk temperature effects (both MHF-5 and MMH)
b. Pressure effects (MHF-5 only)

(U) 4. The measured MHF-5 burnout heat fluxes were higher than expected, particularly at 250 to 650 psia pressure where the MHF-5 values were higher than those of its major constituents at equivalent velocity and subcooling conditions. This apparent improvement and the pressure effect noted

II, Conclusions and Recommendations (cont.)

above have been observed with other mixtures. The burnout heat flux data of MHF-5 at bulk temperatures greater than about 50°F are correlated within ±10% with the following expression:

$$\phi_{Bo} = \left[4.0 + 0.00070V\Delta T_{sub}\right] F_p$$

where: $F_p = 1.33-0.65 \left(\frac{P}{1000}\right)$

$250 \text{ psia} \leq P \leq 1400 \text{ psia}$

The F_p factor accounts for the observed decrease in burnout heat flux with increasing pressure.

(U) 5. Cooling with subcritical pressure MHF-5 for durations up to 8 minutes at 80% of the burnout heat flux has been demonstrated; however, some mild chemical attack by the MHF-5 on the tube wall was noted (347 stainless steel tube).

(U) 6. Inconel 718 is not recommended as a coolant passage material for MHF-5 because significantly lower burnout heat fluxes were measured with this material. Minor material incompatibility appears to be the cause.

(U) 7. The following correlations are recommended for the burnout heat flux of MMH at bulk temperatures greater than 0°F.

$$\phi_{Bo} = 1.0 + 0.00060\ V\Delta T_{sub},\ V\Delta T_{sub} < 8000 \text{ ft °F/sec}$$
$$\phi_{Bo} = 4.2 + 0.00020\ V\Delta T_{sub},\ V\Delta T_{sub} \geq 8000 \text{ ft °F/sec}$$

These expressions predict most of the available MMH burnout data within ±30%.

II, Conclusions and Recommendations (cont.)

(U) 8. For low bulk temperatures, a decrease in MHF-5 and MMH burnout heat flux with decreasing bulk temperature was noted similar to the behavior of RFNA, Corporal Fuel, diethylene triamine, and a 50/50 mixture of aniline and furfuryl alcohol. This low bulk temperature phenomenon appears to be related to viscosity and can be described with the following expression which correlates the majority of the low bulk temperature burnout data within ±30%.

$$\frac{\phi_{Bo}}{(\phi_{Bo})_{HT}} = 1.12 - 0.30 \text{ Ln } (\mu_b \times 10^3)$$

where: μ_b = Bulk temperature viscosity, $lb_m/ft\ sec$

$(\phi_{Bo})_{HT}$ = Burnout heat flux given by a correlation of the higher bulk temperature data

The above equation in conjunction with the correlations given in conclusions 4 and 7 is recommended for evaluating the burnout heat flux of MHF-5 at bulk temperatures less than 50°F and of MMH at bulk temperatures less than 0°F.

(U) 9. At supercritical pressures a burnout-like condition was observed with MHF-5 and MMH. Several types of burnout-like phenomena occurred including:

a. A sudden wall temperature excursion

b. A limited wall temperature excursion (about 200°F)

c. A nucleate boiling-like phenomena followed by a wall temperature excursion.

In addition a burnout condition was evidenced in certain of the MMH tests by the formation of "hot spots" on the tube wall.

II, Conclusions and Recommendations (cont.)

(U) 10. The heat flux at which the above phenomena developed has been defined as the ultimate heat flux. This flux is a design limiting factor analogous to the burnout heat flux at subcritical pressure. The ultimate heat flux data of both MHF-5 and MMH are predicted reasonably well with the conventional forced convection relationship and a maximum wall temperature of 700°F.

$$\phi_{ult} = h\ (700-T_B)$$

(U) In this equation, h is calculated from the Hines Correlation. Ultimate heat fluxes significantly higher than the predictions were indicated in some tests where the nucleate boiling-like behavior occurred. However, insufficient data exist to predict the occurrence or the extent of this boiling-like phenomenon. The maximum wall temperature of 700°F also appears appropriate for avoiding excessive decomposition of MHF-5 and MMH at the tube wall. Significant carbonaceous deposits were noted in tubes which operated at wall temperatures above 700°F.

(U) 11. A 20% reduction in the ultimate heat flux was observed in an extended duration test with supercritical MHF-5. Similar behavior is likely with MMH; therefore, the following equation is recommended as a design correlation for supercritical MHF-5 and MMH ultimate heat flux.

$$\phi_{ult} = 0.8\ h\ (700-T_B)$$

(U) 12. No significant change in the chemical composition of the MHF-5 or MMH occurred during the heat transfer tests. The limited amount of decomposition at the tube wall was insignificant when compared to the total flow through the tubes.

II, Conclusions and Recommendations (ont.)

(U) 13. Transport and physical properties for MMH and MHF-5 have been estimated for pressures up to 5000 psia and temperatures to 700°F.

(U) 14. As more information is collected on the heat transfer characteristics of various propellants, a general picture of the limiting phenomena is developing. The following areas appear to be logical choices for additional work that will aid in this development:

a. Analytical and experimental work to describe the rather complex phenomena of ultimate heat fluxes at supercritical pressures.

b. Experimental and analytical work to define the low temperature burnout heat flux event.

c. Experimental studies on other mixtures of hydrazine type fuels to examine mixture effects.

III. EXPERIMENTAL APPARATUS

A. HIGH PRESSURE HEAT TRANSFER LOOP

(U) All tests were conducted on Aerojet's 5,500 psig blowdown heat transfer loop shown schematically in Figure 1. The principal components of the loop are the nitrogen pressurization system, the feed system, the preheater and precooler, the test section assembly, the heat exchanger, and the flow control valve/dump tank assembly. Electrical power for the preheater and test section assembly was provided by four dc power supplies (each rated at 50 kw-15 volts) which operated from a 440-volt, 3 phase ac line source.

(U) The nitrogen pressurization system consisted of a booster pump and a storage vessel. The booster pump was a Haskel, high-pressure, oil-free gas booster compressor: Model SS-3. Gaseous nitrogen was provided to the booster pump at pressures ranging from 2500 to 3600 psig and compressed up to a maximum pressure of 10,000 psig. The high pressure nitrogen was stored in

III, A, High Pressure Heat Transfer Loop (cont.)

an 18 cu ft, type 304 stainless steel lined, carbon steel receiver. Figure 2 shows the booster pump and the high pressure receiver.

(U) The feed system consisted of a 110 gallon, 5500 psig rated type 321 stainless steel pressure vessel (run tank) for propellant pressurization and storage; a 10,000 psig pressure-reducing regulator, a back-pressure regulator for controlled venting of the vessel, a run valve (tank safety valve); various other valves for filling, draining, venting; and an overpressure relief valve to protect the vessel from excess pressure. The feed system is shown in Figure 3.

(U) The preheater, precooler, and test section assembly were separated from the feed system by a blast wall which offered protection to the feed system in the event of detonation in the test section assembly area. The preheater was constructed from 1/2 in. OD x 0.058 in. wall thickness, type 347 stainless steel tubing approximately 20 ft in length. Electrical taps brazed to the tube at suitable intervals provided an impedance match consistent with the output of the power supplies. During this test program, up to three power supplies were used on the preheater, and preheater outlet bulk temperatures up to 270°F were achieved (Test HT-9-110). The preheater is shown in Figure 3.

(U) In seven of the MHF-5 and MMH tests, the propellant was cooled below ambient temperature. This was done by by-passing the preheater and flowing through a precooler coil which consisted of approximately 40 feet of 1/2 in. OD x 0.035 in. wall thickness, type 347 stainless steel tubing immersed in liquid nitrogen. The precooler coil was electrically heated prior to the initiation of propellant flow to prevent freezing of the propellant during the startup transient. After the desired flow rate was established, power to the cooler coil was reduced until the required inlet temperature was obtained. Using this technique, the lowest test section inlet temperature obtained was -42°F (Test HT-9-112).

III, A, High Pressure Heat Transfer Loop (cont.)

(U) The test section assembly consisted of the test section and related instrumentation (described in Sections II, B. and II, C.), the test section enclosure, propellant mixing sections, and electrical connections. A typical test section and test section assembly are shown in Figures 4 and 5. The test section enclosure was fabricated from stainless steel except for the front cover which was clear acrylic plastic. Connections to this enclosure included a propellant dump line and a low-velocity gaseous nitrogen purge. The nitrogen purge was used to maintain an inert atmosphere around the test section. Water spray nozzles installed inside the enclosure were used to wash down the propellant whenever test section burnout occurred. The nitrogen purge and water spray proved to be very effective for preventing post-burnout fires since no significant propellant burning occurred.

(U) The propellant mixing sections were positioned at the upstream and downstream ends of the test section. Three immersion-type copper constantan thermocouples were installed in each mixer. Each mixer also incorporated insulators which electrically isolated the test section from the rest of the system. The bus-bar connections which clamped onto the test section electrodes were cantilever-mounted in the enclosure. The upper connection was supported with flexures to permit axial movement of the heated test section tube due to thermal expansion.

(U) Propellant cooling downstream of the test section was accomplished with a single tube, multipass, shell-and-tube type heat exchanger. Propellant flowed in the tube and water was used as the coolant on the shell side. The tube was 0.500 OD x 0.058 in. wall thickness and 150 ft long.

(U) Flow control was accomplished using a Control Components, Inc., 1/2 in. valve (C_v = 1.5) operated by a Jordan Controls, Inc., electric motor actuator. After flowing through the flow control valve the propellant was contained in the dump system until after the test. The dump system consisted

III, A, High Pressure Heat Transfer Loop (cont.)

of three 40 gallon type 347 stainless steel spherical vessels connected in parallel, and included an overpressure relief valve, vent, and GN_2 pressurization tie-ins.

(U) The dump system, flow control valve and heat exchanger are shown in Figure 3.

B. TEST SECTIONS

(U) Test sections were fabricated from 347 stainless steel and Inconel 718 tubing with 3/16 and 1/4 in. OD and 0.012 to 0.024 in. wall thickness. The dimensions and material of each test section are listed in Table 1. The unheated entrance length of each test section was 10.75 in.

(U) The heated lengths of the test sections were formed by silver brazing two predrilled cylindrical copper electrodes onto the tubing. These copper cylinders were fitted into the copper bus-bar clamps mounted in the test section enclosure. Figure 5 shows an installed test section. Pressure taps, located upstream and downstream of the test section electrodes, were fabricated by positioning a modified Swagelok union with Teflon ferrules over a 0.031 in. diameter drilled hole. Before installation the union was drilled through at a wrenching flat and a 1/8 in. OD stainless steel tube was Heliarc welded over the hole. The 1/8 in. tube was connected to a high pressure, electrically insulated connector and then to a pressure transducer.

(U) Each test section was instrumented with from two to six chromel-alumel thermocouples for measuring outer wall temperature. The thermocouples were fabricated from 40 gage (about 0.003 in. dia) premium grade thermocouple wire encased in a high temperature varnish-impregnated fiberglass insulation. The junctions were prepared by removing the insulation from the chromel and

III, B, Test Sections (cont.)

alumel wires for about 1/2 in. and capacitance discharge welding them together at a point near the ends of the wires. The excess wire was trimmed away leaving a small loop of uninsulated wire. These loops were positioned around the test section tube over a 0.0005 in. layer of mica (V-1 quality muscovite mica) and were held in firm contact with the tube wall by cantilever spring supports. The thermocouples were installed in pairs as shown in Figure 6. The junctions of each pair of thermocouples were spaced 180° apart on the periphery of the tube and about 1/8 in. apart along the tube axis.

(U) Each test section was also instrumented with one or more incremental voltage taps. These were fabricated by capacitance discharge welding a 0.010-in. stainless steel wire to the tube wall at a given location and insulating this wire with varnish-impregnated fiberglass sleeving.

C. INSTRUMENTATION

The test instrumentation included:

3	Copper-constantan immersion-type thermocouples in the inlet mixer.
3	Copper-constantan immersion-type thermocouples in the outlet mixer.
2 to 6	Chromel-alumel thermocouples on the test section heated length.
2	Turbine-type flowmeters.
2	Pressure transducers for test section pressure (inlet and outlet).
2	Current shunts (preheater and test section circuits).
1 to 3	Test section voltage taps.

III, C, Instrumentation (cont.)

(U) The heat transfer experiments were conducted remotely from the Laboratory Control Room, shown in Figure 7, about 150 ft away from the site of the heat transfer loop. Instrumentation cables from the primary sensing elements at the test site were routed to a central data patchboard system in the control room using shielded transmission lines. The patchboard system connected the signal from primary sensing elements to signal conditioning and calibration equipment and to recording devices.

(U) Astrodata and Kintel differential amplifiers were used in recording the data. These units are capable of operation with high common-mode voltage. The amplifiers convert the low-level data signal to the high-level required for the digital converter and oscillograph systems. Continuous signal shields and a single point ground were employed to maintain signal integrity exclusive of environmental conditions. Test parameters were recorded on a direct reading oscillograph and, via an analog-to-digital data conversion system, on magnetic tape. Printouts of the data in engineering units were prepared from the tape data. A comprehensive block diagram of the instrumentation and data aquisition system in use in the Research Physics Laboratory is shown in Figure 8.

(U) Pressure transducers for this program incorporated 350 ohm, bonded strain gages in a fully active four-arm bridge network. Typical of this configuration is the Taber Model 206. The pressure transducers were maintained and calibrated on a scheduled cycle by Aerojet's Transducer Laboratory. Immediately prior to a heat transfer test all pressure transducer channels were subjected to calibration at 0, 10, 25, 50 and 75 percent of transducer full-scale range.

(U) Both chromel-alumel and copper-constantan premium grade thermocouples were used in the heat transfer tests. Reference junction temperature control was maintained by a conventional water-and-ice bath located at the test site.

III, C, Instrumentation (cont.)

Transmission lines from the thermocouples to the data patchboard were shielded, twisted copper pairs. Temperature calibration was obtained by precision voltage substitution at standard calibration steps of 0, 5, 10, 25 and 50 millivolts as factored by a 1.0 or 0.1 preset value. The thermocouple calibration unit was standardized daily against an internal Eppley Standard Cell.

(U) Propellant flow rate was measured with turbine-type flowmeters (5/8 in. size) manufactured by Potter Aeronautical Corporation. Frequency to dc converters were used to convert the flowmeter output to a dc level suitable for digital recording purposes. These converters were calibrated with a frequency substitution unit which utilizes a precision tuning fork oscillator and binary dividers to supply calibration frequencies of 0, 50, 100, 250 and 500 Hz (Hertz).

Data Recording Systems

(U) Two systems were used to record data from the tests. The primary system incorporated an analog-to-digital data conversion unit having a 420 KHz bit conversion rate with a 1 microsecond sample-and-hold aperture. Twenty Hz passive, low-pass filters on each input signal prevent foldover errors and limit system noise. The converter output data were transmitted over coaxial cables to Aerojet's Central Data Recording facility where the data were converted in format and recorded by Ampex digital tape recorders and subsequently processed on the IBM System 360 data processing unit. The output of this system was a tabulation of all parameters in engineering units.

(U) Secondary data were provided by a Consolidated Electrodynamics Model 5-113 thirty-six-channel direct printout recording oscillograph. The oscillograph records have proven valuable in providing quick-look data as well as data for transient analysis.

III, C, Instrumentation (cont.)

System Measurement Accuracies

(U) Probable error levels for the measurement systems have been established by Aerojet's test division through statistical data analysis. These are best expressed as the one-sigma standard deviation of the calibration and dynamic errors. The following errors are expressed as a percent of nominal operating level of each measurement system (approximately 75% of full-scale capability):

	Measurement System	Probable Error
1.	Pressure	0.300% (1σ)
2.	Thermocouple	
	Immersion type - copper constantan	
	32 - 200°F	.75°F
	200 - 700°F	1.00%
3.	Turbine flowmeters (5/8 in. size)	0.26% (1σ)
4.	Current or voltage (based on analysis only)	0.15% (1σ)

The above estimates do not account for installation errors. These were evaluated in this program by comparing redundant measurements. The bulk temperature thermocouples generally gave readings within 1°F at the test section inlet and 2°F at the outlet. In general, the test section wall temperature thermocouples agreed within 20°F at 500°F, 50°F at 1000°F, and 100°F at 1500°F.

(U) The readings from the test section wall temperature thermocouples were adjusted using the results of previous calibration tests. In these calibration tests an uncooled test section was heated up to 1400°F

III, C, Instrumentation (cont.)

using an ac power supply. Readings from thermocouples welded directly to the tube were compared to readings from spring-loaded thermocouples insulated from the tube wall with mica (the type of installation used on the MHF-5 and MMH test sections). The results of these calibration tests, given in Figure 9, show that the spring-loaded thermocouples read 10°F low at 500°F wall temperature and about 50°F low at 1400°F wall temperature.

(U) Flow rate measurements were obtained from two turbine-type flow meters connected in series upstream of the preheater. Agreement between these meters was generally within 3%. However, some problems were encountered in maintaining good flowmeter agreement with MHF-5 and readings differing by as much as 12% were obtained in a few tests early in the program. This difficulty was possibly caused by a white fluffy deposit which formed on the upstream side of the flowmeter nearest the run tank. It was found that water washed this deposit away. Whenever a discrepancy was observed, the flowmeter nearest the run tank appeared to be the one in error (this was determined by installing new flowmeters and comparing readings). Flowmeters that were recalibrated after being removed from the loop and cleaned compared to their previous calibration within 0.5%. Satisfactory agreement (3%) was maintained for the balance of the MHF-5 program by periodically cleaning or replacing the flowmeters. No difficulty was encountered in obtaining good flowmeter agreement with MMH.

(U) In all cases where redundant measurements were made, the average value was used for data analysis.

D. TEST PROCEDURE

(U) In this section, the procedure followed in the performance of the MHF-5 and MMH heat transfer tests is described. Pretest activity began with the pumping of gaseous nitrogen from a large volume 3600 psig receiver to an

III, D, Test Procedure (cont.)

18 cu ft receiver at 10,000 psig. Other pretest activity included installation of the test section and pressure leak testing at 350 psig, attaching the plexiglass cover on the test section enclosure, preparation of the thermocouple ice bath, and assuring proper bus-bar connections from the power supplies to the preheater and to the test section.

(U) Initial test operations included initiating water flow to the heat exchanger and to the water injection aspirator for the run tank vent, closing the flow control valve, opening the dump tank vent valve, and opening the run valve. With the run valve open, propellant was able to flow through the loop up to the flow control valve. Next, the run tank was pressurized using the pressure reducing regulator to the required test section outlet pressure plus the anticipated pressure drop. Then the flow control valve was opened and adjusted to give the desired flow rate. After flow and pressure were stabilized at the desired values, the recording devices were started and the power supplies were activated.

(U) For the tests in which forced convection heat transfer and the burnout heat flux (subcritical pressure) or the ultimate heat flux (supercritical pressure) were investigated, the following procedure was followed:

1. The desired test section inlet bulk temperature was established by either increasing the preheater power (hot tests) or decreasing the precooler power (cold tests).
2. The test section voltage drop was increased to a predetermined level.
3. After steady conditions were obtained, the pertinent data were recorded.
4. Steps 2 and 3 were repeated until the burnout heat flux or the ultimate heat flux was achieved.

III, D, Test Procedure (cont.)

Testing for extended durations was done in essentially the same manner, except that only two voltage settings were used. At each voltage, steady-state heat transfer was maintained for a period of 4 minutes or until the test section failed.

(U) Posttest operations included deactivation of the test section and preheater power supplies, shutdown of propellant flow (this was followed instantly by automatic purges both upstream and downstream of the test section), initiation of water sprays in the test section enclosure (if test section failure occurred), and venting of the run vessel. The propellant was subsequently returned to the run tank by pressurizing the dump tank system.

IV. PHYSICAL PROPERTIES OF MHF-5 AND MMH

(U) A search of the literature was conducted for data on the physical properties of MHF-5 and MMH needed to conduct the heat transfer tests and interpret the data. These are: density, viscosity, specific heat, thermal conductivity, and vapor pressure. The data found in the literature were extrapolated to about 5000 psia pressure and about 700°F temperature and properties for which no data were available were estimated for this range of conditions. These values are given in appendices to this report along with discussions on the data which were available and the extrapolation or estimation techniques used. MHF-5 properties are given in Appendix A and MMH properties are given in Appendix B.

(U) Significant values and references to appropriate discussions, tables, or figures in the appendices are provided in the following two tables.

IV, Physical Properties of MHF-5 and MMH (cont.)

MHF-5 PROPERTIES

(Citations in Appendix A)

Property	Value	Section	Table	Figure
Critical Pressure	1470 psia	I	-	-
Critical Temperature	685°F	II	-	-
Critical Density	0.316 gm/ml	III	-	-
Density	-	IV	-	3 and 4
Viscosity	-	V	1	5 and 7
Heat Capacity	-	VI	2	9
Thermal Conductivity	-	VII	-	11
Vapor Pressure	-	I,B and VIII	4	1 and 12

MMH PROPERTIES

(Citations in Appendix B)

Property	Value	Section	Table	Figure
Critical Pressure	1195 psia	I	-	-
Critical Temperature	594°F	I	-	-
Critical Density	0.29 gm/ml	I	-	-
Density	-	II	1 and 2	1
Viscosity	-	III	3	2
Heat Capacity	-	IV	4, 5, and 6	3
Thermal Conductivity	-	V	7	4
Vapor Pressure	-	VI	8	5

V. PROPELLANT PREPARATION AND CHEMICAL ANALYSIS

A. MHF-5 PREPARATION

(C) The MHF-5 heat transfer tests were conducted using the mixture of five 20-gallon batches which were each prepared by mixing 92.9 lb of MMH, 54.7 lb of N_2H_4, and 27.01 lb of NH_4NO_3. Ammonia was removed from the mixture by pumping off the vapor generated when the propellant was heated to a temperature of 85 to 100°F. Density measurements of the five batches ranged from 1.008 to 1.001 gm/cc at 77°F temperature.

B. MHF-5 CHEMICAL ANALYSIS

(U) Chemical analyses were determined for several MHF-5 samples taken from the heat transfer system during the course of testing. Samples from a quantity of propellant taken from the system prior to the start of testing were also analyzed for comparison. The tabulation given in Table 2 shows that no appreciable decomposition of the MHF-5 occurred during the testing.

(C) Some difficulties were encountered in obtaining the MHF-5 analyses. The results from a gas chromotograph (the only available device for analyzing MHF-5) tended to be inconsistent due to retention of hydrazine nitrate in the components of the chromatograph system. Several chromatograph column materials were tried with varying degrees of success. The best results were obtained with 5% Carbowax 600 (polyethylene glycol) on Teflon; the material used to analyze AeroZINE 50* samples.

(C) The final analysis procedure consisted of determining the MMH, N_2H_4, H_2O, and NH_3 concentration from gas chromatograph readings. The hydrazine nitrate concentration was determined gravimetrically in a nitron

*AeroZINE 50 is the trade mark registered to the Aerojet-General Corporation for a 50/50 mixture (by weight) of N_2H_4 and UDMH.

V, B, MHF-5 Chemical Analysis (cont.)

precipitation test. These results were considered adequate for this heat transfer investigation but not entirely satisfactory as a precise chemical analysis. The estimated accuracy for the MMH and N_2H_4 constituents is $\pm$ 1 to 2 wt %.

C. MMH CHEMICAL ANALYSIS

(U) Chemical analyses of the MMH obtained before and after testing were determined by iodate titration. The results, tabulated below, indicate that only a slight degradation in purity occurred during testing.

Sample	MMH wt%	H_2O and soluble impurities, wt%
Before Testing	99.70	0.30
After Testing	99.27	0.73

VI. DATA REDUCTION

(U) The data obtained during the MHF-5 and MMH tests were reduced using Aerojet's Data Reduction Computer program, Program 22105 (Ref 2). The output from this program for each test is given in Appendix C.

(U) Local values of heat transfer coefficient were calculated from the relationship:*

$$h = \frac{\phi}{T_i - T_b} \qquad \text{Eq. 1}$$

*See nomenclature at beginning of report.

VI, Data Reduction (cont.)

Values of heat flux were calculated from electrical power measurements and the tube geometry:

$$\phi = 0.000948 \frac{\Delta EI}{\pi (ID)(L)}$$

(U) Inner wall temperatures (T_i) were evaluated assuming radial conduction and no heat transfer at the outer tube wall. The thermal conductivity and electrical resistivity of the tube wall were considered as functions of temperature. The differential equation for this condition is:

$$\frac{d^2T}{dr^2} + \frac{1}{r}\frac{dT}{dr} + \frac{1}{k}\frac{dT}{dr}\frac{dk}{dr} = -\frac{C\,\Delta E^2}{\rho_e k L^2} \qquad \text{Eq. 2}$$

Substitution of finite difference expressions for the derivatives in Equation 2 yields the finite difference equation from which the inside tube wall temperatures were calculated (the outer tube wall temperatures were measured):

$$T_{n+1} = T_n - (T_{n-1} - T_n)\left[\frac{\Delta r}{r_n} + \frac{k_{n-1} - k_n}{k_n} + 1\right] - \frac{C\Delta r^2 \Delta E^2}{k_n \rho_{en} L^2} \qquad \text{Eq. 3}$$

where:

n+1, n, n-1 refer to adjacent radial tube wall increments of thickness Δr.

(U) The thermal conductivity values (k) for 347 stainless steel and Inconel 718 are shown in Figure 10. These data were obtained from Ref 3 and 4. The values of electrical resistivity (ρ_e) shown in Figures 11 and 12 are based on measurements obtained at temperatures from 70 to 1800°F in a resistance heated oven. The measured values of electrical resistivity are summarized in Tables 3 and 4.

VI, Data Reduction (cont.)

(U) Local bulk temperatures were calculated assuming uniform power input along the length of the test section, that is:

$$T_b = T_{bin} + (T_{bout} - T_{bin}) \frac{(L - X)}{L}$$

The local pressure was calculated from a similar expression:

$$P = P_{in} - (P_{in} - P_{out}) \frac{(L - X)}{L}$$

(U) The overall accuracy of the data was evaluated by performing an energy balance across the test section:

$$\text{Energy Balance} = \frac{Q_{in} - Q_{out}}{Q_{in}}$$

The input electrical energy was calculated from

$$Q_{in} = 0.000948\ \Delta EI$$

and the output sensible energy from

$$Q_{out} = \dot{w} \left[(C_p)_{ave} (T_{bout} - T_{bin} - \Delta To) + \frac{(V_{out})^2 - (V_{in})^2}{2\ g_c\ J} \right] \quad \text{Eq. 4}$$

(U) The term ΔTo is the bulk temperature rise observed before application of test section power. This rise is due mainly to frictional heating and was observed to increase with velocity. Incorporation of this term into the energy balance also provides a zero correction for the inlet and outlet bulk temperature thermocouples.

VII. DISCUSSION OF RESULTS

(U) In this section, the results obtained in the MHF-5 and MMH heat transfer tests are summarized and discussed. First some general aspects of the observed heat transfer characteristics are described and then more detailed discussions of the forced convection heat transfer coefficient, subcritical pressure burnout heat flux limits, supercritical pressure ultimate heat flux limits and unusual phenomena are presented. Finally, possible explanations for the unusual phenomena which were observed are evaluated. A complete tabulation of the test results is given in Appendix C.

A. GENERAL HEAT TRANSFER CHARACTERISTICS

(U) The general heat transfer characteristics observed with MHF-5 and MMH are depicted graphically in Figure 13 and discussed in the following paragraphs.

1. Forced Convection - Low Wall Temperature

(U) When the wall temperature was low, i.e., below the saturation temperature in the subcritical pressure tests and/or below the critical temperature in the supercritical pressure tests, a normal forced-convection heat transfer mechanism was observed with both propellants. With this mode of heat transfer, the wall-to-bulk temperature difference is proportional to the applied heat flux and a plot of heat flux vs wall temperature (with bulk temperature essentially a constant) yields a straight line with positive slope. The magnitude of this slope (i.e., the heat transfer coefficient) is proportional to the fluid velocity.

VII, A, General Heat Transfer Characteristics (cont.)

2. Subcritical Pressure Tw > Tsat

(U) At subcritical pressures, a nucleate boiling mechanism was generally observed when the wall temperature slightly exceeded the saturation temperature. With this mechanism, the slope of the heat flux - wall temperature curve increases sharply and relatively large increases in heat flux yield relatively small increases in wall temperature.

(U) The burnout condition at subcritical pressures occurs when the wall temperature increases suddenly. This excursion in wall temperature is attributed to a transition from nucleate boiling to film boiling. Normally, physical failure of the test section accompanies the temperature excursion because the equilibrium wall temperature in film boiling is sufficiently high to either melt the wall locally or cause mechanical failure. This was the case in the subcritical MHF-5 tests; however, in several of the subcritical MMH tests steady conditions were achieved in the film boiling regime. The measured heat transfer coefficients in this regime were, however, quite low as evidenced by the reduced slope of the heat flux - wall temperature curve.

3. Supercritical Pressure Tw > Tcr

(U) At supercritical pressures, a burnout condition occurred with MHF-5 and MMH at wall temperatures somewhat above the critical temperature. A burnout at supercritical pressures is defined as a condition where small increases in heat flux yield large increases in wall temperature. In most cases, the burnout was caused by a sudden degradation in the forced convection heat transfer coefficient which produced an excursion in wall temperature along the line AB shown in Figure 13.

VII, A, General Heat Transfer Characteristics (cont.)

(U) Further increases in heat flux from point B often led to an extended wall temperature excursion which resulted in physical failure of the test section. However, in several tests the temperature excursion AB represented a transition from the normal forced convection mechanism to another stable heat transfer regime. When this occurred the temperature excursion terminated at point B and further increases in heat flux yielded a convection-like characteristic as along lines BC and BC' in Figure 13. Operation in this second regime was generally terminated when a second wall temperature excursion produced physical failure of the test section.

(U) In a few tests, a nucleate boiling-like characteristic was observed; that is, large increases in heat flux produced relatively small increases in wall temperature (line AD in Figure 13). A burnout condition in these tests occurred when the wall temperature suddenly increased and produced test section failure

(U) Some very peculiar phenomena were observed in certain of the MMH tests at supercritical pressure. Achievement of a burnout condition was evidenced by the formation of high temperature regions or "hot spots" which were the result of local temperature excursions as depicted by line AB in Figure 13. These hot spots generally developed first at the inlet and outlet of the test section. As the heat flux was increased beyond point B, the temperature of these spots increased and decreased in an irregular manner as depicted by the dashed line in Figure 13.

VII, Discussion of Results (cont.)

B. FORCED CONVECTION HEAT TRANSFER

(U) The forced convection data of MHF-5 and MMH at subcritical and supercritical pressures are in good agreement with Equation 5 (Hines, Ref 5) as shown by the comparisons in Figures 14 through 17.

$$Nu_b = 0.005\ Re_b^{0.95}\ Pr_b^{0.4} \qquad \text{Eq. 5}$$

where: Nu = Nusselt Number = $\frac{h\ (ID)}{k}\ (3600)(12)$

Re = Reynolds Number = $\frac{V\ (ID)\rho}{12\mu}$

Pr = Prandtl Number = $3600\ \frac{\mu C_p}{k}$

(U) The subcritical pressure data are for heat fluxes below the onset of nucleate boiling. All of the supercritical data are shown except where a large wall temperature excursion occurred (the nucleate boiling-like, and post-transition data are included in Figures 16 and 17).

(U) Most of the data for relatively high bulk temperatures (T_B > 100°F) agree with Equation 5 within ±30% which is considered satisfactory. However at lower bulk temperatures, coefficients significantly higher than the predictions (by up to 150%) were obtained. These high values were related to thermal entrance effects which became significant at lower bulk temperatures and at L/D ratios less than 10 (the low bulk temperature tests were conducted with relatively short test sections).

(U) The thermal entrance effect was correlated in terms of the Prandtl number and the L/D ratio in the form of a dimensionless factor applied to Equation 5.

VII, B, Forced Convection Heat Transfer (cont.)

$$Nu_b = 0.005\ Re_b^{0.95}\ Fr_b^{0.4}\ (F_{L/D}) \qquad \text{Eq. 6}$$

where:

$$F_{L/D} = 1.0 + \frac{0.018\ Pr_b}{(L/D)^{1/2}}$$

Equation 6 correlates nearly all of the data obtained at $L/D \leq 10$ within $\pm 30\%$ as shown in Figure 18. This expression does not, of course, predict the boiling-like behavior observed at low bulk temperatures with supercritical MHF-5.

(U) Equation 6 is for straight round tubes, it is not necessarily a meaningful correlation for design purposes where other geometry effects, for example those produced by noncircular cross-sections and tube curvature, may overshadow the L/D effects. The real significance of Equation 6 is that it further justifies Equation 5 as an acceptable correlation for MHF-5 and MMH forced convection at subcritical and supercritical pressures.

C. SUBCRITICAL PRESSURE BURNOUT HEAT FLUX LIMITS

1. MHF-5 Burnout Heat Flux Limits

a. Testing

(U) The burnout heat flux of MHF-5 at subcritical pressures was investigated in 22 tests at the following conditions:

Velocity:	17.7 to 188.8 ft/sec
Pressure:	253 to 1412 psia
Bulk Temperature:	-24.6 to 291.3°F
Burnout Heat Flux:	7.5 to 49.6 Btu/in.^{2} sec

VII, C, Subcritical Pressure Burnout Heat Flux Limits (cont.)

(U) The objective of 20 of these tests was to achieve a burnout condition and provide data relative to the forced convection heat transfer characteristics. Extended duration heat transfer was evaluated in the two other tests at heat fluxes up to 80% of the burnout heat flux. A burnout condition was observed in 19 tests (no burnout in Test HT-8-101) and the results of these are summarized in Table 5. Physical failure of the test section occurred during 18 tests. A burnout was achieved in Test HT-8-120 although test section failure did not occur. This particular test was terminated due to duration considerations; however, the test section began to "glow" just as the test section power was shut off. Such "glowing" normally preceded test section failure in the other MHF-5 tests.

b. Burnout Heat Flux

(U) Figures 19 through 24 indicate that the heat transfer mechanism observed with MHF-5 consists of forced convection regime, then a nucleate boiling regime, followed by a burnout phenomenon. Burnout occurred when the tube wall experienced a sudden excursion in temperature. Outside tube wall temperatures ranging from 900 to 1750°F were observed just prior to the excursion.

(U) The burnout heat flux level for subcritical MHF-5 has been found to depend on velocity, subcooling, pressure, bulk temperature, and test section material. This is demonstrated in Figure 25 which shows MHF-5 burnout heat flux as a function of $V\Delta T_{sub}$, the product of velocity and subcooling. Previous studies (Ref 1) have shown that, aside from compatibility and low bulk temperature effects, the $V\Delta T_{sub}$ parameter generally correlates subcritical burnout heat flux data. This is true for MHF-5 also, but three other major effects seem apparent. These are (1) a pressure effect, (2) a low bulk temperature effect, and (3) a material effect.

VII, C, Subcritical Pressure Burnout Heat Flux Limits (cont.)

(1) The Pressure Effect

(U) At a given pressure (and at bulk temperatures greater than 100°F), the burnout heat flux correlates with the velocity - subcooling product quite well. At given velocity and subcooling conditions, the burnout heat flux, however, definitely decreases with increasing pressure. This is similar to AeroZINE 50 burnout data (Ref 6), where pressure effects were noted but not to the same extent.

(U) A significant influence of pressure on burnout heat flux has also been noted for other mixtures and it appears that pressure effects are characteristic of mixtures. Additional discussion on the pressure effect is given in Section VII,F,2. Test section examinations indicate that chemical phenomena may have accentuated the pressure effect with MHF-5 (see Section VII,E,1).

(U) For MHF-5 the pressure variations can be correlated empirically with an expression of the form:

$$\phi_{Bo} = [A + B(V\Delta T_{sub})] \; F_p \qquad \text{Eq. 7}$$

where: F_p = a factor dependent on pressure

Correlations employing Equation 7 for pressures of 250, 500, 1000, and 1400 psia and for bulk temperatures greater than 100°F are shown in Figure 25. The 500 and 1000 psia correlations were first established by drawing lines through the data. Comparison of these two lines revealed that the ratio of slope to intercept was a constant, therefore suggesting the form of Equation 7. The lines for 250 and 1400 psia were established assuming this proportionality (only one data point was obtained at each of these two pressures).

VII, C, Subcritical Pressure Burnout Heat Flux Limits (cont.)

(U) Further examination of the correlations shown in Figure 25 indicated that the F_p factor decreased linearly with pressure. The data were normalized with respect to the 500 psia line (i.e., F_p was assumed equal to 1.0 at about 500 psia pressure) and the correlation shown in Figure 26 was developed.

$$\phi_{Bo} = [4.0 + 0.00070\ V\Delta T_{sub}]\ F_p \qquad \text{Eq. 8}$$

where: $F_p = 1.33 - 0.65\ (\frac{P}{1000})$

for: $250\ \text{psia} \leq P \leq 1400\ \text{psia}$

$T_b > 100°F$

This expression agrees with the data for bulk temperatures higher than 100°F within ±10%.

(2) The Low Bulk Temperature Effect

(U) The data obtained at bulk temperatures from -25 to +25°F indicate that at these temperatures the burnout heat flux at subcritical pressures is significantly less than would be predicted from the higher temperature data. As shown in Figure 27, this low bulk temperature effect appears to exist for temperatures up to 100°F, but is most significant at temperatures below 50°F. For bulk temperatures greater than 100°F, the effects of bulk temperature are predicted by the normal subcooling term.

(U) It is apparent that the lower burnout fluxes associated with low bulk temperatures are not a unique characteristic of MHF-5 since similar effects, although less severe, were observed with MMH in this investigation and with Corporal Fuel, diethylene triamine, RFNA, and a 50/50

VII, C, Subcritical Pressure Burnout Heat Flux Limits (cont.)

mixture of aniline and furfuryl alcohol. The plot in Figure 27 provides an empirical correlation of the low bulk temperature effect for MHF-5. A more general correlation is obtained with bulk temperature viscosity as discussed in Section VI,C,3 of this report.

(3) The Material Effect

(U) The burnout heat fluxes achieved with Inconel 718 test sections are noticeably lower than those obtained with 347 stainless steel. This appears to be the result of a minor incompatibility between MHF-5 and Inconel 718 (at subcritical pressures). For this reason, only the stainless steel data have been considered in the development of subcritical burnout heat flux correlations.

c. Extended Duration Heat Transfer

(U) Cooling with MHF-5 for an extended duration was evaluated in Tests HT-8-113 and -114 for a total duration of 8 min each. The conditions are tabulated below and shown graphically in Figures 28 and 29. Stainless steel test sections were used.

Test	Duration, min	V(1) ft/sec	P(1) psia	T_b(1) °F	ϕ_2 Btu/in.^{2} sec	ϕ/ϕ_{Bo}(2)
HT-8-113	4	51	520-514	144	8.4	0.49
	4	51	514-510	144	9.3	0.58
HT-8-114	4	159	1058-1052	154	25.5	0.70
	4	158	1039-1034	163	29.4	0.81

(1) Test section outlet conditions
(2) ϕ_{Bo} calculated from Equation 8

VII, C, Subcritical Pressure Burnout Heat Flux Limits (cont.)

(U) Burnout did not occur and no unusual phenomena were observed. Some degradation in the integrity of the tube wall thermocouples is evident, particularly in Test HT-8-114 (Figure 29). A slight whistling was heard throughout Test HT-8-113.

(U) The results of these tests indicate that operation with subcritical MHF-5 for extended durations at heat fluxes up to 80% of the burnout heat flux is feasible.

d. Whistling Phenomena

(U) As noted in Table 5, a slight whistling was heard in each test conducted at velocities of 50 ft/sec or less and at pressures below 1100 psia (no whistling was heard at 50 ft/sec velocity and 1400 psia pressure in Test HT-8-126). This whistling was not very loud and sounded rather like a "muffled teapot". Whistling always began in the nucleate boiling regime at heat fluxes ranging from 35% to 95% of the burnout heat flux and, once started, continued until burnout occurred. No quantitative measurements of this phenomena were obtained. Whistling had no apparent detrimental effect on MHF-5 heat transfer characteristics even in tests with durations up to 8 min (Test HT-8-11[illegible]).

2. MMH Burnout Heat Flux Limits

a. Testing

(U) The burnout heat flux of MMH was investigated in nine tests at the following conditions.

VII, C, Subcritical Pressure Burnout Heat Flux Limits (cont.)

Velocity:	57.0 to 159.8
Pressure:	490 to 841 psia
Bulk Temperature:	-37.5 to 302.7°F
Burnout Heat Flux:	6.78 to 19.9 Btu/in.^{2} sec

The objectives were to achieve the burnout heat flux and to provide data relative to the forced convection heat transfer characteristics of MMH. A burnout condition was attained in each test; the results are summarized in Table 6.

(U) The heat flux-wall temperature relationships shown in Figures 30 through 33 demonstrate that in certain tests, stable heat transfer was maintained in the film boiling regime as well as the forced convection and nucleate boiling regimes. For this reason, test section failure did not always occur when the burnout heat flux was achieved (the burnout heat flux is defined as the heat flux when the transition from nucleate boiling to film boiling takes place). Film boiling heat transfer was observed in all 800 psia tests (Test HT-9-101, -104, and -116) and in one 500 psia test (Test HT-9-103).

(U) Unusual phenomena were observed in the low bulk temperature test at 100 ft/sec velocity and 500 psia pressure (Test HT-9-111). The burnout condition for this test is taken as the lowest heat flux where "hot spots" were visually observed on the test section. These spots developed between wall thermocouple stations and consequently no severe temperature excursion was ever recorded. The hot spots were similar to those which were seen in supercritical pressure tests with MMH (discussed in Section VI,D,2 of this report).

VII, C, Subcritical Pressure Burnout Heat Flux Limits (cont.)

b. Burnout Heat Flux Correlations

(U) The burnout heat flux of MMH at subcritical pressures correlates with the product of velocity and subcooling. This is demonstrated in Figure 34 where the values of burnout heat flux obtained in this investigation and in previous experiments by Aerojet* (Ref 7, 8) and Rocketdyne* (Ref 9) are shown as a function of $V\Delta T_{sub}$.

(U) Two distinct regions are apparent in this data, a high $V\Delta T_{sub}$ region and a low $V\Delta T_{sub}$ region, and different correlations are indicated for each. The existence of two regions for correlating burnout heat flux data has also been observed with other fluids (Ref 1, 6) including N_2H_4, AeroZINE 50 and numerous others.

(U) At high values of $V\Delta T_{sub}$, the following correlation was derived by curve fitting the data at bulk temperatures greater than 0°F with the method of least squares.

$$\phi_{Bo} = 4.2 + 0.00020\ V\Delta T_{sub} \qquad \text{Eq. 9}$$

for: $V\Delta T_{sub} \geq 8000$ ft°F/sec

$T_b > 0$°F

(U) Equation 9 predicts 90% of the data (18 out of 20 data points) within ±30%. The data obtained in this investigation at the higher bulk temperatures are correlated within ±20%. None of the high bulk temperature data are over predicted by more than 30%; however, two of the Ref 7 data points are under predicted by 40 to 50%.

*Since most of these previous data are unpublished, they are listed for reference in Table 7.

VII, C, Subcritical Pressure Burnout Heat Flux Limits (cont.)

(U) The burnout heat flux achieved at -38°F bulk temperature in this investigation (Test HT-9-118) is about 33% lower than predicted by Equation 9, while the data obtained at bulk temperatures down to 7°F are predicted within ±20%. This appears to be the result of low bulk temperature effects similar to those encountered with MHF-5. Therefore, Equation 9 does not appear applicable for bulk temperatures below 0°F. (The low bulk temperature effect is discussed further in Section VI,C,3 of this report.)

(U) At values of $V\Delta T_{sub}$ less than about 8000 ft°F/sec, a somewhat different data correlation is indicated. The following correlation appears appropriate for this region because it approximates the low $V\Delta T_{sub}$ region fairly well and provides a logical transition to the high $V\Delta T_{sub}$ region.

$$\phi_{Bo} = 1.0 + 0.00060\ V\Delta T_{sub} \qquad \text{Eq. 10}$$

$$V\Delta T_{sub} \leq 8000 \text{ ft°F/sec}$$

(U) About 83% of the low $V\Delta T_{sub}$ data are predicted within ±30% by Equation 10. Certain of the Ref 7 data are under predicted by about 50%. No low bulk temperature data are available for the low $V\Delta T_{sub}$ region.

c. Whistling

(U) A whistling phenomena was heard in each of the MMH tests where a transition from nucleate boiling to film boiling occurred without test section failure. This whistling was significantly louder than in the MHF-5 tests and was actually more of a "screeching" noise than a "whistling" noise. The MMH whistling, appears to be associated with the film boiling phenomena since it was always heard during or after the transition from nucleate boiling to film boiling.

VII, C, Subcritical Pressure Burnout Heat Flux Limits (cont.)

3. Low Bulk Temperature Effects

(U) The burnout heat flux of fluids at subcritical pressures is generally considered to increase with decreasing bulk temperature. In data correlations, this relationship is usually accounted for with the subcooling term, ΔT_{sub} (as, for example, in Equations 8 and 9). The reduced values of burnout heat flux observed with MHF-5 and MMH at low bulk temperatures indicate that the effects of bulk temperature are completely accounted for by the subcooling term only at bulk temperatures above a certain level.

(U) This low bulk temperature phenomenon is not a unique characteristic of MHF-5 and MMH, as similar behavior has been reported for: (1) red fuming nitric acid, RFNA (Ref 10); (2) diethylene triamine, DETA, (Ref 11); (3) a 50/50 mixture of aniline and furfuryl alcohol (Ref 12); and (4) Corporal Fuel* (Ref 13). Data for these four fluids showing an inverse bulk temperature effect are plotted in Figure 35.

(U) The reduction in burnout heat flux at low bulk temperature appears related to the bulk temperature viscosity, μ_b. This can be seen by plotting a bulk temperature factor, F_T, (defined below) as a function of viscosity.

$$F_T = \frac{\phi_{Bo}}{(\phi_{Bo})_{HT}}$$

where:

ϕ_{Bo} = Experimental burnout heat flux

$(\phi_{Bo})_{HT}$ = Burnout heat flux predicted by the correlation established from the higher bulk temperature data

*Corporal Fuel is a mixture consisting of 45.8% aniline, 46.4% furfuryl alcohol, 0.2% triethylamine, 7.3% N_2H_4, 0.5% water.

VII, C, Subcritical Pressure Burnout Heat Flux Limits (cont.)

(U) This has been done for the MHF-5, MMH, RFNA, 50 aniline/50 furfuryl alcohol, and Corporal Fuel data, and the results are plotted in Figure 36. The manner in which F_T and μ_b were obtained for each propellant is described below:

MHF-5 and MMH

ϕ_{Bo} was taken from Tables 5 and 6, and $(\phi_{Bo})_{HT}$ was calculated from Equations 8 and 9. Viscosity values were obtained from Figures 5A, 7A (Appendix A) and 2B (Appendix B).

RFNA

F_T was calculated from Figure 35 (which is taken from Ref 10) where $(\phi_{Bo})_{HT}$ was evaluated from the straight-line drawn through the higher temperature data. A considerable amount of other high temperature RFNA data exists and a best estimate correlation has been established (Ref 1). The straight-line in Figure 35 appears more appropriate than the best estimate correlation for evaluating bulk temperature effects because a high degree of scatter exists in the RFNA data (Ref 1) and ϕ_{Bo} has been observed to vary from one batch of propellant to another. Viscosity values were taken from Ref 14.

50 Aniline/50 Furfuryl Alcohol

F_T was calculated from Figure 35 where $(\phi_{Bo})_{HT}$ was taken from the straight-line drawn through the higher temperature data. The viscosity of this mixture was obtained by cross-plotting the values given for aniline in Ref 15, for furfuryl alcohol in Ref 16, and for a 65/35 mixture in Ref 17.

VII, C, Subcritical Pressure Burnout Heat Flux Limits (cont.)

Corporal Fuel

F_T was calculated from the data given in Ref 13 using the correlation: $(\phi_{Bo})_{HT} = 2.7 + 0.00045\ V\Delta T_{sub}$ which was derived from the plot shown in Ref 1. The viscosity was estimated on a modal average basis from the 50 aniline/50 furfuryl values and from the N_2H_4 values given in Ref 14.

(U) The plot in Figure 36 shows that bulk temperature viscosity yields a fairly general correlation of the low bulk temperature effect. At relatively low values of viscosity (higher bulk temperature) only random deviations from the best estimate correlations are evident. At viscosities above 0.001 to 0.0015 $lb_m/ft\ sec$ (1.5 to 2.2 centipoise) a definite trend toward decreased burnout heat flux is apparent. This trend continues at higher viscosities and F_T values in the range of 0.35 to 0.70 are evident at 0.01 $lb_m/ft\ sec$ viscosity.

(U) A reasonable estimate for F_T is obtained by drawing straight lines through the data in Figure 36. This yields the following expressions.

$$F_T = 1.0, \qquad (\mu_b \times 10^3) < 1.5$$

$$F_T = 1.12 - 0.3\ \mathrm{Ln}\ (\mu_b \times 10^3), \qquad (\mu_b \times 10^3) > 1.5 \qquad \text{Eq. 11}$$

where: μ_b is in $lb_m/ft\ sec$ units

Equation 11 was constructed to fit the MHF-5 and MMH data since the RFNA burnout data exhibit considerable scatter (Ref 1) and only estimates were available for the viscosity of 50 aniline/50 furfuryl and Corporal Fuel. However, most of the data in Figure 36 are correlated within $\pm 30\%$ by Equation 11.

VII, C, Subcritical Pressure Burnout Heat Flux Limits (cont.)

(U) The viscosity of MHF-5 and MMH is 0.0015 lb_m/ft sec at 55°F and 0°F, respectively. Therefore, it is recommended that for bulk temperatures below these values the burnout heat flux of MHF-5 and MMH be calculated from:

$$\phi_{Bo} = (\phi_{Bo})_{HT} (F_T) \qquad \text{Eq. 12}$$

where: F_T is given by Equation 11
$(\phi_{Bo})_{HT}$ is given by Equation 8 for MHF-5
and by Equations 9 and 10 for MMH

Furthermore, it appears that Equation 12 is applicable to other fluids when the viscosity is greater than 0.0015 lb_m/ft-sec provided an appropriate expression for $(\phi_{Bo})_{HT}$ is known (several are given in Ref 1).

D. SUPERCRITICAL PRESSURE ULTIMATE HEAT FLUX LIMITS

(U) A burnout condition at supercritical pressures is defined as a point where small increases in heat flux produce large increases in wall temperature. In this report, the heat flux at which this occurs is termed the ultimate heat flux in an attempt to avoid confusion with the burnout heat flux which is usually associated with the transition from nucleate boiling to film boiling at subcritical pressures.

(U) The results from tests to determine the ultimate heat flux of MHF-5 and MMH at supercritical pressures are discussed in the following paragraphs. A burnout condition was achieved in each test; however, the manner in which this condition developed was found to vary considerably.

VII, D, Supercritical Pressure Ultimate Heat Flux Limits (cont.)

1. MHF-5 Ultimate Heat Flux Limits

a. Testing

(U) The ultimate heat flux limits of MHF-5 were measured in 16 tests covering the following conditions.

Velocity:	19.3 to 205 ft/sec
Pressure:	2018 to 3874 psia
Bulk Temperature:	8 to 308°F
Heat Flux:	up to 45.1 Btu/in.^{2} sec

(U) The objective was to determine the ultimate heat flux limits and forced convection characteristics of supercritical MHF-5. This was accomplished and the ultimate heat flux results are summarized in Table 8. Heat transfer conditions with supercritical MHF-5 for extended durations were investigated in one test (HT-8-134).

b. Burnout Conditions

(U) Two types of behavior were observed with supercritical MHF-5, one characteristic of low velocity (V<110 ft/sec) and another at high velocity (V>120 ft/sec).

2. Low Velocity Heat Transfer

(U) The burnout condition at velocities less than 110 ft/sec consisted of a sudden excursion in wall temperature which caused test section failure. This excursion began at inside (liquid side) wall temperatures in the range of 700 to 850°F. Heat transfer for fluxes up to the ultimate heat flux was generally characterized by a normal forced convection mechanism;

VII, D, Supercritical Pressure Ultimate Heat Flux Limits (cont.)

however, some boiling-like behavior was observed. Verification of the temperature excursion was provided by thermocouple data, visual observation via closed circuit TV, and color movies.

20 ft/sec Velocity

(U) At 20 ft/sec velocity, ultimate heat fluxes of 3.0 and 3.5 Btu/in.^{2} sec were achieved in two tests at 3000 psia pressure and 150°F bulk temperature. The wall temperature data indicate nucleate boiling-like behavior at heat fluxes above 2 Btu/in.^{2} sec (Figure 37). Figure 38 shows that the energy balances for these tests tend toward excess sensible energy (over the input electrical energy) as the ultimate heat flux is approached. Excess sensible energies amounting to 30 to 50% were indicated at the ultimate heat flux (no such indications were obtained at subcritical pressures with MHF-5 or MMH). Relatively low wall temperatures (800 to 900°F on the outer wall) were measured just prior to the temperature excursion.

50 ft/sec Velocity

(U) Ultimate heat fluxes ranging from 5.7 to 9.1 Btu/in.^{2} sec were observed in four tests at 50 ft/sec velocity, 2000 to 4000 psia pressure, and 100 to 180°F bulk temperature. Slight amounts of boiling-like behavior occurred as shown in Figure 39. The energy balances for these tests also indicated a general trend toward excess sensible energy as the ultimate heat flux was approached. This was most pronounced for the test conducted with an Inconel 718 test section (HT-8-109) as shown in Figure 38. Outer wall temperatures ranging from 950 to 1200°F were recorded prior to the temperature excursion.

VII, D, Supercritical Ultimate Heat Flux Limits (cont.)

100 ft/sec Velocity

(U) Normal forced convection behavior which terminated in a wall temperature excursion at heat fluxes of 11 to 12 Btu/in.^{2} sec was observed in three tests at 100 ft/sec velocity, 3000 psia pressure, and 150 to 300°F bulk temperature. This is displayed in Figures 40 and 41. Steadily increasing excess energy up to 15-20% was measured in the two tests at 150°F bulk temperature (HT-8-107, -108) but no such indications were observed at 300°F bulk temperature (Figure 36). In these tests, outer wall temperatures ranged from 1200 to 1300°F just prior to test section failure.

(U) A very pronounced nucleate boiling-like characteristic occurred in test HT-8-132 which was conducted at low bulk temperature (8 to 40°F), 100 ft/sec velocity and 3000 psia pressure (Figure 41). This behavior was followed by a temperature excursion at 22.75 Btu/in.^{2} sec heat flux which produced test section failure. Outer wall temperatures increased from 1700 to 1950°F just before test section failure. A very significant L/D effect on forced convection heat transfer coefficient is apparent at the lower heat fluxes. The significance of the nucleate boiling behavior at low bulk temperature becomes apparent when the ultimate heat fluxes in the four tests at 100 ft/sec velocity are compared. The low bulk temperature value is 90% greater than the higher bulk temperature values.

(U) The energy balances for all the 100 ft/sec tests are good, generally within 10%. However, Figure 38 shows that a trend toward excess energy occurs as the ultimate heat flux is approached.

VII, D, Supercritical Ultimate Heat Flux Limits (cont.)

3. High Velocity Heat Transfer

(U) A transition from normal forced convection to a second stable heat transfer regime was observed in each test conducted at 125 to 205 ft/sec velocity. Figures 42 through 44 show that the transitions consisted of only a limited wall temperature excursion of 100 to 200°F. It occurred at heat fluxes of 15 to 21 Btu/in.^{2} sec and at about the same range of wall temperature where large excursions occurred in the lower velocity tests (700 to 850°F).

(U) As the heat flux was increased, operation in this second heat transfer regime was terminated by sudden failure of the test section, apparently the result of a second wall temperature excursion at heat fluxes ranging from 24.5 to 45.1 Btu/in.^{2} sec. It is difficult to verify the occurrence of the second excursion from the outer wall thermocouple data because with temperature readings of 1600 to 2200°F the tube wall thermocouples tend to be undependable. Wall temperature excursions were visually evidenced, however, as the test section was seen to become very hot locally just before failure. The fact that at 150 ft/sec velocity a higher heat flux was achieved at 3000 psia pressure than at 2000 psia in the same type of tubing indicates that failure during these tests was probably not simply a case of gradually overstressing a pressurized tube.

(U) The slope of the heat flux-wall temperature curve in the second heat transfer regime is either greater than or about the same as the slope in the forced convection region. From this standpoint, normal operation in the second regime could be considered. However, the limited temperature excursions which were evident upon entering this second regime do not appear conducive to design conservatism. For this reason, the ultimate heat flux limit in the supercritical MHF-5 high velocity tests has been defined as the heat flux where the transition occurs.

VII, D, Supercritical Ultimate Heat Flux Limits (cont.)

(U) The energy balances obtained for the high velocity tests are shown in Figure 45. At 3000 and 4000 psia, peculiar behavior is apparent at the heat flux where the transition occurred. Below the transition point, the energy balances are within ±10% and no general trend is indicated. However, as the transition heat flux is approached the excess energy increases by 5 to 15%. Then at heat fluxes above the transition point, energy balances similar to those at the lower heat fluxes are indicated. This behavior is not indicated for test HT-8-135 at 2000 psia pressure and 160 ft/sec velocity. A gradual trend toward excess energy is indicated throughout this test, but all the energy balances are within normally acceptable limits (±12%).

c. Extended Duration Heat Transfer

(U) Cooling with supercritical MHF-5 in a stainless steel test section for extended durations was investigated in test HT-8-134. The conditions are listed below and shown graphically in Figure 46.

Duration	*V, ft/sec	*P, psia	*T_B, °F	ϕ, $\frac{Btu}{in.^2\ sec}$
4 min	53	3043	146	4.57
3.25 min (failure)	53	3030	153 to 158	5.05

*Test section outlet conditions

(U) At the lower heat flux level, steady-state heat transfer was maintained for a duration of four minutes. Apparently normal forced convection heat transfer occurred during this period. However, a barely perceptible increase in excess sensible energy was indicated by the energy balances.

VII, D, Supercritical Ultimate Heat Flux Limits (cont.)

(U) The test was terminated at the higher heat flux level after 3.25 minutes of steady state when the test section failed. A more pronounced increase in excess energy was indicated for this portion of the test (Figure 46). This is evidence that the exothermic decomposition of the MHF-5 increased and degraded the liquid side heat transfer mechanism.

(U) Although the outer wall thermocouple data do not show a sudden increase in temperature before tube failure, certain of the data do indicate a gradually increasing wall temperature for about one minute before burnout. Other indications of a temperature excursion before the tube failed are apparent, however, in that about two seconds before the burnout the voltage drop increased and the current decreased. These are both indications of increasing resistance and, therefore, increasing temperature.

(U) The results of this test suggest that lower ultimate heat flux limits exist for extended duration operation with supercritical MHF-5 than for relatively short duration operation. For shorter durations, ultimate heat flux limits of 6.4 Btu/in.^{2} sec (HT-8-123, stainless steel test section) and 5.5 Btu/in.^{2} sec (HT-8-109, Inconel 718) were observed at conditions which were very close to those of the extended duration test. Therefore, ultimate heat flux limits 10 to 20% less than those observed in the shorter duration tests appear appropriate for extended duration operation with supercritical MHF-5. It is not clear however exactly what the percentage is or that it even exists at high velocities because of the different characteristics observed at low and high velocities in the shorter duration tests.

VII, D, Supercritical Ultimate Heat Flux Limits (cont.)

d. Ultimate Heat Flux Correlations

(U) The ultimate heat flux of supercritical MHF-5 has been plotted against velocity as shown in Figure 47. The data in which no significant boiling-like behavior occurred fall within a narrow band (within ±20%) around the dashed line in Figure 45. This line also indicates the heat flux at which boiling behavior (if any) began, however, the values of ultimate heat flux with boiling-like behavior are up to 100% higher.

(U) Some criteria for predicting the boiling-like phenomena and its extent are needed to correlate the ultimate heat flux data more accurately. Unfortunately, the data to date are simply not sufficient to establish such criteria. These data do show the low velocities and low bulk temperatures where this exceptional behavior can occur.

(U) The effect of extended duration is certainly an additional factor to be considered in the establishment of a design correlation for supercritical MHF-5 ultimate heat flux since a 20% reduction in ultimate heat flux was observed in the extended duration test (50 ft/sec velocity, 3000 psia pressure, and 150°F bulk temperature). It is not known whether this reduction would occur at other conditions since this can only be determined by testing. In a previous investigation with 98% H_2O_2 (Ref 4), a significant extended duration effect was found to exist over a fairly wide range of pressures (2800 to 3700 psia) and velocities (50 to 150 ft/sec) at 100 to 150°F bulk temperature. It appears therefore that a duration effect must be assumed at all conditions with supercritical MHF-5 until experimental evidence to the contrary is obtained.

(U) A design correlation has thus been established from the plot in Figure 47 which appears to adequately account for the extended duration result and the scatter in the ultimate heat flux data.

VII, D, Supercritical Ultimate Heat Flux Limits (cont.)

$$\phi_{Bo} = 0.094V \qquad \text{Eq 13}$$

(U) Equation 13 provides an upper limit criterion for heat flux which can be rather easily applied and could prove useful for preliminary design analyses. However, an alternate procedure for predicting supercritical MHF-5 ultimate heat flux based on a heat transfer coefficient and a limiting wall temperature appears more appropriate because the burnout condition generally developed at about the same wall temperature (700 to 800°F) and convection was generally the heat transfer mechanism which was evident up to the ultimate heat flux.

(U) The applicability of this alternate procedure is demonstrated in Figure 48 where it is shown that the ultimate heat flux without boiling-like behavior is predicted within ±20% with the conventional convection equation:

$$\phi = h(T_w - T_b)$$

in conjunction with the convection correlation established in Section VI,B:

$$h = \frac{0.005}{12(3600)} \left(\frac{k}{d}\right) Re_b^{0.95} \; Pr_b^{0.4} \; (F_{L/D}) \qquad \text{Eq 14}$$

and a limiting wall temperature of 700°F. Here again the ultimate heat flux with boiling-like behavior is underpredicted.

(U) The extended duration ultimate heat flux is about 20% lower than the prediction in Figure 48. Therefore, in order to account for extended duration effects, the following equation is recommended as a design correlation for supercritical MHF-5:

VII, D, Supercritical Ultimate Heat Flux Limits (cont.)

$$\phi_{ult} = 0.8\ h\ (700 - T_b) \qquad \text{Eq 15}$$

Since the L/D term in Equation 14 is not necessarily applicable to all geometries, it is further recommended that h in Equation 15 be evaluated from the Hines Correlation, Equation 5 (or Equation 14 with $F_{L/D} = 1$).

2. MMH Ultimate Heat Flux Limits

a. Testing

(U) The ultimate heat flux of MMH at supercritical pressure was measured in eight tests covering the following ranges:

Velocity:	48 to 152 ft/sec
Pressure:	2060 to 3960 psia
Bulk Temperature:	-37 to 305°F
Heat Flux:	Up to 28.66 Btu/in.^{2} sec

(U) The objectives were to determine the ultimate heat flux and forced convection heat transfer characteristics of supercritical MMH. A burnout condition was observed in each test. The results are summarized in Table 9.

(U) The majority of tests were conducted at a pressure level of 3000 psia and 100 to 200°F bulk temperature with velocities ranging from 50 to 150 ft/sec. Heat transfer at low (-37°F) and elevated (300°F) bulk temperature was examined at 50 ft/sec velocity and 3000 psia pressure. Pressure levels of 2000 to 4000 psia were tested at 100 ft/sec velocity and 100 to 200°F bulk temperature.

VII, D, Supercritical Ultimate Heat Flux Limits (cont.)

b. Burnout Conditions

(1) General Observations

(U) The achievement of a burnout condition with supercritical MMH was evidenced by one of the following four events:

1. A gradual degradation of the heat transfer coefficient.
2. A transition or limited wall temperature excursion.
3. A large wall temperature excursion which followed nucleate boiling-like behavior.
4. The occurrence of localized "hot spots".

(U) The ultimate heat flux is defined as the lowest heat flux where any one of these events occurred. In general, a normal forced convection heat transfer mechanism was indicated at heat fluxes below the ultimate heat flux. General indications of excess sensible energy were not obtained with supercritical MMH as the ultimate heat flux was approached.

(2) 50 ft/sec Velocity

(U) Three types of burnout conditions were observed at 50 ft/sec velocity and 3000 psia as shown in Figure 49. The ultimate heat fluxes range from 5.9 to 6.9 Btu/in.^{2} sec. At high bulk temperature (286°) a transition occurred when the wall temperature was about 650°F and the wall temperature suddenly increased about 200°F. After this transition, a convection-type mechanism was apparent until the test section failed due to a second wall temperature excursion. (This behavior is identical to that observed with supercritical MHF-5 at high velocities).

VII, D, Supercritical Ultimate Heat Flux Limits (cont.)

(U) A more gradual temperature excursion was evident at the low bulk temperature (-37°). This appeared to be a gradual degradation in heat transfer coefficient which developed at wall temperatures of 800 to 900°F. Some nucleate boiling-like behavior was also observed in the downstream portion of the test section (The bulk temperature was -20°F in this region at the ultimate heat flux).

(U) Very unusual behavior was observed in test HT-8-108 at 100 to 200°F bulk temperature. A burnout condition was attained at 5.9 Btu/in.^{2} sec heat flux by the sudden formation of relativel hig' wall temperature regions, termed "hot spots", at the test section inlet and outlet. These hot spot regions were about 1/2 in. long and became red hot while the rest of the test section remained relatively cool. The wall temperature data show that the hot spots were visual evidence of a sudden increase in the outer tube wall temperature from 1000°F to 1300°F (calculated inner wall temperature increased from 800°F to 1100°F). Test section failure did not accompany the formation of the hot spots. When the heat flux was further increased, additional hot spots developed and the temperature of certain areas on the test section increased and decreased in a.. irregular manner. Eventually the entire test section glowed. Test section failure occurred when the heat flux was increased to 13.3 Btu/in.^{2} sec.

(3) 100 ft/sec Velocity

(U) Transition, nucleate boiling-like and hot spot phenomena were observed in four tests at 100 ft/sec velocity and 100 to 200°F bulk temperature. The heat flux and wall temperature data obtained in these tests are shown in Figure 50.

VII, D, Supercritical Ultimate Heat Flux Limits (cont.)

(U) Hot spots occurred in two tests at 3000 psia. In both of these a hot spot was first observed at the test section inlet when the heat flux was 12.7 Btu/in.^{2} sec (this demonstrates the reproducibility of the hot spot phenomenon). An additional spot developed at the test section outlet when the heat flux was increased to about 14 Btu/in.^{2} sec. During the development of the hot spots, the inside tube wall temperature increased from about 700°F to 1000-1200°F. Subsequent increases in heat flux produced the same type of irregular behavior which occurred in test HT-8-108 (50 ft/sec velocity). Test section failure eventually occurred at heat fluxes of 25.3 and 27.7 Btu/in.^{2} sec.

(U) At 2000 psia, nucleate-boiling like behavior was observed at a wall temperature of about 700°F and at heat fluxes of 11.7 to 17.9 Btu/in.^{2} sec. The upper limit of heat flux represents the ultimate heat flux since at this point a sudden excursion in wall temperature occurred and the test section failed.

(U) A transition occurred at 4000 psia pressure when a wall temperature of about 700°F was achieved at 21.7 Btu/in.^{2} sec heat flux. Comparison of the 4000 psia wall temperatures to the 2000 and 3000 psia values (Figure 50) reveals that an apparent gradual enhancement in heat transfer coefficient occurred between about 6 Btu/in.^{2} sec and the ultimate heat flux. After the transition, a convection type heat transfer mechanism existed which terminated in a wall temperature excursion at 28.5 Btu/in.^{2} sec heat flux (the wall temperature data in Figure 48 show the beginning of this second excursion).

(4) 150 ft/sec Velocity

(U) The ultimate heat flux at 150 ft/sec velocity, 3000 psia pressure, and 150°F bulk temperature was also indicated by a

VII, D, Supercritical Ultimate Heat Flux Limits (cont.)

transition as shown in Figure 51. The wall temperature data show that a sudden increase in wall temperature of about 200°F occurred when a heat flux of 24.69 Btu/in.^{2} sec and a wall temperature of about 900°F had been achieved. This test was terminated before test section failure occurred.

c. Ultimate Heat Flux Correlation

(U) A reasonable correlation of the supercritical MMH ultimate heat flux data is obtained with velocity as shown in Figure 52. The 3000 psia data correlate quite well for a wide range of bulk temperatures (-37 to 286°F) and velocities (50 to 150 ft/sec). The 2000 and 4000 psia values are considerably higher than the 3000 psia values (25 to 50%) apparently because of boiling-like phenomena that occurred.

(U) Certain of the 3000 psia data indicate a stronger influence of velocity than was found for MHF-5, and an exponential relationship may be applicable (Figure 52). However, additional data at 150 to 200 ft/sec velocity are really needed to verify the existence of an exponential relationship.

(C) The expression developed for MHF-5 ultimate heat flux also appears appropriate for MMH as demonstrated in Figure 53. No extended duration testing was done with MMH; however, behavior similar to MHF-5 is likely since MMH is the principal component of MHF-5. Therefore, based on these considerations the design correlation recommended for supercritical MHF-5 is also recommended for supercritical MMH:

$$\phi_{ult} = 0.8\ h\ (700 - T_b), \qquad \text{Eq 15}$$

where: h is given by Equation 5.

VII, Discussion of Results (cont.)

E. TEST SECTION EXAMINATIONS

(U) After testing, most of the MHF-5 and MM[illegible]est sections were cut in half and examined for evidence of deposition (or coking) and chemical attack. The observations are discussed in the following paragraphs.

1. MHF-5 Test Sections

a. Subcritical Pressure

(U) The majority of test sections from the subcritical MHF-5 tests were relatively clean. Notable exceptions were the two Inconel 718 tubes used in tests HT-8-104 and -105. The interior of these was coated with a black layer of carbonaceous material. The existence of this layer is indicative of propellant decomposition at the tube wall. Such decomposition would be exothermic and is certainly a factor contributing to the lower burnout heat fluxes in the Inconel 718 tubes.

(U) The interior coloration of the 347 stainless steel tubes varied with pressure. In general, discoloration increased with pressure. The test sections used at 250 to 650 psia pressure were quite clean, although some bronze staining was evident. This staining was darkest and most uniform in the tube from the 500 psia, 50 ft/sec velocity, extended duration test (HT-8-113). The 1000 psia test sections were all bronze-stained, but darker and more uniformly discolored than the tubes used at lower pressures. Dark grey stains were also evident in some of the 1000 psia test sections. A somewhat different discoloration was seen in the test section from the 1400 psia pressure test (HT-8-126). The colora ion of this tube ranged from grey-blue to purple and some carbonaceous residues were apparent near the burnout site.

VII, E, Test Section Examinations (cont.)

(U) Some longitudinal troughs were also noted in the walls of the stainless steel test sections. They were in general quite small and could be seen plainly only with the aid of a microscope. They were also found in sections of unused tubing. The troughs were apparently tooling marks left on the tubing during the drawing process. In the extended duration test sections the troughs were somewhat enlarged, particularly in the test section from the 1000 psia pressure and 150 ft/sec velocity test (HT-8-114). A view of one of these is shown in Figure 54; photomicrographs taken of specimens from the HT-8-114 test section are shown in Figures 54 and 55. These larger troughs were on the order of 0.001 in. deep. They appear to be the result of a corrosion-erosion attack on the tube wall which started in the tooling marks. A general increase in surface roughness was also noted on this particular test section.

b. Supercritical Pressure

(U) All of the test sections from the supercritical pressure MHF-5 tests contained a thin layer of carbonaceous deposit on the interior surface. In general, the Inconel 718 tubes appeared somewhat blacker than the stainless steel tubes and contained more deposit. The extent of this deposition did not appear to vary appreciably with bulk temperature, pressure, or velocity.

(U) The stainless steel tube which failed in the supercritical pressure extended duration test (HT-8-134) was examined in detail. The cross sectioned tube is shown in Figure 56. Failure occurred in two places; a complete severance occurred about 3 in. from the test section outlet and the wall bulged and split 1.25 in. from the test section outlet (total heated length = 6 in.). Bending of the tube also occurred upon failure. Most of the interior was blackened and evidence of chemical attack was found between the two failure points ("shiny area" in Figure 56). Photomicrographs were taken

VII, E, Test Section Examinations (cont.)

of specimens from a typical blackened region, the region of the bulge, and the "shiny" region. These are shown along with a photomicrograph of an unheated tube specimen (control specimen) in Figures 56, 57, and 58.

(U) Figure 56 shows that the carbonaceous residues in the blackened regions produced a uniform carburized layer on the interior tube surface. Intergranular penetration by carbon from the residues occurred in the bulge, severance, and shiny regions as shown in Figures 57 and 58. The penetration was quite severe in the shiny region where whole grains of metal were lifted from the surface and apparently washed away producing a wall thickness reduction of about 30%.

2. MMH Test Sections

a. Subcritical Pressure

(U) Two types of interior appearance were noted on the test sections used with MMH at subcritical pressures (all were 347 stainless steel). In the tests were tube failure coincided with the transition from nucleate to film boiling (for example tests HT-9-106, and -117) the tube was essentially unmarked except in the immediate vicinity of the burnout site. Some black deposits and small amounts of chemical attack were noted near the burnout site where wall temperatures on the order of 2000°F occurred during the process of burnout. A general darkening of the tube sur and somewhat more chemical attack were observed in the tests were stable film boiling was maintained (for example, test HT-9-103) and in the low-bulk-temperature test where hot spots developed (test HT-9-111). This apparent increased chemical activity is probably due to the relatively high wall temperatures which occurred during these tests (900 to 1200°F).

VII, E, Test Section Examinations (cont.)

b. Supercritical Pressures

(U) A thin layer of black carbonaceous deposit was found on the interior surface of each supercritical MMH test section. The appearance of these tubes was in general quite similar to the supercritical MHF-5 test sections. A notable exception was the HT-9-113 test section which was light gray in color rather than black, indicating that only very small amounts of deposition occurred in this test.

(U) It is significant that HT-8-113 was the test in which a very pronounced boiling-like characteristic was observed. As a result of this phenomena, the maximum inner wall temperature during this test was relatively low, about 750°F. Inner wall temperatures of 1000°F or more occurred on the other supercritical MMH test sections. It appears, therefore, that formation of the carbonaceous layer started at wall temperatures slightly less than 750°F.

(U) The test section from test HT-9-107, one of the tests in which the "hot spot" phenomena was observed, was examined in detail near the point where the test section eventually failed. Photomicrographs taken at the locations noted in Figure 59 show a carbonaceous layer, a carburized layer, and evidence of intergranular penetration by carbon (Figures 59 and 60). This specimen is very similar to the HT-8-134 test section (supercritical MHF-5 duration test) and there are no indications of peculiar phenomena which might have produced the "hot spots".

F. DISCUSSION OF UNUSUAL PHENOMENA

(U) Several of the phenomena mentioned in the preceding are somewhat unusual and warrant further consideration. This section contains additional discussions in the following areas:

VII, F, Discussion Unusual Phenomena (cont.)

1. Burnout Heat Flux at Low Bulk Temperature
2. Effect of Pressure on MHF-5 Burnout Heat Flux
3. Hot Spot Phenomena
4. Other Burnout Phenomena at Supercritical Pressure

(U) The program scope did not permit detailed analyses of each of these, however, we have tried to alert the designer to anomalous behavior and to provide adequate empirical expressions for their prediction. Furthermore some of the events occurred after the burnout or ultimate heat flux was attained, thus from a design consideration they are primarily of scientific interest.

1. Burnout Heat Flux at Low Bulk Temperature (Subcritical Pressure)

(U) This investigation was not the first in which burnout heat flux was found to decrease with bulk temperature at temperatures below a certain value. The phenomenon has been termed the "low bulk temperature effect" in other sections of this report but the term "viscous effect" is probably more appropriate because its occurrence certainly appears related to viscosity (see Figure 36). Not much discussion exists in the literature, probably because it has not been observed with the more commonly used coolants. For example, the Figure 36 correlation indicates that viscous effects will not be observed with water since water freezes before its viscosity becomes as high as 0.0015 lb_m/ft sec (Ref 14).

(U) Apparently the subcooled nucleate boiling mechanism is altered significantly when the viscosity becomes sufficiently large. As discussed in Reference 18, heat transfer in nucleate boiling is accompanied by a vigorous turbulent mixing process at the heated wall, produced by the formation and collapse of vapor bubbles. It seems reasonable that the structure of the turbulence induced by this bubble action could be affected by viscosity. For

VII, F, Discussion of Unusual Phenomena (cont.)

example, one of the principal features of subcooled nucleate boiling bubble action is that collapsing bubbles draw streams of subcooled liquid to the wall (Ref 18), which "impinge" against the wall at a fairly high velocity. The eddies formed by the impinging subcooled stream will re-enter the main cooling stream more slowly when the viscosity is high. Thus coolant temperatures will be locally higher near the wall and burnout fluxes consequently lower.

(U) Further investigation into the mechanism of burnout with and without viscous effects is certainly needed to adequately explain this phenomenon. The correlation in Figure 36 appears, however, to be a first attempt to quantify the phenomenon and it should be sufficient for estimation of these viscous effects. A correlation involving a dimensionless parameter would seem more appropriate but attempts to correlate the Figure 36 data with Prandtl number (Pr) yielded a family of lines (one for each propellant) rather than a single correlation. No relationship between Reynolds number (based on tube ID and bulk temperature properties) and the viscous effect was found.

2. Effect of Pressure on MHF-5 Burnout Heat Flux

(C) The effect of pressure on MHF-5 burnout heat flux is very significant, as shown in Section VII,C,1 of this report. The burnout heat flux decreases with increasing pressure at constant velocity and subcooling conditions. A similar but much less pronounced trend seen in the AeroZINE 50 burnout data has been attributed to the low critical pressure and temperature of UDMH (785 psia, 480°F). At higher pressure (and correspondingly higher saturation temperature) the UDMH in AeroZINE 50 becomes a supercritical fluid which does not contributed to the nucleate boiling action. The MMH component in MHF-5 may play the same role as the UDMH in Aerozine 50.

(U) The results of other experiments indicate that a pressure dependent burnout heat flux may be a characteristic of mixtures. In burnout

VII, F, Discussion of Unusual Phenomena (cont.)

studies with monisopropyldiphenyl and benzene mixtures (Ref 24), the burnout heat flux was found to very considerably with pressure while the pure component burnout values did not. For these mixtures, the burnout heat flux increased with increasing pressure.

(U) In addition, it appears that increased chemical activity near the wall could be contributing factor to the MHF-5 pressure effect. This concluded from the interior coloration of the test sections noted in Section VII,E,1, where progressively darker test sections at higher pressure indicate increasing propellant decomposition at the tube wall. Any decomposition would tend to accelerate the transition from nucleate boiling to film boiling since the decomposition is exothermic. It is not clear, however, whether the increased chemical action is due to the increased pressure alone or to the higher wall temperatures which are encountered as a result of the increased saturation temperature (Figure 20). The temperature effect is the more reasonable assumption since it has a more pronounced influence on chemical reactions. Here again, the mechansim is not clearly defined but the empirical approach shown in Figure 26 provides the means to treat the phenomenon in a quantitative manner.

3. Hot Spot Phenomena

(U) The most unusual phenomenon was the occurrence of test section hot spots in the MMH tests. These hot spots were very localized and, once formed, behaved quite erratically as the "glowing" was observed to diminish and increase irregularly as the heat flux was increased. These spots were possibly caused by the formation of carbon deposits on the interior tube surface. A fairly rapid buildup of a very thin carbon layer could produce a locally high tube wall thermal resistance and, correspondingly, locally high wall temperature. Flaking off of this deposit could then cause the test section to cool off locally.

VII, F, Discussion of Unusual Phenomena (cont.)

(U) The above mechanism appears plausible since carbon deposits were found inside the MMH test sections where hot spots were noted. On the other hand, it is possible that the carbon deposits were formed after the hot spots developed. No hot spots were seen in the supercritical MHF-5 tests, and posttest examinations revealed that the general appearance of the supercritical MHF-5 and supercritical MMH test sections was about the same. In any case, no confirmed explanation is available, but as noted above, the inception of hot spots was defined as the ultimate heat flux limit and their peculiar behavior after formation is only of general interest.

4. Other Burnout Phenomena at Supercritical Pressure

a. General Discussion

(U) It has been consistently observed that burnout phenomena can occur with fluids at supercritical pressures when the bulk temperature is less than the critical temperature (Ref 1). These phenomena usually occur when the wall temperature exceeds the critical temperature and some work toward relating these occurrences to fluid property variations in the boundary layer has been done (Ref 19). However, for rocket propellants these phenomena are often complicated by chemical reactions in the boundary layer.

(U) Several types of burnout phenomena have been observed but, for the purposes of discussion they can be classed as one of two basic types:

Type 1. A general decrease in heat transfer coefficient which produces a wall temperature excursion.

Type 2. Nucleate - boiling like behavior followed by a wall temperature excursion.

VII, F, Discussion of Unusual Phenomena (cont.)

(U) In each type, a heat flux is reached where a relatively low value of heat transfer coefficient exists at the wall (temperature excursion) but this is sometimes preceded by the occurrence of very high values of heat transfer coefficient (nucleate boiling - like behavior). It appears that chemical reactions in the boundary layer can either influence these phenomena or be the controlling factor in their occurrence.

(U) Both types of behavior occurred with supercritical MHF-5 and MMH. In addition, a transition or limited temperature excursion phenomenon was observed. The transition phenomenon is considered a special case of Type 1 since the sudden increase in wall temperature is indicative of a reduced heat transfer coefficient. The heat flux at which the transition occurred has been termed an ultimate (limiting) heat flux because the sudden (but admittedly limited) increase in wall temperature is not consistent with conservative design methods.

b. Decreasing Heat Transfer Coefficient

(U) A burnout condition associated with a decreasing heat transfer coefficient has been previously observed with ClF_3, AeroZINE 50, and 98% H_2O_2 at supercritical pressures. In this investigation it was noted with MHF-5 at the higher bulk temperatures (T_b>100°F) and with MMH at 3000 psia.

(U) The decrease can occur gradually or very rapidly. The gradual reduction noted with ClF_3 (Ref 1) can logically be expected at supercritical pressures when the wall temperature exceeds the critical temperature if no chemical reaction occurs. It is reasonable that as the wall temperature approaches the critical temperature, the fluid near the wall becomes gas-like rather than liquid-like, and gradually lower heat transfer coefficients result.

VII, F, Discussion of Unusual Phenomena (cont.)

(U) The rapid, almost instantaneous decrease in heat transfer coefficient and abrupt tube failure observed with AeroZINE 50 and 98% H_2O_2 (Refs 20 and 4) has been related to an exothermic decomposition in the boundary layer. Exothermic decomposition was also apparently a contributing factor in the MHF-5 and MMH burnouts of this type as evidenced by the carbonaceous residues found in the test sections. Decomposition may only be a contributing factor, however, because each failure occurred at wall temperature near or above the critical temperature where property variations can also become significant.

c. Nucleate Boiling-Like Phenomena

(U) Nucleate boiling-like behavior has been reported for N_2O_4 (Ref 21), CO_2 (Ref 22), and water (Ref 23). The pronounced nucleate-boiling characteristic observed with supercritical N_2O_4 can be directly related to the endothermic dissociation of this propellant. An actual boiling-like mechanism involving interactions between high and low density fluid has been postulated for CO_2 and water. This latter process appears to be the mechanism observed with supercritical MHF-5 and MMH. It is not clear from the data obtained in this investigation exactly what general circumstances cause nucleate boiling-like behavior but the indications are that this behavior can be expected with MHF-5 at low velocities and at low temperature, and with MMH at a pressure of 2000 psia.

VIII. THRUST CHAMBER DESIGN CONSIDERATIONS

(U) The most critical parameter to be considered in the design of thrust chamber cooling systems is the burnout or ultimate heat flux since normally the liquid-side thermal resistance (1/h) does not seriously influence the design. The adequacy of a given propellant as a thrust chamber coolant is usually judged by the level of heat flux that it can accept at reasonable coolant velocities. In this section, the cooling capabilities of MHF-5 and MMH at subcritical and supercritical pressures are compared to the capabilities of other well known coolants.

A. BURNOUT HEAT FLUX (SUBCRITICAL PRESSURE)

(U) The burnout heat flux characteristics of MHF-5 and MMH are compared to those previously established for water, N_2H_4, and AeroZINE 50 in Figure 61. In this plot, burnout heat flux is shown as a function of pressure for 100 ft/sec velocity and 150°F bulk temperature, and as a function of bulk temperature for 100 ft/sec velocity and 500 psia pressure. The MHF-5 and MMH curves shown were obtained from equations 8 and 9, and the water, N_2H_4, and AeroZINE 50 burnout values were calculated from the correlations given in Reference 1.

(U) Figure 61 shows that the cooling capabilities of MHF-5 are relatively good and that the burnout heat flux of MHF-5 is significantly greater than the MMH burnout heat flux throughout the range of subcritical pressures. MMH compares roughly with AeroZINE 50 as a coolant, however the MMH burnout heat flux is somewhat lower than the AeroZINE 50 values.

(U) The effect of pressure on MHF-5 burnout heat flux is quite pronounced and is the opposite of the normally observed effect. At low pressures, 500 psia or less, MHF-5 is a very attractive coolant as it is comparable to water and superior to its major constituents, N_2H_4 and MMH. At higher pressures the cooling capabilities of MHF-5 are diminished somewhat but the burnout heat

VIII, A, Burnout Heat Flux (Subcritical Pressure) (cont.)

flux is still relatively high, being about the same as N_2H_4 at 1000 psia and about the same as AeroZINE 50 at 1400 psia.

(U) The adverse effect of low bulk temperature on MHF-5 and MMH burnout heat flux is also displayed in Figure 61. These temperature effects were calculated from Equation 11 and are more pronounced for MHF-5 because the viscosity is higher than the MMH viscosity. It is apparent that a potential problem exists in cooling with very cold MHF-5 or MMH since a significant reduction in burnout heat flux exists.

B. ULTIMATE HEAT FLUX (SUPERCRITICAL PRESSURE)

(U) Ultimate heat flux limits for MHF-5 and MMH at supercritical pressures are compared to those determined for N_2O_4, 98% H_2O_2, and AeroZINE 50 in Figure 62. The MHF-5 and MMH curves were established from Equation 15. The N_2O_4, 98% H_2O_2, and AeroZINE 50 curves were taken from Reference 1. It is apparent that MHF-5, MMH, and AeroZINE 50 have about the same ultimate heat flux limits and that these fuels are not particularly promising coolants for high heat flux regions at supercritical pressures.

C. HEAT FLUX LIMITS FOR OTHER HYDRAZINE TYPE FUELS

(U) Generalized correlations for heat flux limits are highly desirable for estimating the burnout and ultimate heat flux of fluids for which no data exist. Unfortunately, no general correlations which are completely satisfactory have been developed, although the burnout heat flux can be estimated reasonably well with the procedure outlined in Reference 1. However, considerable burnout and ultimate heat flux data now exist for hydrazine type fuels and some general aspects regarding the heat flux limits of this particular class of propellants are apparent. These are discussed in the following paragraphs.

VIII, C, Heat Flux Limits for Other Hydrazine Type Fuels (cont.)

1. Burnout Heat Flux

(U) In Reference 1 it was shown that for high values of $V\Delta T_{sub}$ ($V\Delta T_{sub}$ > 2000 to 8000 ft°F/sec) a reasonably good estimate for the burnout heat flux of fluid 1 could be obtained from the burnout correlation established (from data) for fluid 2 using the following equation which relates the burnout heat flux of the two fluids to their critical pressures.

$$(\phi_{Bo})_1 = \left[A_2 + B_2\ V\Delta T_{sub}\right] \quad \frac{(P_{cr})_1}{(P_{cr})_2} \qquad \text{Eq 16}$$

where: A_2, B_2 are correlation constants established for fluid 2.

Equation 16 was found to work best when the molecular structure of fluids 1 and 2 was similar. Predictions for hydrazine type fuels were obtained from Equation 16 and the correlation for hydrazine (Pcr = 2131 psia). Combination of Equation 16 and the hydrazine correlation yie' :

$$\phi_{Bo} = \left[5.0 + 0.000445\ V\Delta T_{sub}\right] \frac{Pcr}{2131} \qquad \text{Eq 17}$$

Predictions from Equation 17 were within 20% of the best estimate correlation for AeroZINE 50, UDMH, 75% N_2H_4/25% UDMH, 25% N_2H_4/75% UDMH, and 40% MMH/60% UDMH.

(U) The prediction from Equation 17 also compares well with the best estimate correlation established for MMH at high values of $V\Delta T_{sub}$ (Figure 34). The predicted equation,

$$\phi_{Bo} = 2.8 + 0.00025\ V\Delta T_{sub}$$

VIII, C, Heat Flux Limits for Other Hydrazine Type Fuels (cont.)

is within ±15% of the best estimate correlation,

$$\phi_{Bo} = 4.2 + 0.00020\ V\Delta T_{sub}$$

for $V\Delta T_{sub}$ up to 60,000 ft °F/sec (the upper limit of the MMH data).

(U) Equation 17 does not compare well with the correlations established for MHF-5. The predicted equation for MHF-5,

$$\phi_{Bo} = 3.5 + 0.00031\ V\Delta T_{sub}$$

is about the same as the 1400 psia correlation (within 20%) but burnout heat fluxes which are too low are predicted for the lower pressures. The 1000 psia data are about 40% higher than predicted and the 250 and 500 psia data are 100% or more higher than predicted. This can be seen by examining the MHF-5 correlations and noting that the $V\Delta T_{sub}$ term is generally large compared to the constant term. The MHF-5 correlations are listed below.

P, psia	Correlation
250	$\phi_{Bo} = 4.7 + 0.00082\ V\Delta T_{sub}$
800	$\phi_{Bo} = 4.0 + 0.00070\ V\Delta T_{sub}$
1000	$\phi_{Bo} = 2.8 + 0.000425\ V\Delta T_{sub}$
1400	$\phi_{Bo} = 1.7 + 0.000294\ V\Delta T_{sub}$

(C) It is not clear why the low-pressure MHF-5 burnout values are so high, higher in fact than either of the principal constituents of MHF-5, N_2H_4 and MMH, at equivalent conditions. This behavior is not unique, however, because monoisopropyldiphenyl and benzene mixtures (Ref 24) also indicate maximums in burnout heat flux at a certain composition (pressure, velocity and subcooling remaining constant). This maximum value is up to 300% higher than

VIII, C, Heat Flux Limits for Other Hydrazine Type Fuels (cont.)

the burnout heat flux of the pure components. Conversely, no enhancemen' in the burnout heat flux exists for N_2H_4/UDMH or UDMH/MMH mixtures (Equation 17 works quite well for these). Additional experimental work is needed to clarify the nature of this effect in the N_2H_4/MMH/$N_2H_5NO_3$ system.

2. Ultimate Heat Flux

(U) No generalized correlations for the ultimate heat flux of supercritical pressure fluids have been developed. However, the plot in Figur` shows that the ultimate heat fluxes of the hydrazine type fuels which have been investigated (AeroZINE 50, MHF-5, and MMH) are about the same at a given velocity. Therefore, Figure 62 may be used to estimate the ultimate heat flow of hydrazine type fuels.

(U) An alternate procedure for estimating ultimate heat flux may also be used. As noted in this investigation for MMH and MHF-5, and in Reference 20 for AeroZINE 50, the ultimate heat flux for these fuels is generally reached when the wall temperature is near the critical temperature. Furthermore, heat transfer at heat fluxes below the ultimate value can generally be described by a conventional forced convection correlation (such as the Hines Correlation). Therefore the relationship:

$$\phi_{ult} = h\,(T_{cr} - T_B)$$

will yield a reasonable estimate for the ultimate heat flux. This expression is recommended for hydrazine type fuels for which no data are available.

REFERENCE LIST

*1. N. E. Van Huff and D. C. Rousar, "Ultimate Heat Flux Limits of Storable Propellants," 8th Liquid Propulsion Symposium, CPIA Publication No. 121, Vol II, October 1966

2. H. Tayama, Liquid-Side Heat Transfer Analysis With Several Fluids, Program B22105 Job Report, Aerojet Computing Sciences Division, 15 April 1966

3. Report on Physical Properties of Metals and Alloys from Cryogenic to Elevated Temperatures, American Society for Testing Materials, ASTM Special Publication No. 296, April 1961

4. D. C. Rousar and N. E. Van Huff, Heat Transfer Characteristics of 98% H_2O_2 at High Pressure and High Velocity, Technical Report AFRPL-TR-66-263, Aerojet-General Corporation, Contract AF 04(611)-10785, August 1966

5. W. S. Hines, Turbulent Forced Convection Heat Transfer to Liquids at Very High Heat Fluxes and Flow Rates, Rocketdyne Research Report No. 61-14, November 1961

6. D. C. Rousar, Heat Transfer Characteristic of AeroZINE 50 at High Velocities and Subcoolings, Aerojet-General Internal Report TCER 9648-003, Contract AF 04(695)-941, 11 November 1966

7. K. Sato, Heat Transfer Characteristics of Project 107A Storable Propellant; Aerojet-General Internal Memorandum, Monthly Progress Report for May 1959, Contract AF 04(645)-8.

*8. Application of Alkyl Hydrazines to Rocket Power Plants, Aerojet-General Report No. 1293, Volumes I and II, May 1958 (Confidential)

*9. J. R. McCarthy and W. S. Hines, Heat Transfer With Monomethylhydrazine, Rocketdyne Internal Memorandum CHTUM 59-62, 12 June 1959 (Confidential)

10. L. E. Dean, Heat Transfer Characteristics of RFNA, Bell Aircraft Report No. 117-982-004, July 1956

*11. Combined Bimonthly Summary No. 51, Jet Propulsion Laboratory, Pasadena, Calif, Feb 1956 (Confidential)

*12. Combined Bimonthly Summary No. 50, Jet Propulsion Laboratory, Dec 1955 (Confidential)

13. Combined Bimonthly Summary No. 44, 45, 46, and 47, Jet Propulsion Laboratory, Nov 1954, Jan 1955, April 1955, June 1955

REFERENCE LIST (cont.)

14. Performance and Properties of Liquid Propellants, Aerojet-General Report 8160-65, June 1961

15. Liquid Propellants Handbook, Vol 1, Batelle Memorial Institute, Sept 1957

16. Liquid Propellants Handbook, Vol 2, Batelle Memorial Institute, Sept 1957

17. Design Studies of Liquid Fuel Booster Rockets, The M. W. Kellogg Co., Jersey City, New Jersey, Report SPD 168, April 1948, p. 21

18. F. Kreith, Principles of Heat Transfer, 1st Edition, p. 403, International Textbook Co., Scranton, Penn.

19. B. S. Petukhov, E. A. Krasnoschekov, and V. S. Protopopov, "An Investigation of Heat Transfer to Fluids Flowing in Pipes under Supercritical Conditions," International Developments in Heat Transfer, 1961

20. W. R. Thompson and E. L. Geery, An Experimental Investigation of Heat Transfer to AeroZINE 50 at Supercritical Pressures, Advanced Research Division, Aerojet-General Corporation Special Report No. 2654, August 1963

21. W. R. Thompson, E. L. Geery, J. F. Harkee, An Experimental Study of The Heat Transfer Characteristics of Nitrogen Tetroxide at Supercritical Pressures, Von Karman Center, TM 183-64-39, Aerojet-General Corporation, 12 June 1964

22. K. Nishikawa, K. Miyabi, "On The Boiling-Like Phenomena at Supercritical Pressures," Memoirs of the Faculty of Engineering, Kyushu University, Fukuoka Japan, Dec 1965

23. K. Goldman, "Heat Transfer to Supercritical Water at 5000 psi Flowing at High Mass Flow Rates Through Round Tubes," International Developments in Heat Transfer, 1961

24. K. V. Naboichenko, A. A. Kiryutin, B. S. Gribov, "A Study of Critical Heat Flux with Forced Flow of Monoisopropyldiphenyl-Benzene Mixtures," Thermal Engineering, Vol 12, No. 11, November 1965

TABLE 1

TEST SECTION DIMENSIONS

Test	Nominal Values			Measured Values		
	OD, in.	Wall Thickness, in.	Material	OD, in.	ID, in.	Heated Length, in.
HT-8-101, 102	1/4	0.016	347 Stainless	0.251	0.219	6.00
(MHF-5) -103	3/16	0.016	347 Stainless	0.187	0.155	4.00
-104	3/16	0.015	Incorel 718	0.190	0.160	3.50
-105	3/16	0.015	Inconel 718	0.190	0.160	3.50
-106	3/16	0.016	347 Stainless	0.187	0.155	4.00
-107	3/16	0.024	Inconel 718	0.189	0.139	5.00
-108	3/16	0.024	347 Stainless	0.187	0.139	5.00
-109	3/16	0.015	Inconel 718	0.254	0.222	5.50
-110	1/4	0.016	347 Stainless	0.251	0.218	5.50
-111	1/4	0.016	347 Stainless	0.251	0.216	5.00
-112	3/16	0.012	347 Stainless	0.188	0.164	4.00
-113	1/4	0.016	347 Stainless	0.251	0.218	6.00
-114	3/16	0.016	347 Stainless	0.187	0.153	4.00
-115	3/16	0.024	347 Stainless	0.186	0.139	4.00
-116	3/16	0.024	347 Stainless	0.186	0.139	6.00
-117	3/16	0.024	347 Stainless	0.187	0.141	6.00
-118	1/4	0.015	Inconel 718	0.254	0.222	5.50
-119	1/4	0.016	347 Stainless	0.251	0.218	4.50
-120	3/16	0.012	347 Stainless	0.187	0.163	1.50
-121	1/4	0.016	347 Stainless	0.251	0.218	4.50
-122	3/16	0.012	347 Stainless	0.188	0.164	1.50
-123	3/16	0.024	347 Stainless	0.187	0.139	6.00
-124	3/16	0.024	347 Stainless	0.187	0.138	4.00
-125	3/16	0.024	347 Stainless	0.187	0.138	5.00
-126	1/4	0.016	347 Stainless	0.251	0.218	6.00
-127	3/16	0.024	347 Stainless	0.187	0.138	4.00
-128	1/4	0.015	Inconel 718	0.253	0.221	5.00
-130	3/16	0.024	347 Stainless	0.187	0.138	1.00
-131	3/16	0.024	347 Stainless	0.187	0.138	1.00
-132	3/16	0.024	347 Stainless	0.187	0.139	1.50
-133	3/16	0.024	347 Stainless	0.186	0.138	5.50
-134	3/16	0.024	347 Stainless	0.186	0.138	6.00
-135	3/16	0.024	347 Stainless	0.186	0.138	3.00
-136	3/16	0.015	Inconel 718	0.189	0.159	2.00
-137	3/16	0.024	347 Stainless	0.187	0.139	5.00
-138	1/4	0.015	Inconel 718	0.253	0.221	5.50
-139	3/16	0.016	347 Stainless	0.187	0.155	5.50
HT-9-101	3/16	0.016	347 Stainless	0.187	0.155	4.50
-102	3/16	0.024	347 Stainless	0.187	0.139	5.00
(MMH) -103	3/16	0.024	347 Stainless	0.187	0.140	5.00
-104	3/16	0.024	347 Stainless	0.187	0.139	5.00
-105	3/16	0.024	347 Stainless	0.187	0.138	5.00
-106	3/16	0.012	347 Stainless	0.188	0.164	5.00
-107	3/16	0.024	347 Stainless	0.187	0.139	5.00
-108	3/16	0.024	347 Stainless	0.187	0.139	6.00
-109	3/16	0.024	347 Stainless	0.187	0.140	3.00
-110	3/16	0.024	347 Stainless	0.186	0.137	2.00
-111	3/16	0.016	347 Stainless	0.187	0.155	1.50
-112	3/16	0.024	347 Stainless	0.187	0.139	1.50
-113	3/16	0.024	347 Stainless	0.187	0.139	5.00
-115	3/16	0.015	Inconel 718	0.189	0.157	4.00
-116	3/16	0.012	347 Stainless	0.188	0.163	4.00
-117	3/16	0.024	347 Stainless	0.186	0.139	6.00
-118	3/16	0.024	347 Stainless	0.187	0.139	1.50

TABLE 2

MHF-5 CHEMICAL ANALYSIS RESULTS (u)

	Sample	MMH Wt%	N_2H_4 Wt%	$N_2H_5NO_3$ Wt%	H_2O Wt%	NH_3 Wt%	Date
1.	Lab Standard*	54.0 53.5	23.9 24.3	19.8 19.8	0.2 0.5	2.1 1.9	8-31-66
2.	From Run Tank Prior to Testing	55.7 56.3	25.6 24.6	17.7 17.7	0.8 1.2	0.2 0.2	8-31-66
3.	Before Test -110	54.2	26.0	18.4	0.9	0.3	9-16-66
4.	From Run Tank Prior to Testing	53.8	26.5	18.4	1.0	0.3	9-16-66
5.	Before Test -114	53.5	26.9	18.35	1.0	0.3	9-23-66
6.	After Test -114	53.0	27.3	18.40	1.0	0.3	9-23-66
7.	From Run Tank Prior to Testing	52.7	27.5	18.35	1.0	0.3	9-23-66
8.	After Test -139	53.3	25.8	18.8	1.9	0.2	11-09-66
9.	From Run Tank Prior to Testing	53.4	26.9	18.6	0.7	0.4	11-09-66
Nominal Values		55.0	26.0	19.0	-	-	

*A small separately prepared batch

TABLE 3

MEASURED ELECTRICAL RESISTIVITY OF 347 STAINLESS STEEL TUBING

Tube Size		Temperature °F	Electrical Resistivity ohm-in.
OD, in.	Wall Thickness, in.		
1/4	0.016	75	28.10
		500	33.17
		900	38.34
		1350	42.78
		1800	45.61
		70*	27.91
3/16	0.024	75	29.83
		484	34.93
		869	40.57
		1317	45.31
		1753	47.67
		70*	29.53
3/16	0.016	75	29.58
		467	34.38
		837	40.28
		1283	44.81
		1706	47.25
		70*	29.35
3/16	0.012	75	28.97
		450	33.60
		805	39.39
		1250	43.52
		1660	46.35
		70*	28.68

*Measured after tubes cooled to room temperature.

TABLE 4

MEASURED ELECTRICAL RESISTIVITY OF INCONEL 718 TUBING

Tube Size		Temperature °F	Electrical Resistivity ohm-in.
O.D, in.	Wall Thickness, in.		
1/4	0.015	70	53.17
		500	55.46
		900	57.58
		1350	57.49
		1800	57.58
		70*	54.28
3/16	0.015	70	49.13
		487	51.68
		857	53.77
		1285	54.60
		1745	53.32
		70*	49.96
3/16	0.024	70	47.07
		475	49.92
		815	51.65
		1220	51.63
		1690	51.46
		70*	48.47

*Measured after tubes cooled to room temperature.

TABLE 5

BURNOUT TEST RESULTS FOR MHF-5 AT SUBCRITICAL PRESSURE

Test No.	ϕ, $\frac{Btu}{in^2 sec}$	V ft/sec	P psia	T_b °F	(1) Heat Balance, %	(2) Conditions	Test Section	Remarks
HT-8-139	14.15	50.4	253	195.9	-2.3	FP	3/16 x 0.016 x 5.5 347 Stainless	(3) Burnout, x (4) = 0.08 (severance) Whistling at ϕ = 9 to burnout
-115	39.71	156.6	654	178.1	+0.8	FP	3/16 x 0.024 x 4.0 347 Stainless	Burnout, x = 0.05 (severance)
-116	22.81	111.1	552	276.8	-1.0	FP	3/16 x 0.024 x 6.0 347 Stainless	Burnout, x = 0.07 (severance)
-121	11.89	49.7	530	291.3	+2.2	FP	1/4 x 0.016 x 4.5 347 Stainless	Burnout, x = 0.06 (severance) Whistling near burnout
-119	12.77	51.7	536	265.2	+1.3	FP	1/4 x 0.016 x 4.5 347 Stainless	Burnout, x = 0.08 (severance) Whistling at ϕ = 7 to burnout
-101,-102	14.48	50.8	531	203.0	-8.3	FP	1/4 x 0.016 x 6.0 347 Stainless	Burnout, x = 0.10 (severance) Whistling at ϕ = 7 to burnout
-122	17.86	49.8	532	24.4	+3.5	FP	3/16 x 0.012 x 1.5 347 Stainless	Burnout, x = 1.4 (severance) Whistling near burnout
-130	8.31	52.2	513	-24.6	+9.9	FP	3/16 x 0.024 x 1.0 347 Stainless	Burnout, x = 0.5 (multiple cracks) Whistling at ϕ = 3 to burnout
-110	7.50	51.7	512	217.4	+7.5	FP	1/4 x 0.016 x 5.5 347 Stainless	Burnout, x = 0.08 (severance) Whistling at ϕ = 3 to burnout
-120	49.60	188.8	1071	108.7	+0.9	0	3/16 x 0.012 x 1.5 347 Stainless	No physical burnout; test section "glowed" as power was shut off
-103	33.25	156.1	1075	178.5	-8.5	FP	3/16 x 0.016 x 4.0 347 Stainless	Burnout, x = 0.4 (severance)
-106	33.44	156.1	1074	167.8	-7.9	FP	3/16 x 0.016 x 4.0 347 Stainless	Burnout, x = 1.0 (severance)

TABLE 5 (cont.)

Test No.	ϕ, Btu/in²sec	V, ft/sec	P, psia	T_b, °F	(1) Heat Balance, %	(2) Conditions	Test Section	Remarks
MT-8-103	24.84	154.4	1055	154.4	-5.4	FP	3/16 x 0.015 x 3.5 Inconel 718	Burnout, x = 0.9 (severance)
-104	22.00	142.7	1067	144.1	-5.8	FP	3/16 x 0.015 x 3.5 Inconel 718	Burnout, x = 1.0 (severance)
-117	19.50	98.8	1071	264.6	-10.3	FP	3/16 x 0.024 x 6.0 347 Stainless	Burnout, x = 0.07 (severance)
-112	22.96	96.8	1031	141.0	-2.3	FP	3/16 x 0.024 x 1.0 347 Stainless	Burnout, x = 0.62 (severance)
-131	23.83	102.9	1073	9.7	-0.6	FP	3/16 x 0.024 x 1.0 347 Stainless	Burnout, x = 0.9 (severance)
-111	11.64	50.1	1024	215.1	-1.2	FP	1/4 x 0.016 x 5.0 347 Stainless	Burnout, x = 0.08 (severance) Whistling at ϕ = 9 to burnout
-126	8.66	48.4	1412	176.7	-7.0	FP	1/4 x 0.016 x 6.0 347 Stainless	Burnout, x = 0.15 (severance)

(1) Heat Balance = $(Q_{in} - Q_{out})/Q_{in}$, Q_{in} = input electrical energy, Btu/sec
Q_{out} = output sensible energy, Btu/sec

(2) FP = Failure point conditions
O = Outlet conditions

(3) Burnout: Indicates test section failure produced by the transition from nucleate boiling to film boiling.

(4) x = Distance between point of failure and downstream end of test section

TABLE 6

BURNOUT TEST RESULTS FOR MMH AT SUBCRITICAL PRESSURE
(All Test Sections 347 Stainless Steel)

Test No.	ϕ, $\frac{Btu}{in^2 sec}$	V, ft/sec	P, psia	T_b, °F	(1) Heat Balance, %	(2) Conditions	Test Section	Remarks
MT-9-103	(a) 16.8*	159.6	502	158	-4.5	0	3/16 x 0.024 x 5.0	(3) Transition whistling
	(b) 17.76	159.8	518	151.4	-3.2	FP		Tube failure, x (4) = 0.5 (severance)
-117	7.83*	99.2	500	302.7	-1.7	FP	3/16 x 0.024 x 6.0	Normal burnout (5), x = 0.15 (hole)
-105	10.17*	101.4	533	196.7	+3.7	FP	3/16 x 0.024 x 5.0	Normal burnout, x = 0.45 (severance)
-106	9.59*	100.0	496	134.8	-7.3	x = 0.60	3/16 x 0.012 x 5.0	Normalbburnout, x = 0.1,1.1 (severance at two locations)
-111	(a) 12.53*	103.1	512	7.0	+6.0	Midpoint	3/16 x 0.016 x 1.5	Hot spots near midpoint.
	(b) 32.54	103.9	490	44.7	+3.4	0		Max. heat flux (no failure)
-118	6.78*	57.0	530	-37.5	-1.0	I	3/16 x 0.024 x 1 5	Transition near inlet (No failure test terminated)
-101	(a) 17.6*	153.0	841	141.6	-3.6	0	3/16 x 0.016 x 4.5	Transition, loud whistling ϕ = 19.1
	(b) 19.9	150.7	836	116.1	-2.3	FP		Tube failure, x = 2.25 (crack)
-104	(a) 10.25*	99.5	815	206.2	+3.1	0	3/16 x 0.024 x 5.0	Transition, loud whistling ϕ = 11.06
	(b) 14.63	100.6	765	226.8	+4.5	x = 0.3		Tube failure, x = 0.1,0.6
-116	(a) 10.46*	90.8	802	83	-10.8	x = 1.25	3/16 x 0.012 x 4.0	Transition, loud whistling, ϕ = 13.8
	(b) 16.8	92.7	775	100.7	-6.3	FP		Tube failure, x = 1.25 (severance)

*Denotes burnout heat flux

(1) Heat balance = $(Q_{in}-Q_{out})/Q_{in}$

(2) FP = Failure point conditions
I = Inlet conditions
0 = Outlet conditions

(3) Transition - indicates transition from nucleate boiling to film boiling.

(4) x = Distance from failure point to downstream end of test section.

(5) Normal burnout - indicates failure occurred at transition from nucleate to film boiling.

TABLE 7

SUBCRITICAL MMH BURNOUT HEAT FLUX DATA
OBTAINED IN PREVIOUS INVESTIGATIONS (u)

Source	V ft/sec	P psia	T_B °F	ϕ_{BO} Btu/in.^{2}-sec	Remarks
(u) Aerojet, Ref 7	33	312	298	4.98	This data is unclassified
	30	328	161	8.85	
	23	322	239	3.55	
	21	337	209	5.55	Stainless steel tubes
	55	455	212	7.58	3/16-in. OD
	51	464	140	9.76	0.035-in. wall thickness
	18	216	252	2.63	3, 12, and 36 in.
	20	315	171	6.70	heated lengths
	53	258	129	10.10	
	54	303	232	6.25	
(c) Aerojet, Ref 8	30.6	301	158	4.66	Classified Confidential
	29.9	502	165	5.29	
	60.9	311	142	7.19	321 stainless steel tubes
	60.2	502	142	6.98	0.210-in. ID
					8.0 in. heated length
(c) Rocketdyne, Ref 9	16.6	217	210	3.21	Classified Confidential
	17.2	225	213	3.42	12 June 1959
	34.2	722	240	4.22	(Declassified after 12
	33.2	228	216	4.52	years)
	16.8	215	256	2.35	Nickel tubing
	16.4	730	193	3.32	OD = 0.250 in.
	17.7	730	267	2.82	0.012-in. wall thickness
	17.8	215	290	2.17	Heated lengths ranging
	17.9	720	307	2.57	from 9 to 25 in.
	34.5	215	250	3.62	
	16.8	208	188	3.36	
	32.5	705	164	5.01	
	16.4	210	182	2.99	
	32.5	193	156	4.63	

TABLE 8

BURNOUT TEST RESULTS FOR MHF-5 AT SUPERCRITICAL PRESSURE

Test No.	ϕ, $\frac{Btu}{in.^2 sec}$	V ft/sec	P psia	T_b °F	(1) Heat Balance, %	(2) Conditions	Test Section	Remarks
HT-8-127	~7.0	---	---	---	---	---	3/16 x 0.024 x 4.0	Onset of slight "boiling"(3)
	7.71*	49.0	2018	178.7	-18.2	FP	347 Stainless	(4)Degradation, x (5) = 0.15 (hole)
-135	(a) 21.00*	163.5	2074	175.2	+1.3	0	3/16 x 0.024 x 3.0	(a) Transition(6)
	(b) 25.89	163.8	2078	179.5	-1.9	FP	347 Stainless	(b) Failure, x = 0.56 (severance)
-118	(a) 2.33	19.3	2964	131.2	-39.0	0	1/4 x 0.015 x 5.5	Onset of "boiling"
	(b) 3.07*	19.3	2962	148.7	-49.2	FP	Inconel 718	Failure, x = 0.5 (severance)
-138	(a) 2.16	19.3	2997	107.6	-24.6	0	1/4 x 0.015 x 5.5	Onset of "boiling"
	(b) 3.50*	19.4	2995	124.4	-31.1	FP	Inconel 718	Failure, x = 1.15 (bulge, hole)
-109	(a) 5.46	50.0	2992	153.3	-46.5	FP	1/4 x 0.015 x 5.5	Onset of slight "boiling"
	(b) 5.74*	50.0	2990	156.2	-50.0	FP	Inconel 718	Degradation, x = 1.3 (severance bulge)
-123	6.39*	50.8	2946	103.5	-28.8	FP	3/16 x 0.024 x 6.0 347 Stainless	Degradation, x = 4.0 (crack)
-133	12.17*	102.9	3088	294.9	+1.6	FP	3/16 x 0.024 x 5.5 347 Stainless	Degradation, x = 1.0 (severance)
-107	11.15*	103.1	3036	162.9	-19.8	FP	3/16 x 0.024 x 5.0 Inconel 718	Degradation, x = 0.7 (severance)
-108	12.22*	104.5	2987	157.1	-14.2	FP	3/16 x 0.024 x 5.0 347 Stainless	Degradation, x = 1.3 (severance)
-132	(a) 11.92	100.7	3037	8.8	-0.7	I	3/16 x 0.024 x 1.5	Onset of "boiling"
	(b) 22.75*	99.9	3035	9.7	-3.0	FP	347 Stainless	Degradation, x = 1.45 (severance)

TABLE 8 (cont.)

Test No.	ϕ, $\frac{Btu}{in^2 sec}$	V ft/sec	P psia	T_b °F	(1) Heat Balance, %	(2) Conditions	Test Section	Remarks
HT-8-137	(a) 15.34*	123.1	3020	171.1	-9.6	0	3/16 x 0.024 x 5.0	Transition
	(b) 28.70	125.7	2995	217.1	+0.6	FP	347 Stainless	Failure, x = 0.25 (hole)
-125	(a) 16.2*	152.7	2832	149.3	-0.9	0	3/16 x 0.024 x 5.0	Transition
	(b) 33.0	154.1	2804	204.3	-0.9	FP	347 Stainless	Failure, x = 0.15 (severance)
-124	(a) 19.12*	205.3	3011	135.3	-1.6	0	3/16 x 0.024 x 4.0	Approximate transition point
	(b) 45.12	205.4	2825	187.8	+0.2	FP	347 Stainless	Failure, x = 0.15 (severance)
-128	(a) 7.3	- -	---	---	---	---	1/4 x 0.015 x 5.0	Onset of slight "boiling"
	(b) 9.15*	50.9	3829	179.7	-20.4	FP	Inconel 718	Degradation, x = 0.25 (crack)
-136	(a) 14.99*	130.6	3874	166.3	---	0	3/16 x 0.015 x 2.0	Approximate transition point
	(b) 24.53	129.3	3744	182.1	-2.7	FP	Inconel 718	Failure, x = 0.05 (severance)

*Denotes Ultimate Heat Flux

(1) Heat Balance = $(Q_{in}-Q_{out})/Q_{in}$

(2) FP = Failure Point Conditions.
I = Inlet conditions.
(3) O = Outlet conditions.

(3) "Boiling" - indicates nucleate boiling-like behavior.

(4) Degradation - indicates severe degradation of heat transfer coefficient produced tube failure.

(5) x = Distance between failure point and downstream end of test section.

(6) Transition - indicates limited wall temperature excursion.

TABLE 9

BURNOUT TEST RESULTS FOR MMH AT SUPERCRITICAL PRESSURE

Test No.	ϕ, Btu/in.^{2} sec	V ft/sec	P psia	T_B °F	(1) Heat Balance, %	(2) Conditions	Test Section	Remarks
HT-9-113	(a) 11.68	111.5	2062	155.3	-18.2	O	3/16x0.024x5.0	Onset of "Boiling"(3)
	(b) 17.92*	114.8	2054	183.0	-11.9	FP	347 Stainless	(4)Degradation, x(5)= 0.25 (crack)
-110	(a) 6.05*	57.4	3027	286.0	+25.1	O	3/16x0.024x2.0	(6)Transition
	(b) 11.05	56.6	3025	305.6	+18.6	FP	347 Stainless	Tube failure, x=1.0 (bulge and hole)
-108	(a) 5.90* (in)	48.6	3026	82.9	-15.1	I	3/16x0.024x6.0	(7)Hot spots at inlet and outlet
	(out)	50.9	3021	172.7		O	347 Stainless	
	(b) 13.28	52.9	3015	258.5	-3.5	FP		Tube failure, x=0.6 (severance)
-112	(a) 6.88*	49.6	3114	-36.6	+1.8	I	3/16x0.024x1.5	Degradation
	(b) 11.39	48.1	2922	-35.1	-1.8	FP	347 Stainless	Tube failure, x=1.25 (severance)
-102	(a) 12.7*	106.7	3056	90.2	-9.8	I	3/16x0.024x5.0	Hot Spot at inlet
	(b) 13.71	111.5	3027	167.7	-10.2	O	347 Stainless	Additional hot spot at outlet
	(c) 27.65	115.3	3012	221.3	-0.1	FP		Tube failure, x=0.1 (severance)
-107	(a) 12.75*	106.5	3062	87.1	-12.7	I	3/16x0.024x5.0	Hot spot at inlet
	(b) 14.09	111.3	3031	168.3	-12.3	O	347 Stainless	Additional hot spot at outlet
	(c) 25.3	107.3	3049	86.0	-2.5	I		Tube failure, x=4.3 (severance)
-109	(a) 24.69*	152.1	3025	155.5	-0.3	O	3/16x0.024x3.0	Transition
	(b) 28.66	152.0	2984	158.4	+0.3	O	347 Stainless	Max. heat flux (no failure)
-115	(a) 21.67*	115.0	3957	187.5	-6.7	O	3/16x0.015x4.0	Transition
	(b) 28.47	115.8	3951	200.7	-3.5	FP	Inconel 718	Tube failure, x=0.10 (hole)

* - Denotes Ultimate Heat Flux

(1) Heat Balance = (Q in - Q out)/Q in
(2) FP = Failure point conditions
I = Inlet conditions
O = Outlet conditions
(3) "Boiling" - indicates nucleate boiling - like behavior.
(4) Degradation - indicates severe degradation of heat transfer coefficient.
(5) x = distance between failure point and downstream end of test section.
(6) Transition - indicates limited temperature excursion.
(7) Hot Spot - denotes appearance of high temperature region.

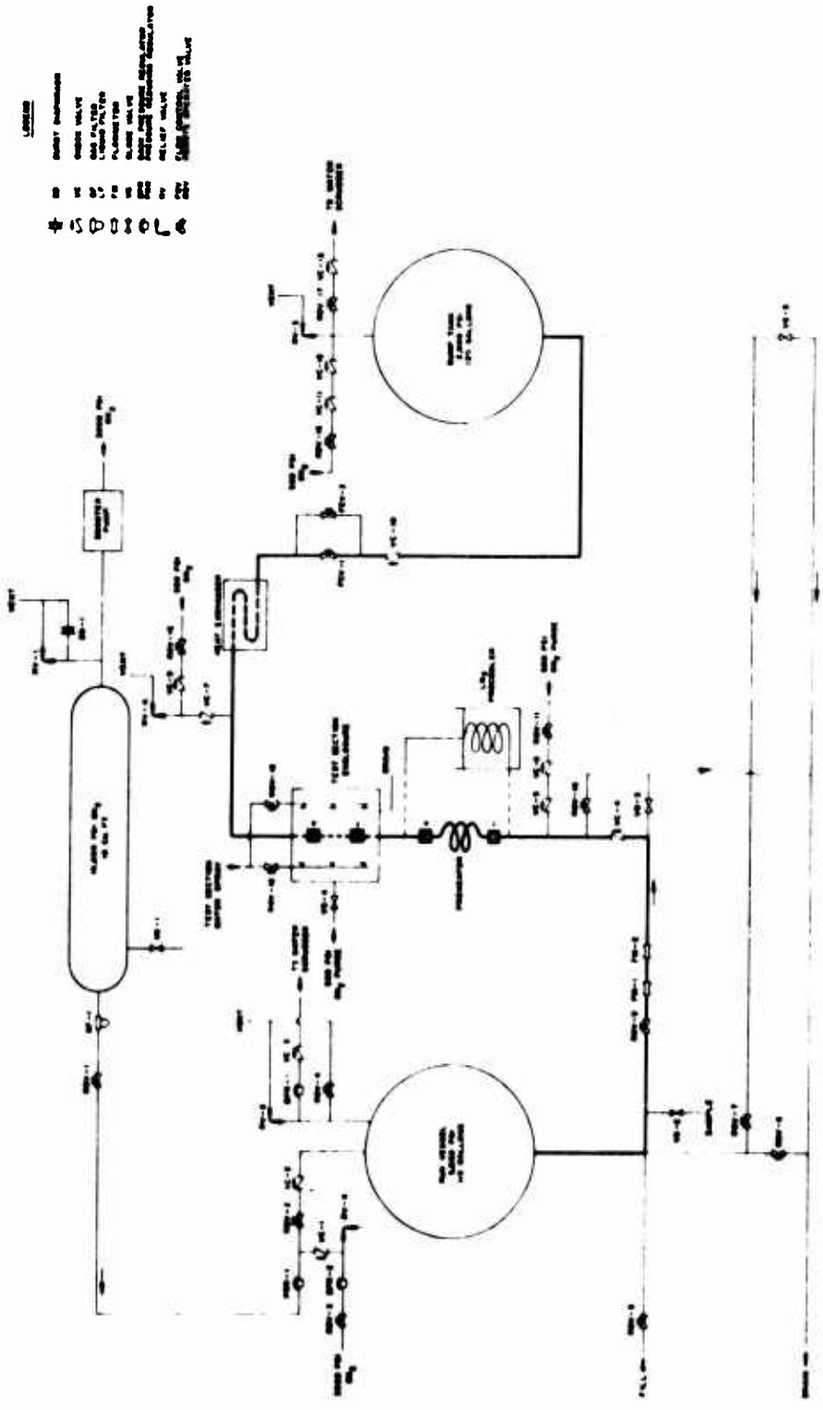

Schematic Diagram of the High Pressure Heat Transfer Loop

Figure 1

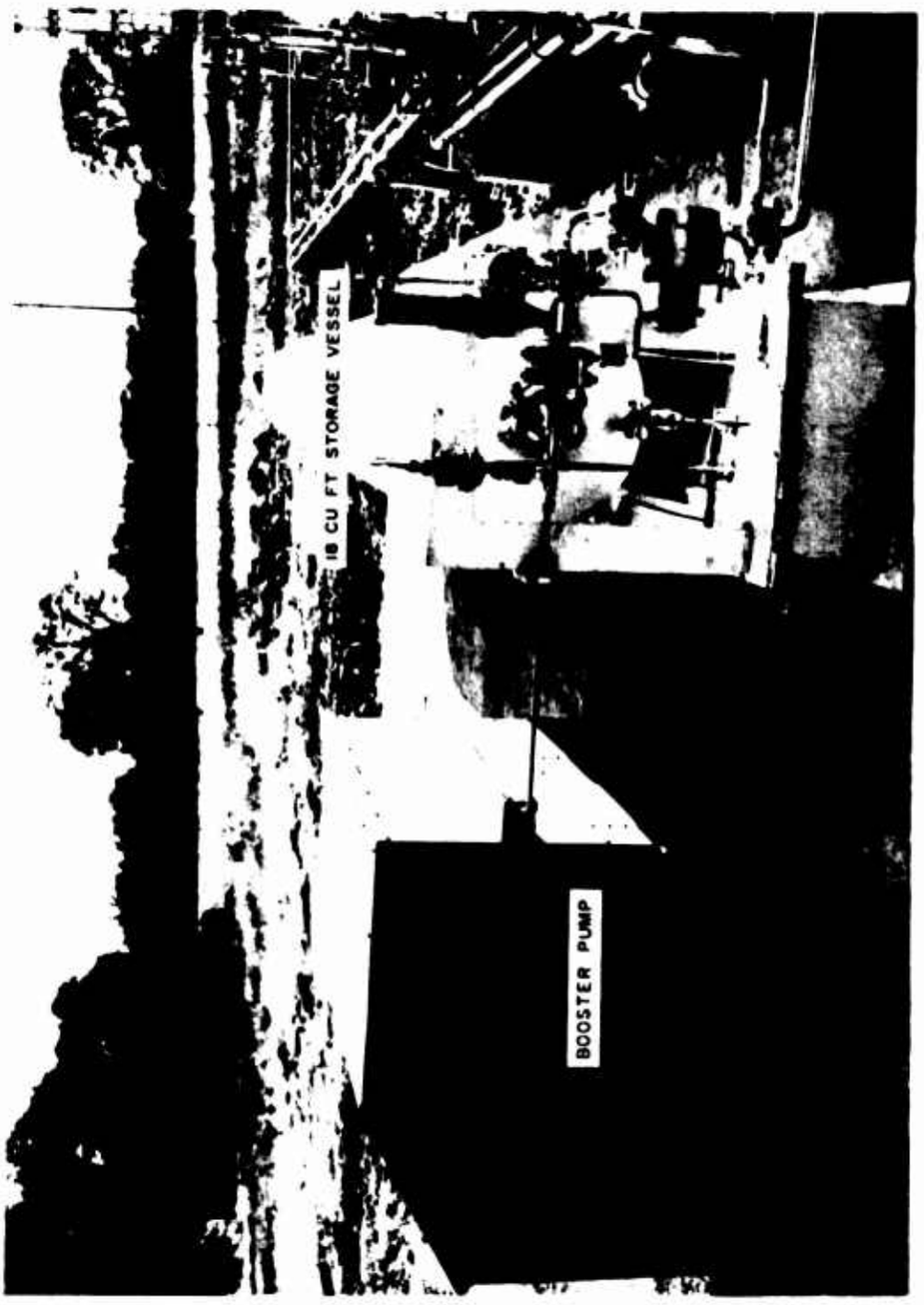
18 CU FT STORAGE VESSEL
BOOSTER PUMP

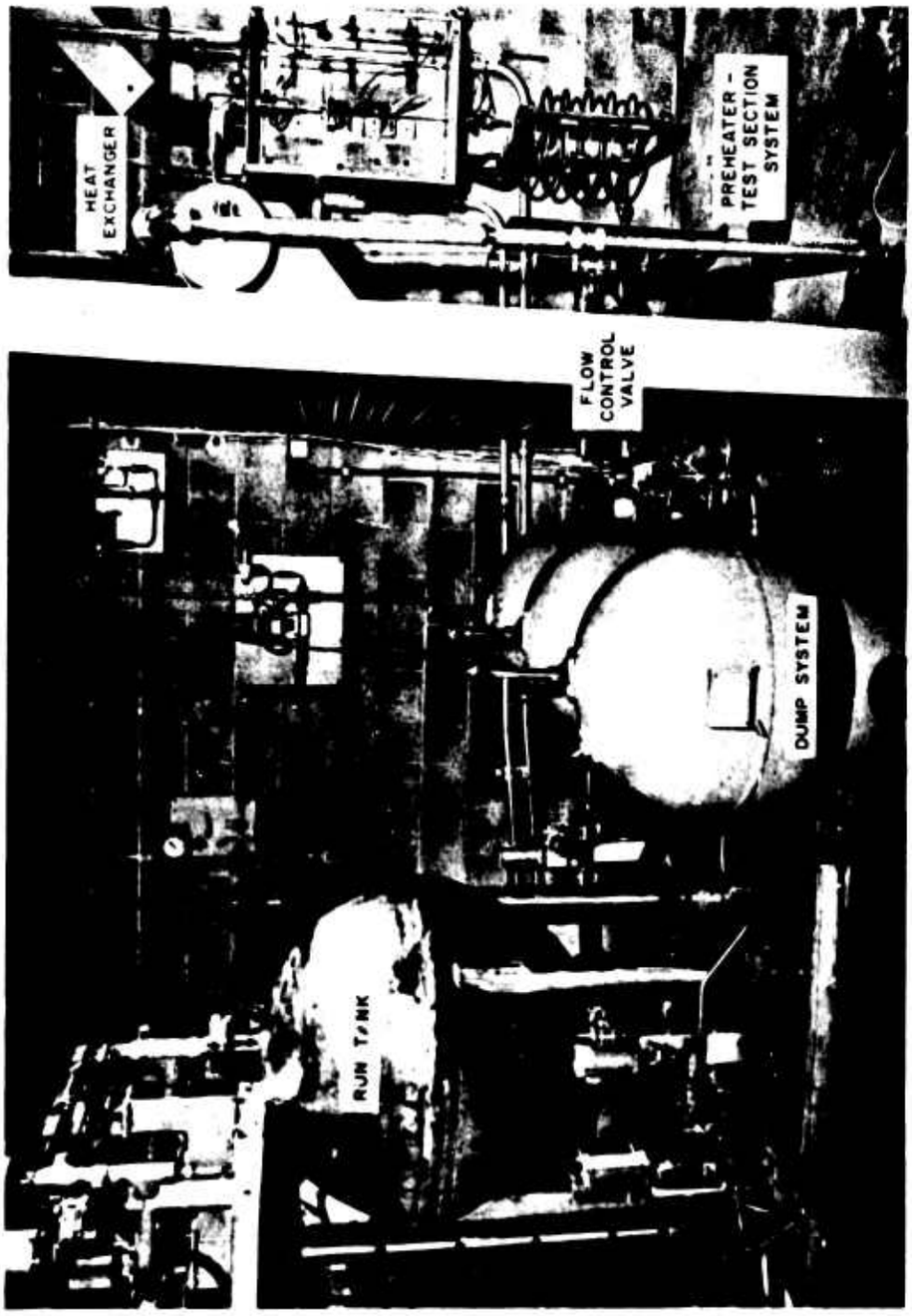
HEAT EXCHANGER
PREHEATER - TEST SECTION SYSTEM
FLOW CONTROL VALVE
DUMP SYSTEM
RUN TANK

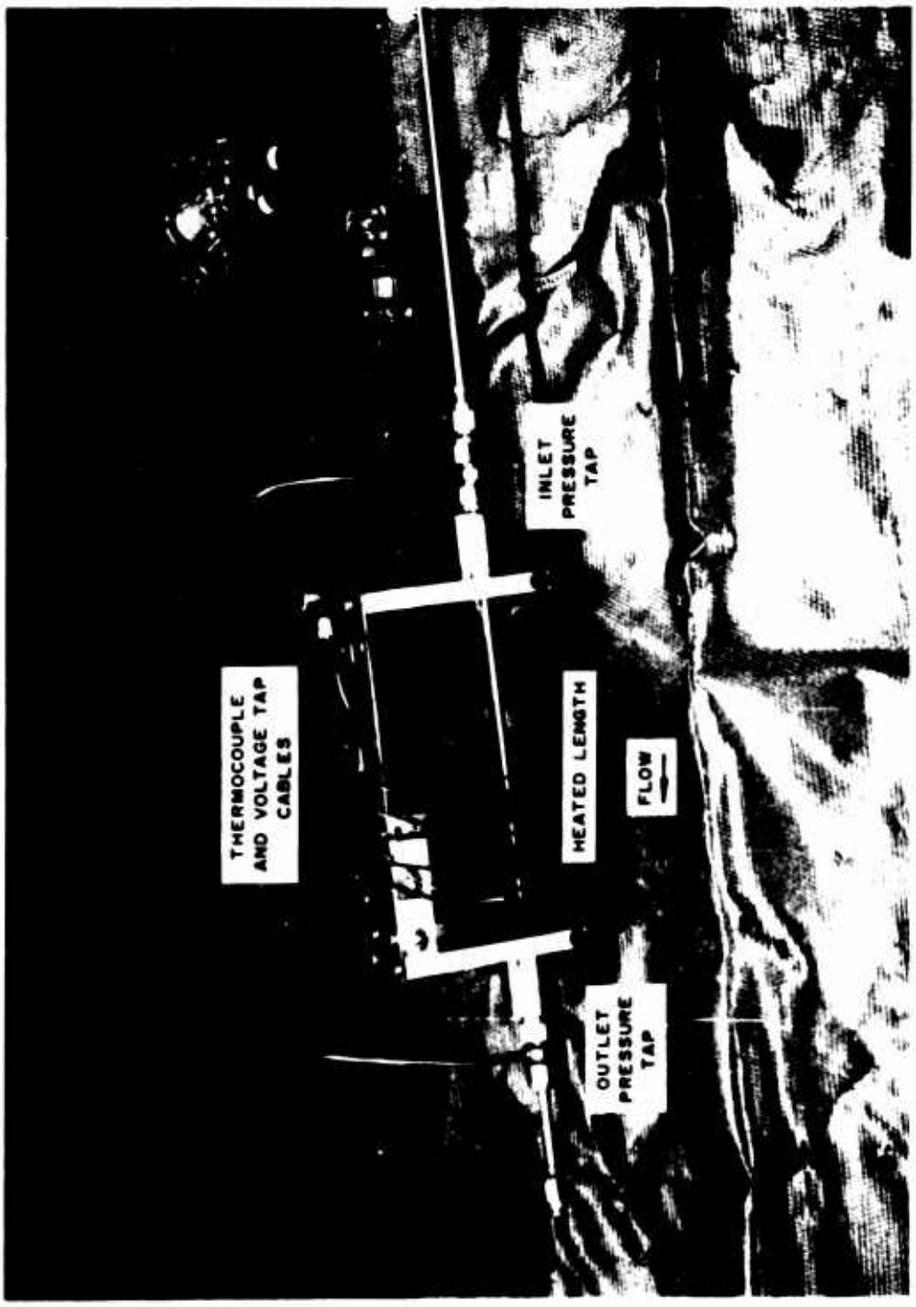

Typical Test Section Assembly

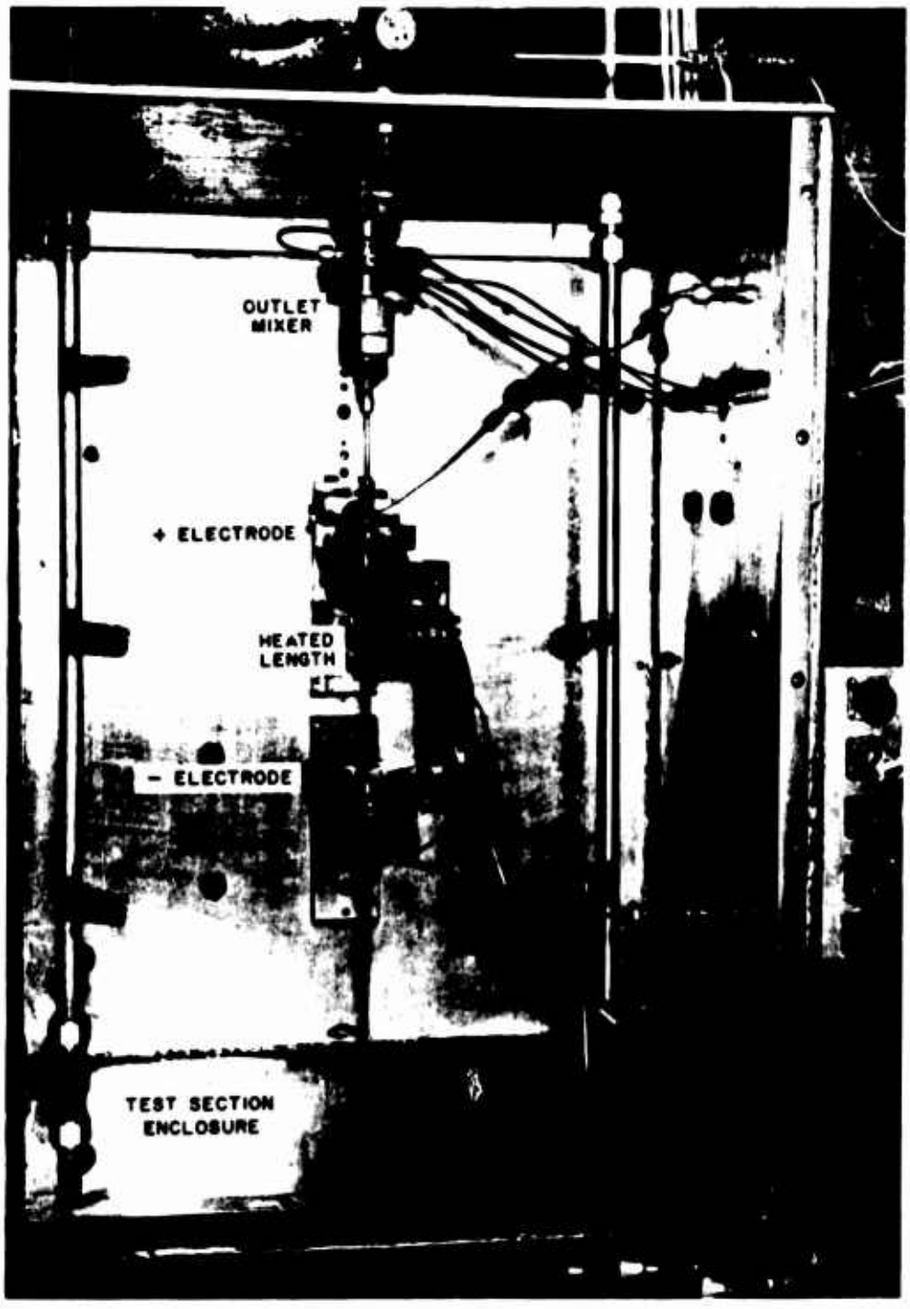
OUTLET
MIXER
+ ELECTRODE
HEATED
LENGTH
- ELECTRODE
TEST SECTION
ENCLOSURE

[illegible]

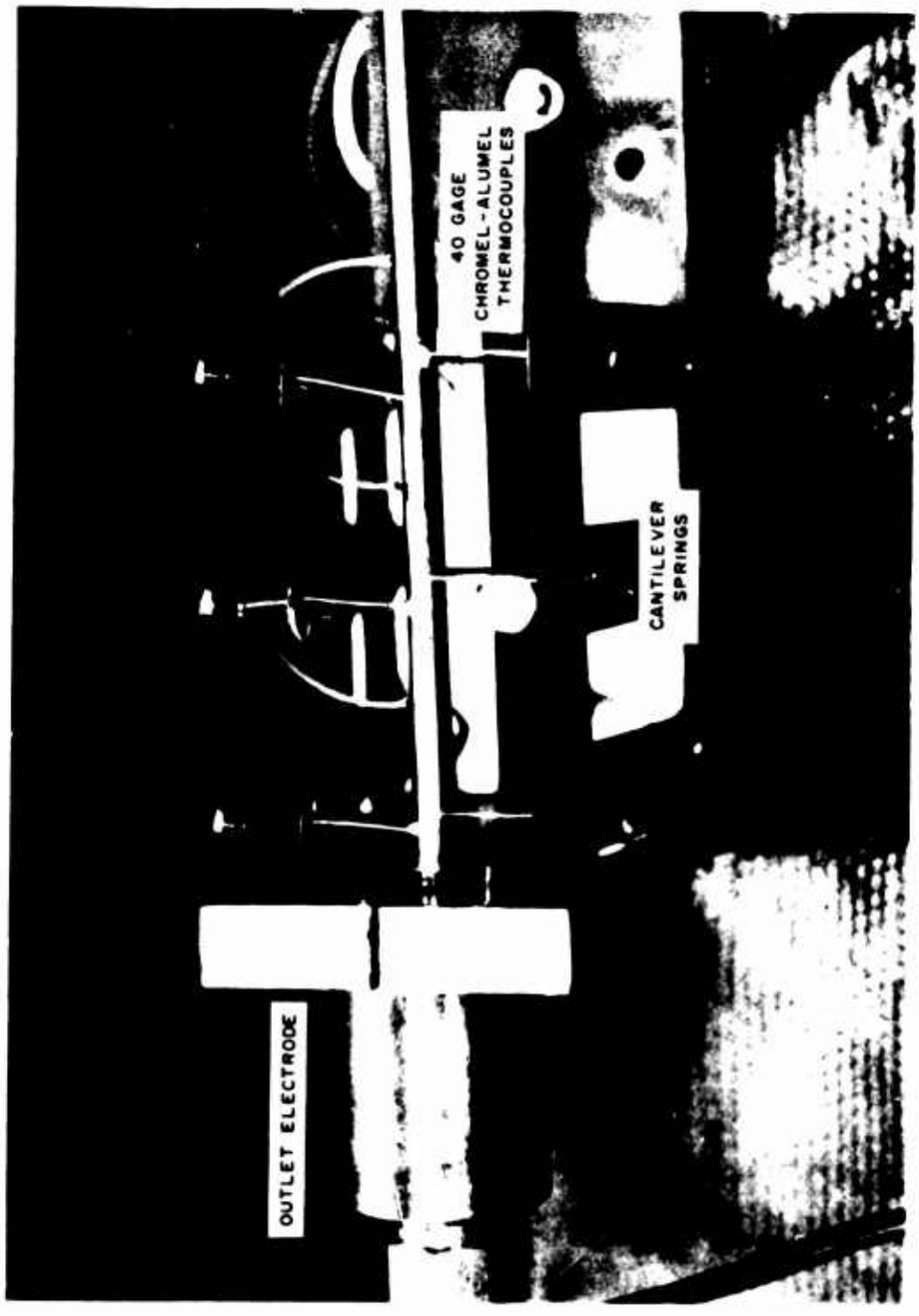

Tube Wall Thermocouple Installation

Figure [illegible]

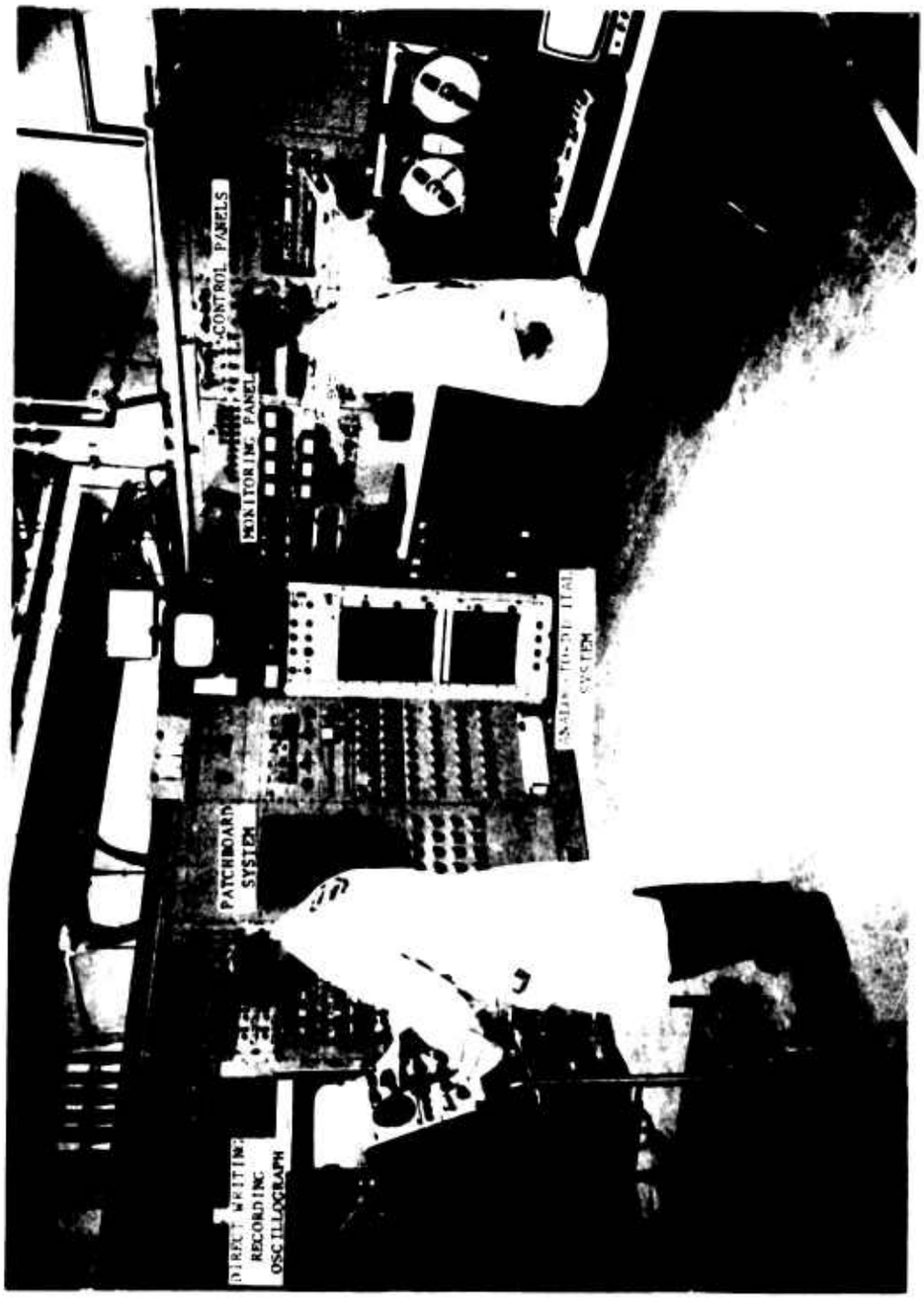

Laboratory Control Room

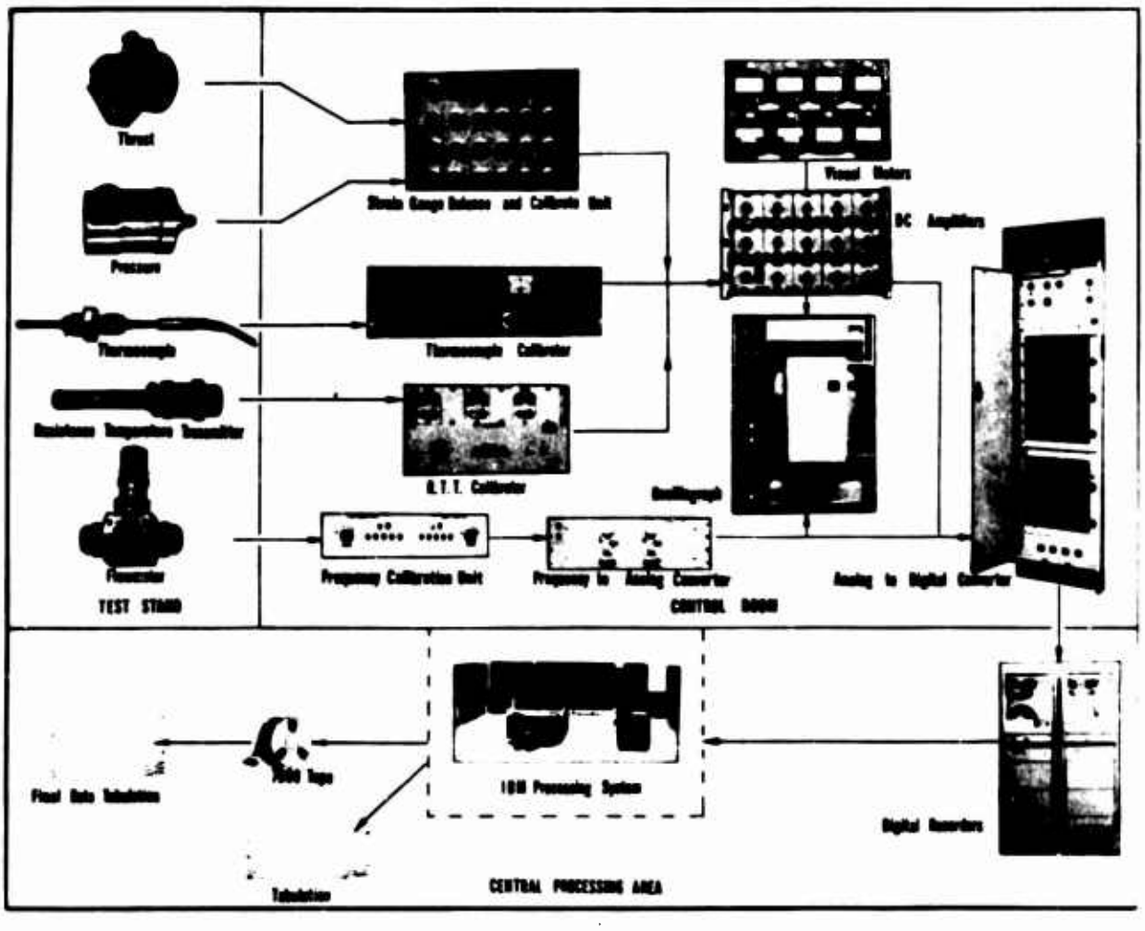

Instrumentation/Data Acquisition Block Diagram

Figure 3

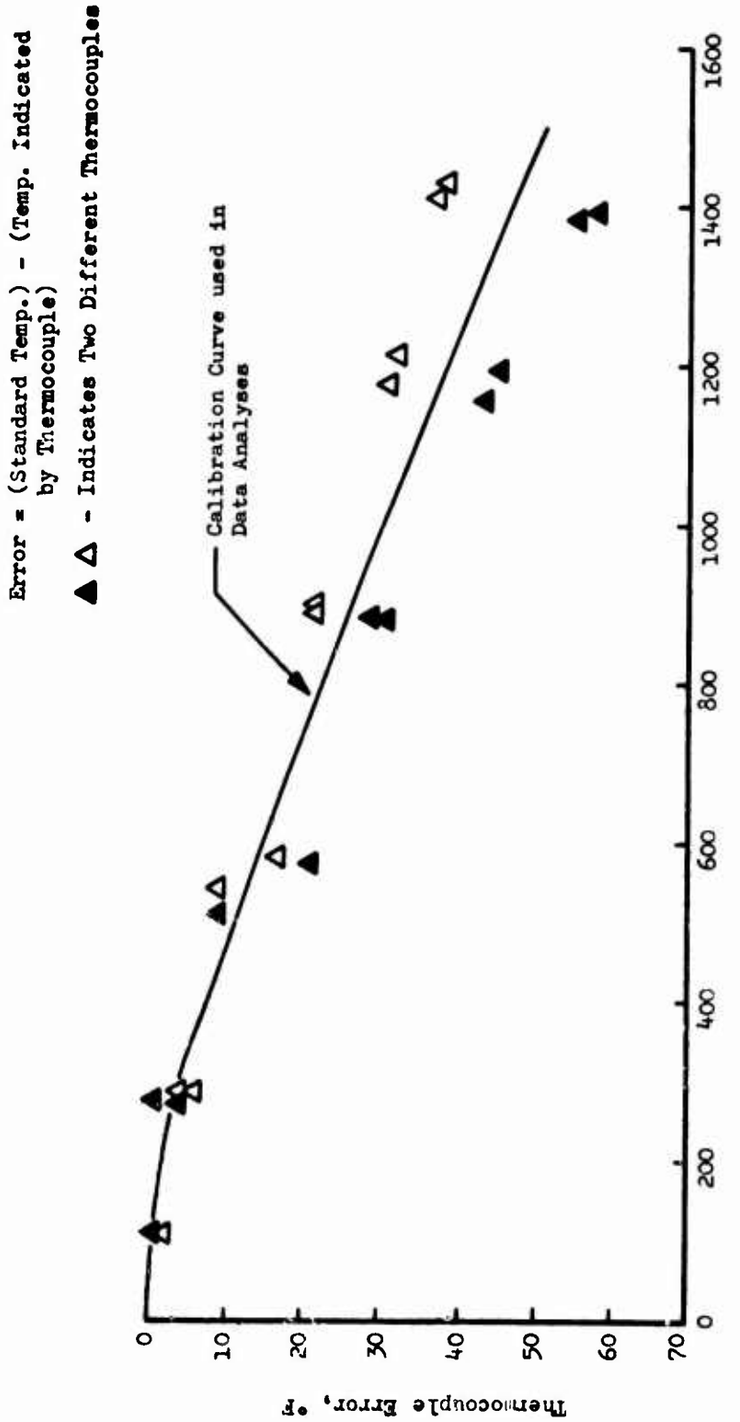

Wall Temperature Thermocouple Calibration

Figure 9

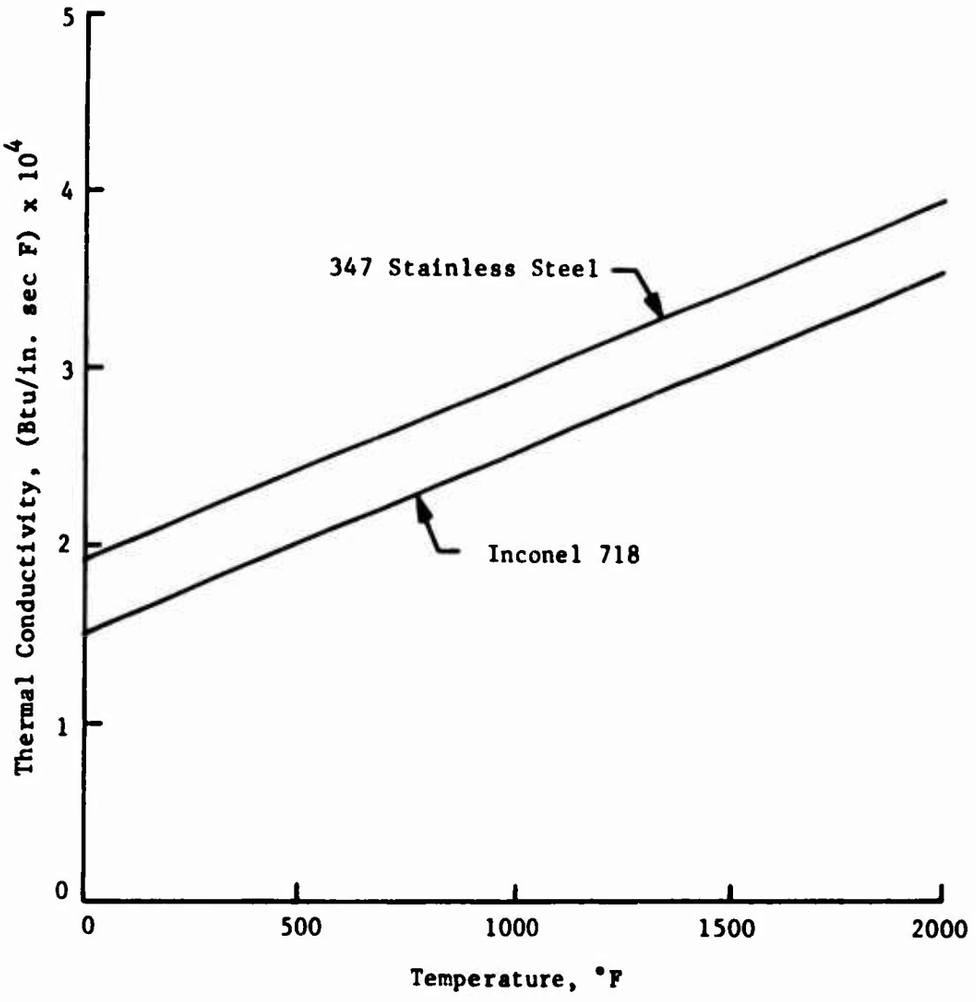

Thermal Conductivity of Stainless Steel and Inconel 718

Figure 10

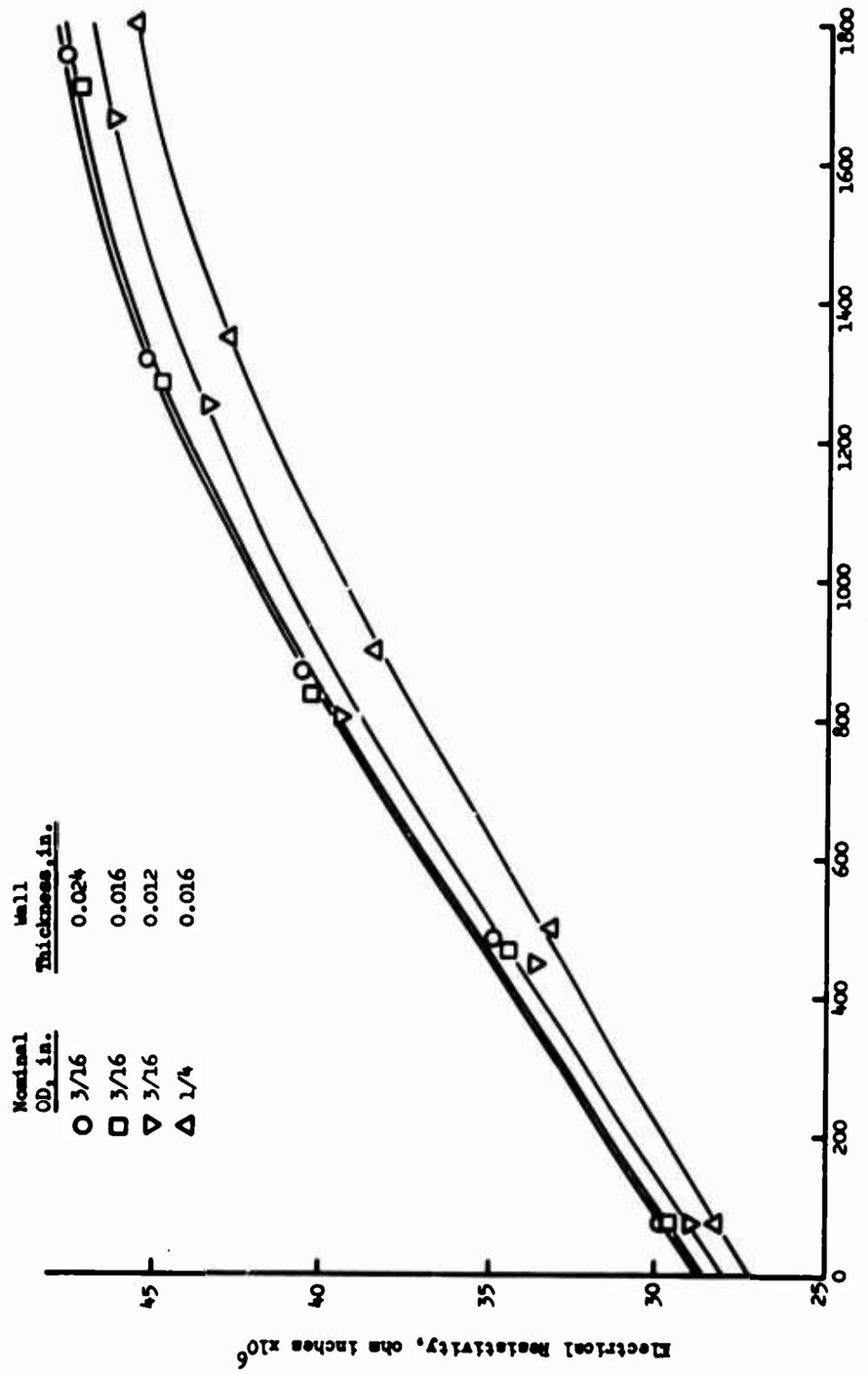

Electrical Resistivity of 347 Stainless Steel

Figure 11

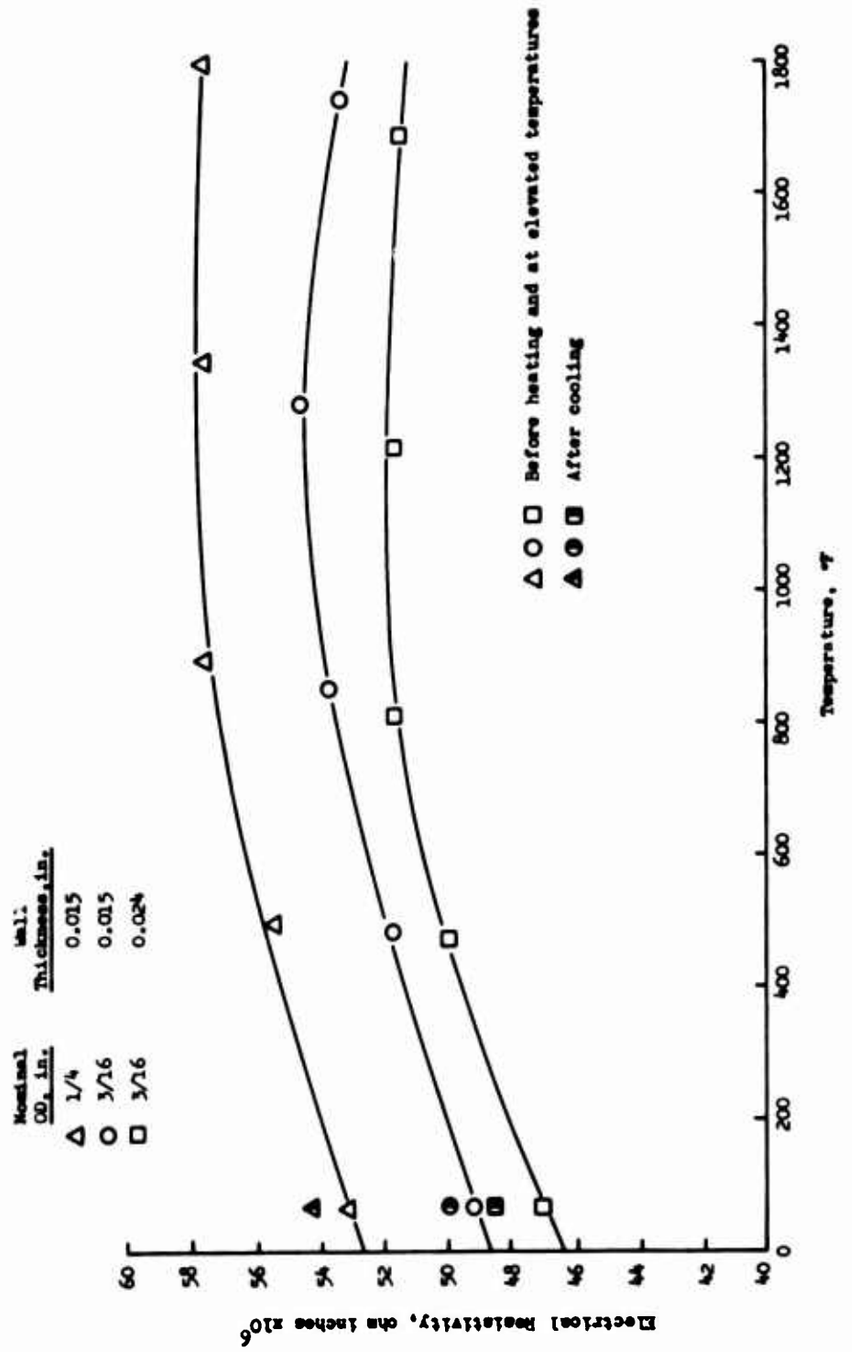

Electrical Resistivity of Inconel 718

Figure 12

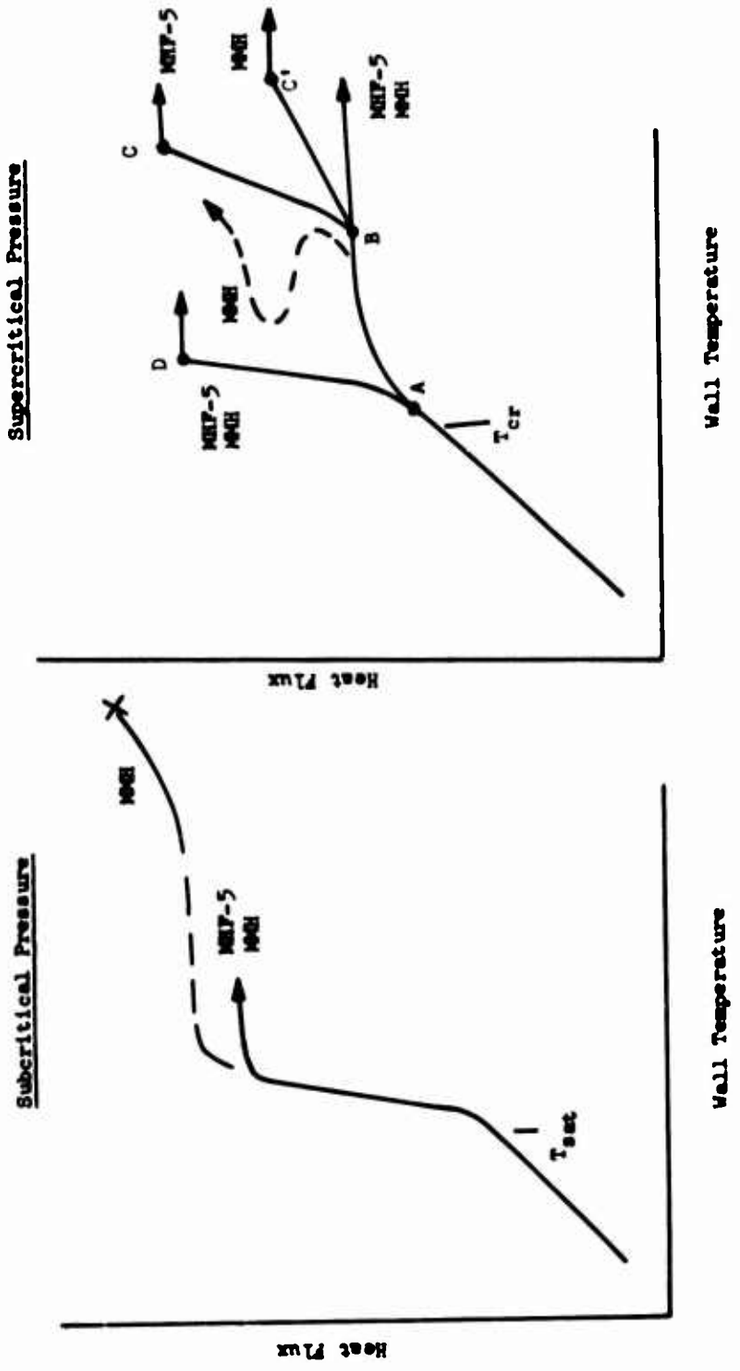

General Heat Transfer Characteristics of MHF-5 and MMH

Figure 13

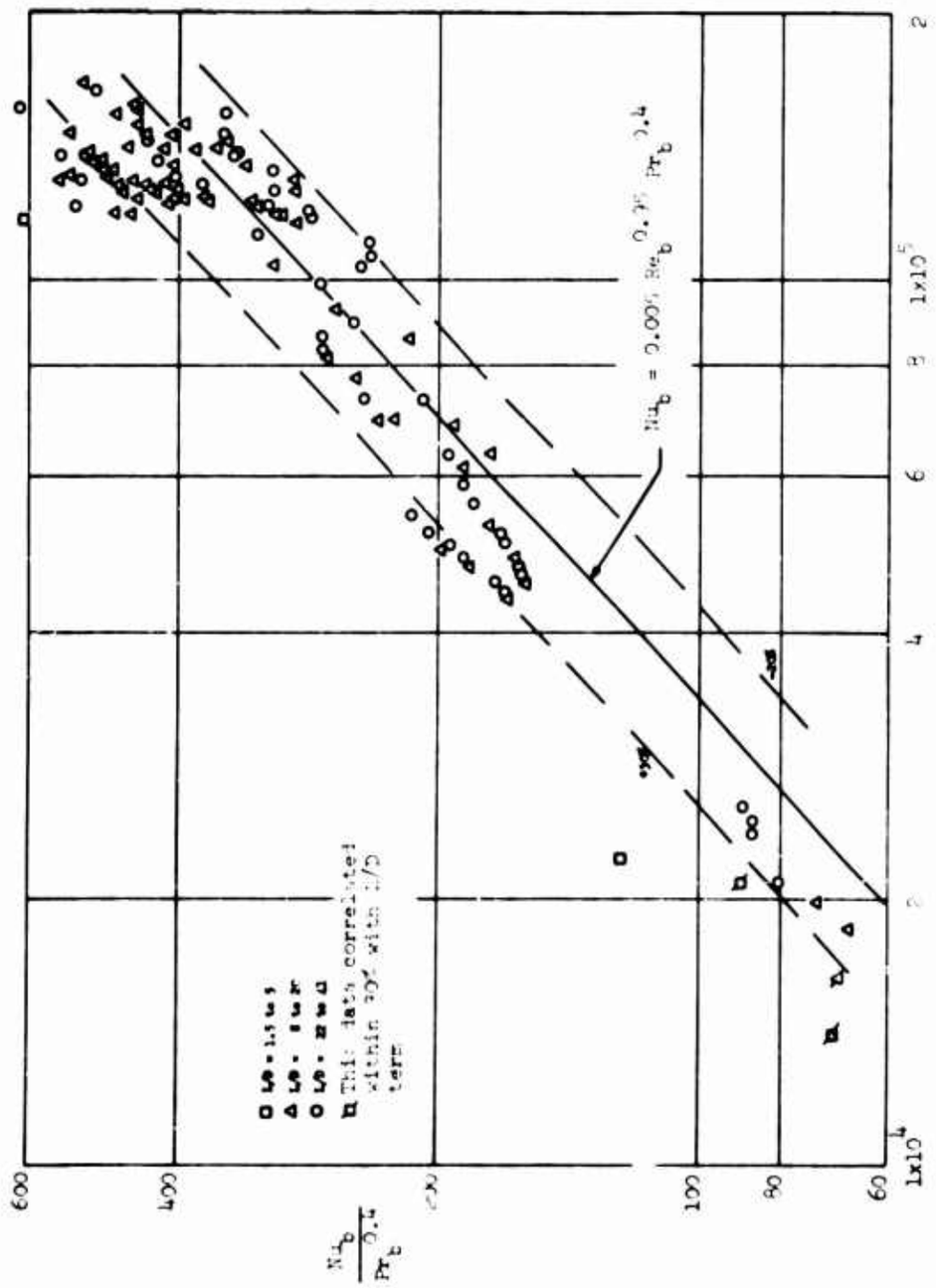

Subcritical MHF-5 Forced Convection Data

Figure 14

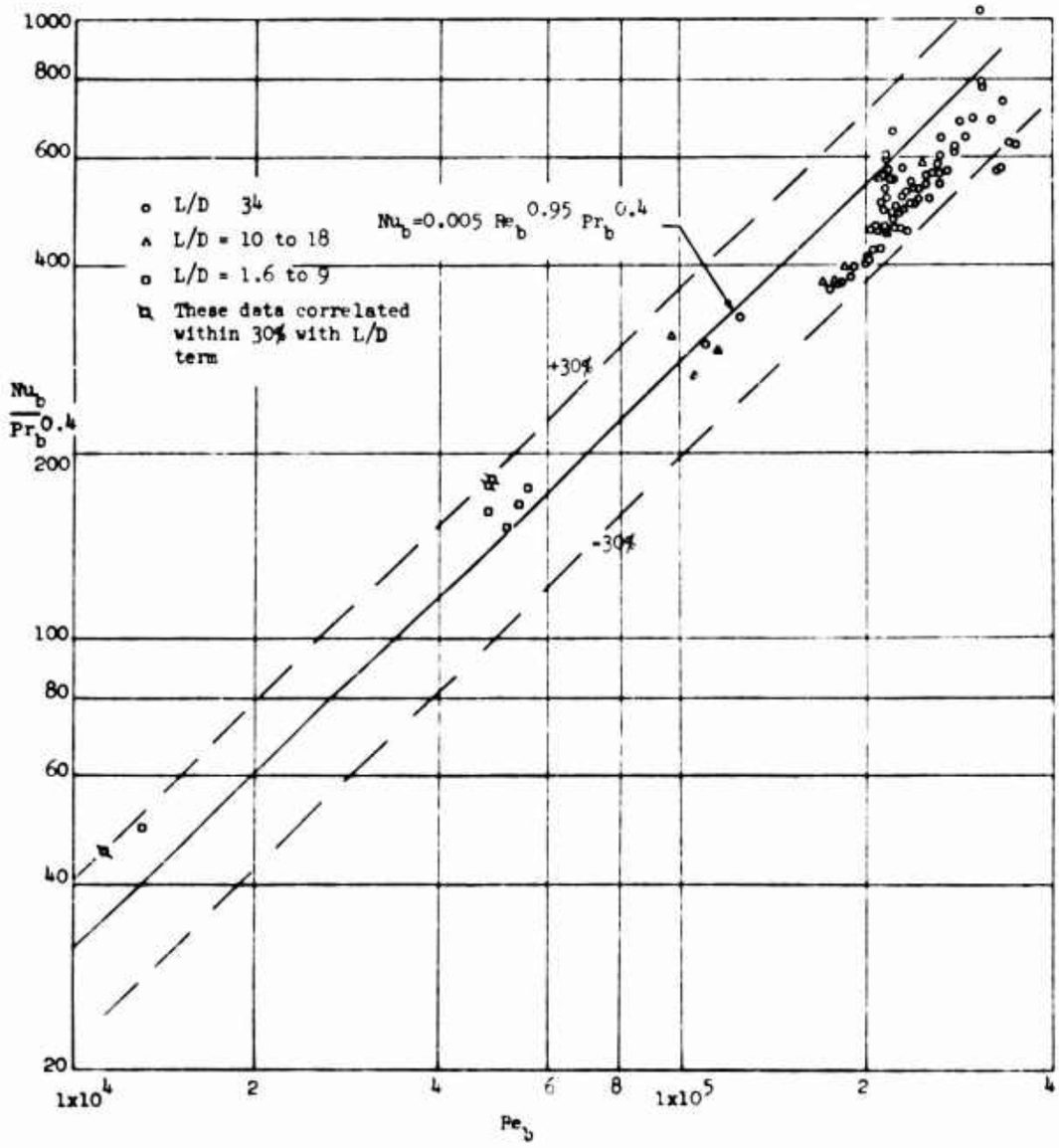

Subcritical MMH Forced Convection Data

Figure 15

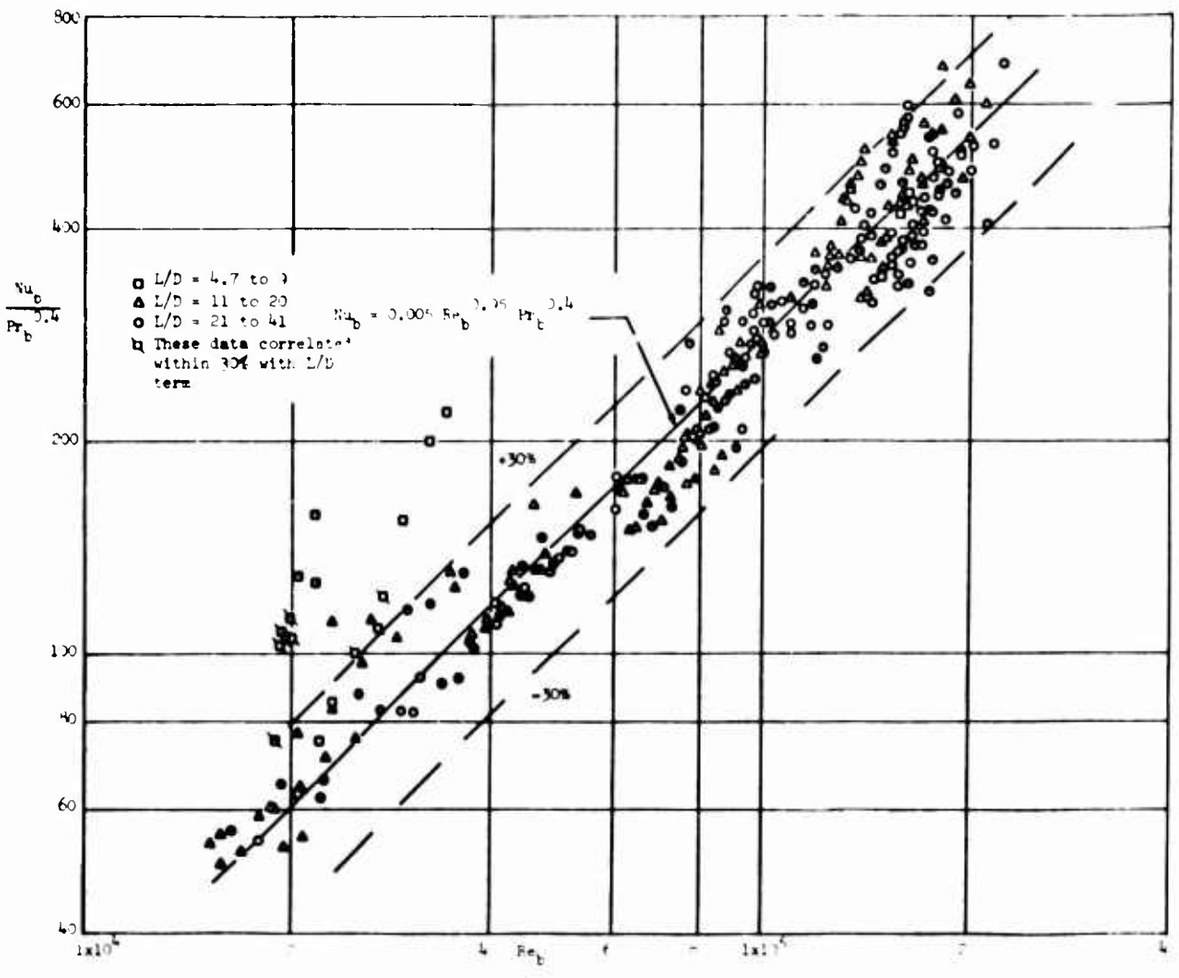

Supercritical MHF-5 Forced Convection Data

Figure 16

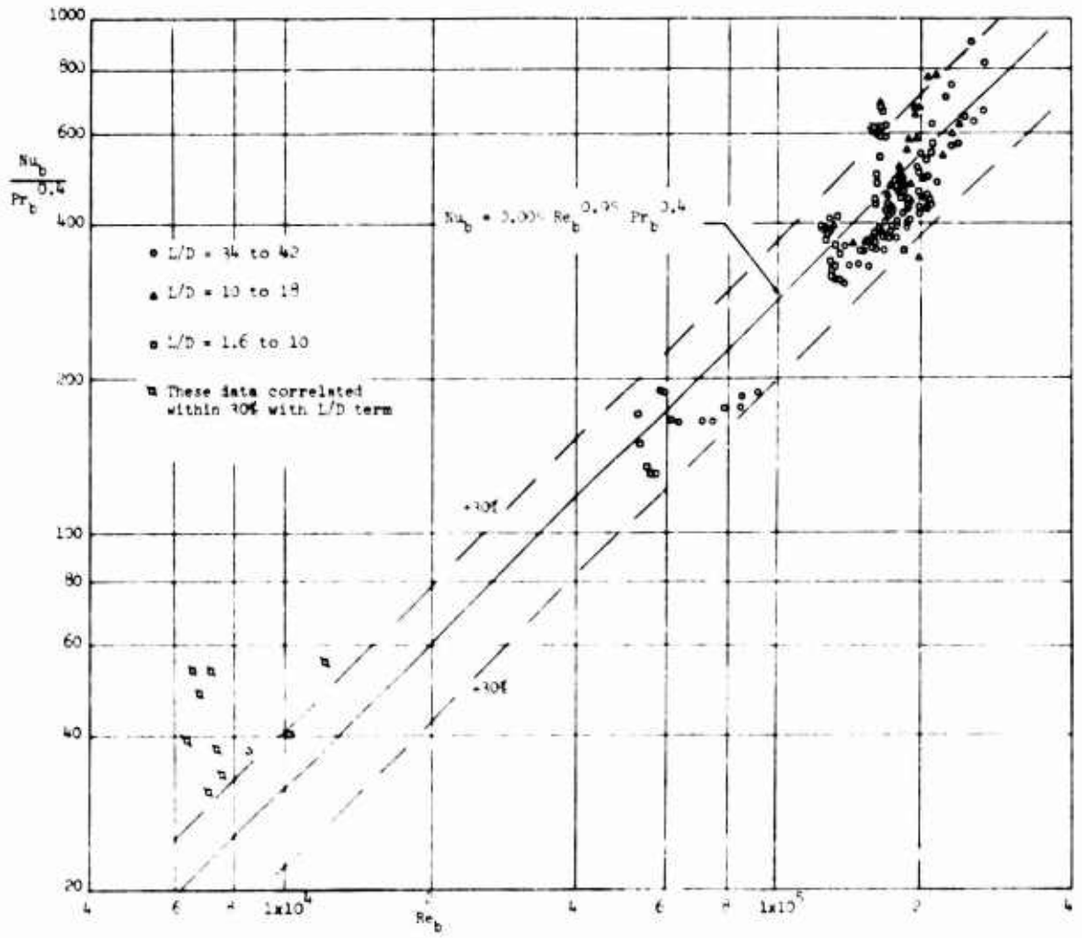

Supercritical MMH Forced Convection Data

Figure 17

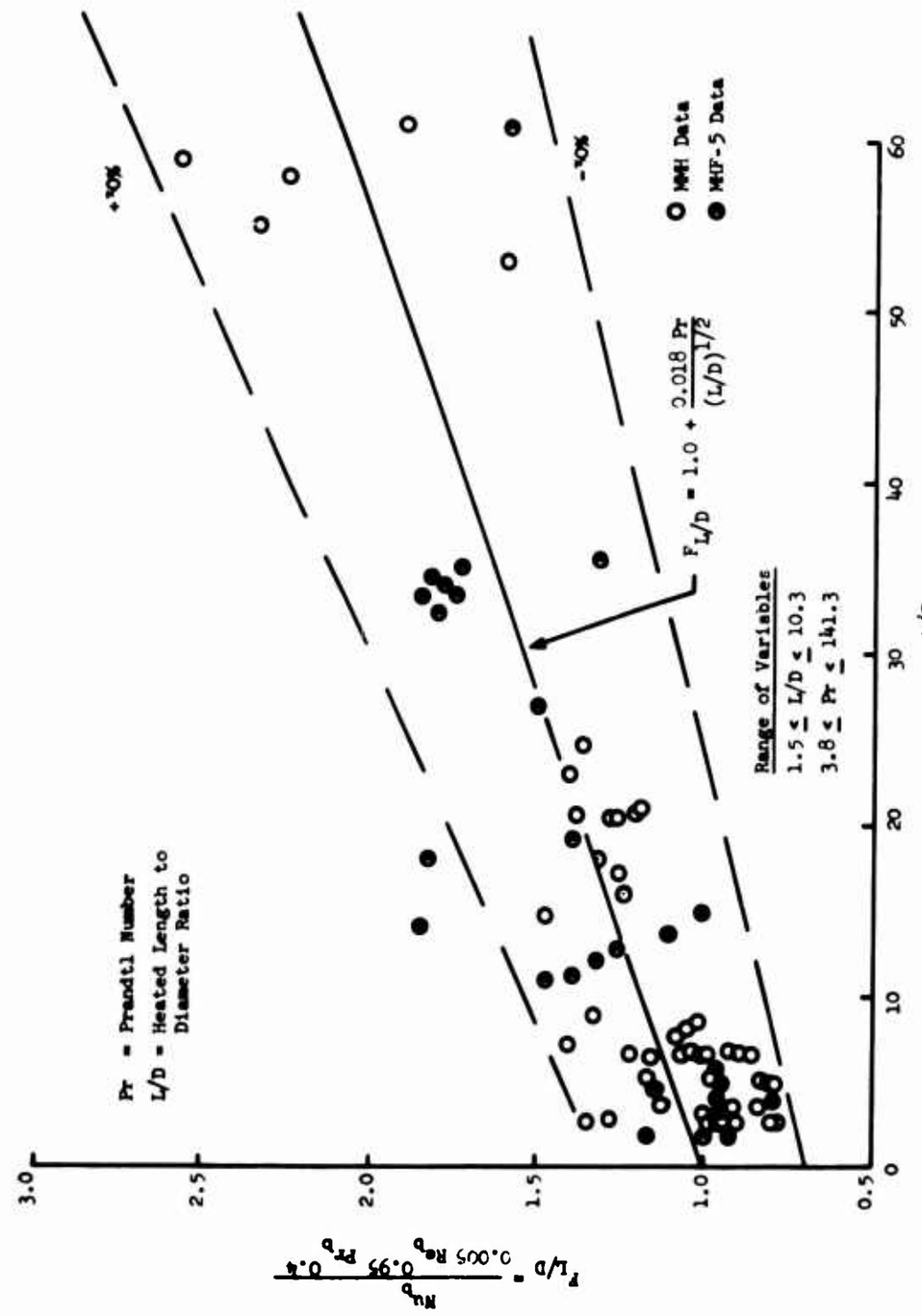

Correlation of L/D Effects

Figure 18

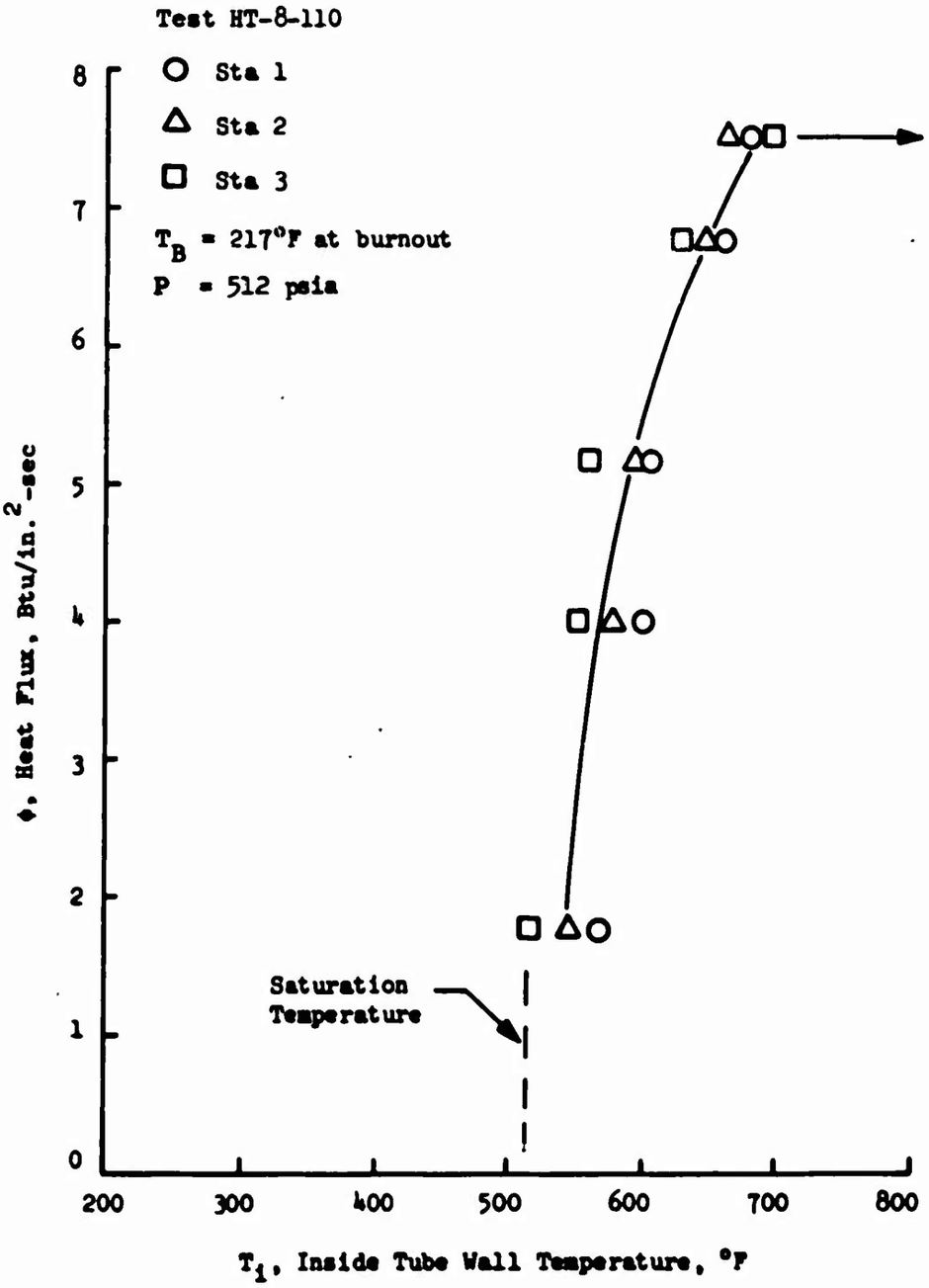

Subcritical MHF-5 Heat Transfer at 20 ft/sec Velocity

Figure 19

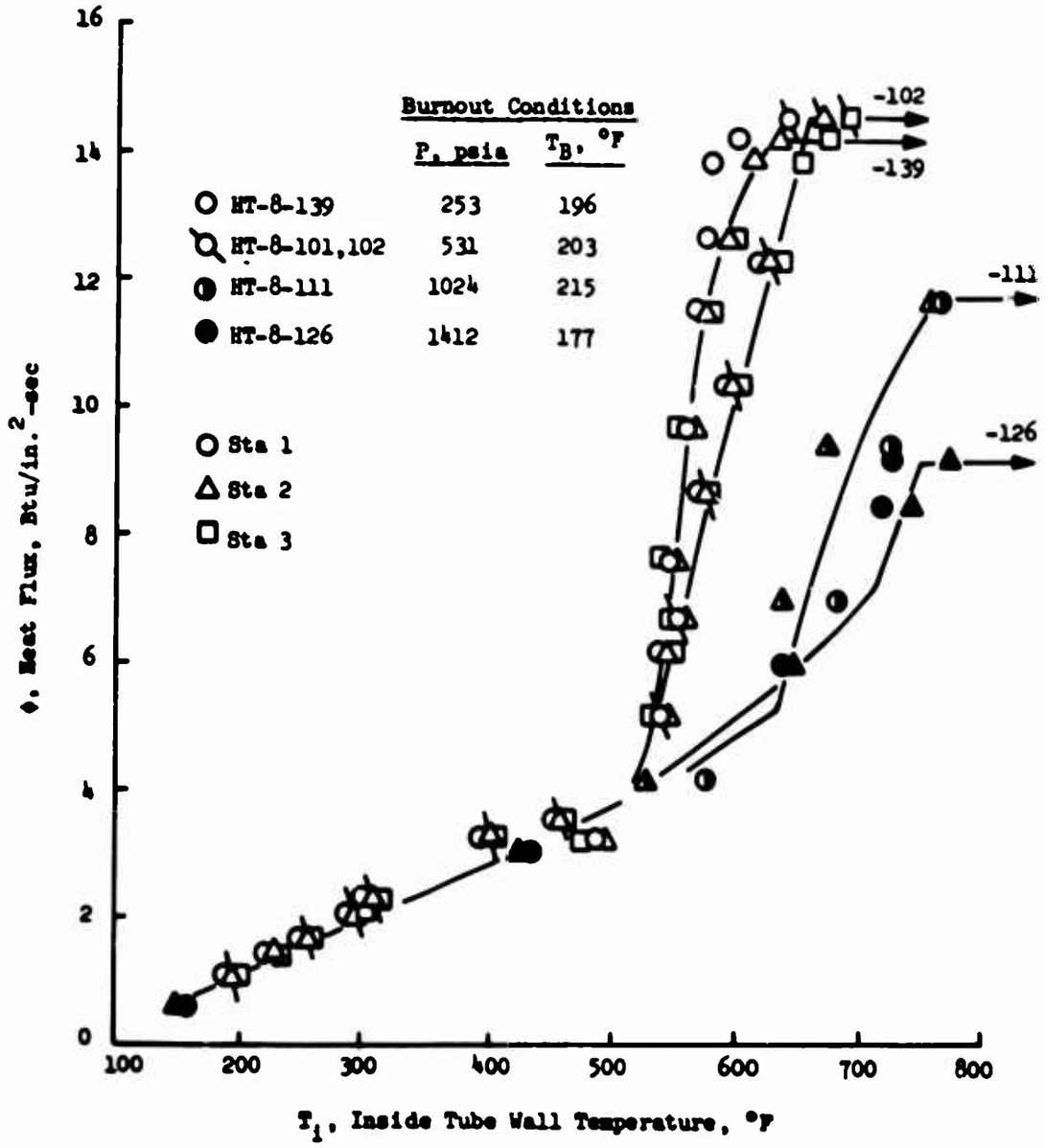

Subcritical MHF-5 Heat Transfer at 50 ft/sec Velocity and 250 to 140 psia Pressure

Figure 20

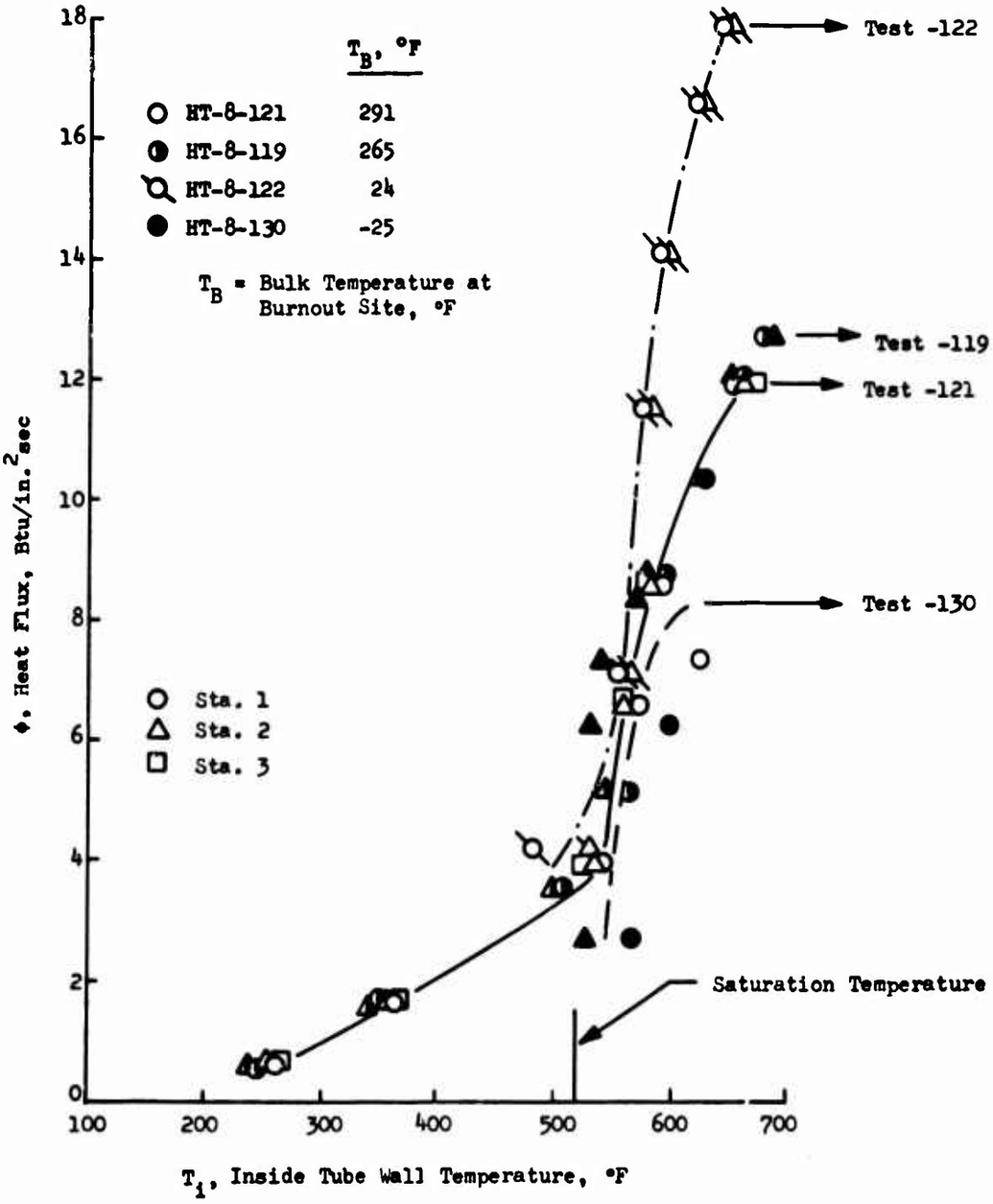

Subcritical MHF-5 Heat Transfer at 50 ft/sec Velocity and 500 psia Pressure

Figure 21

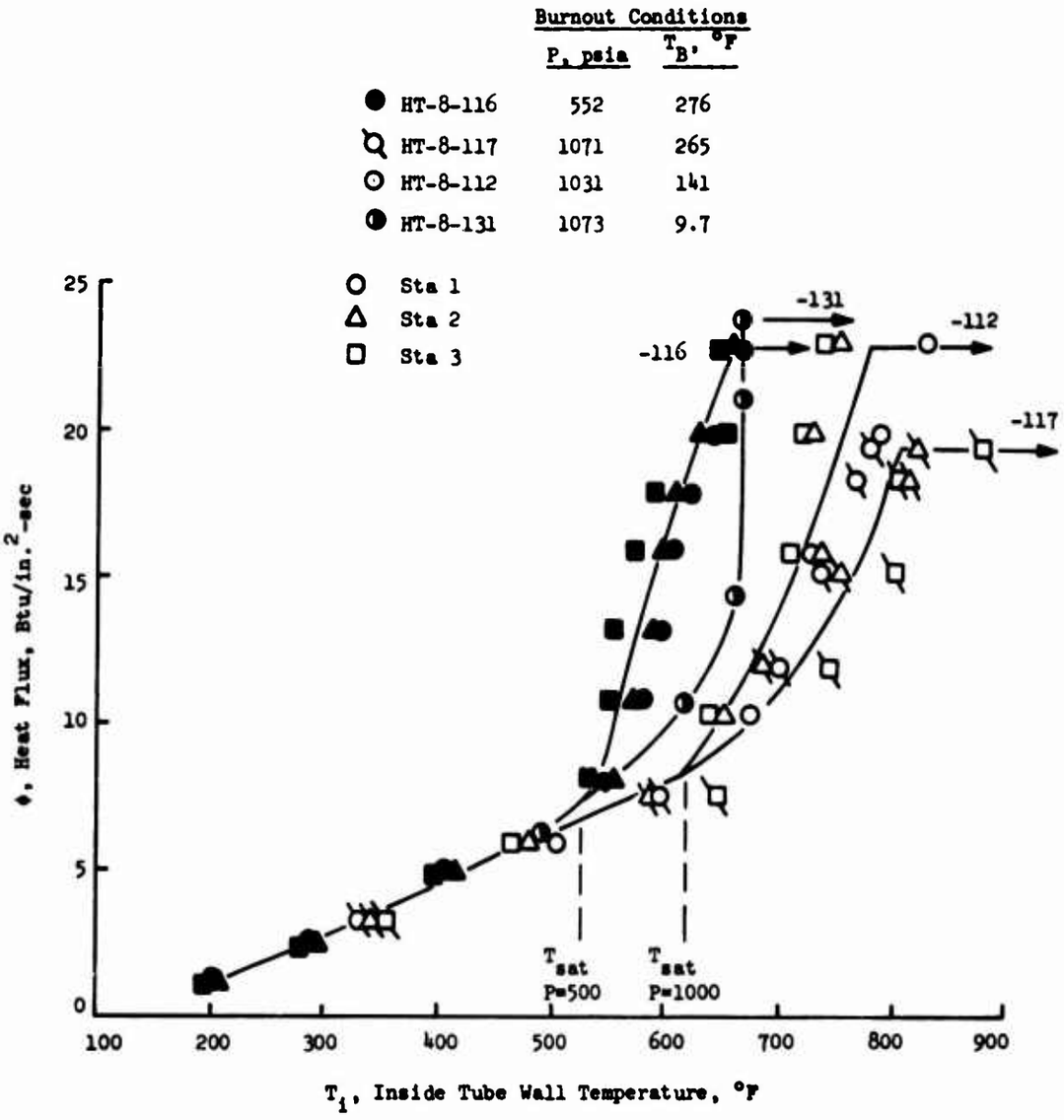

Subcritical MHF-5 Heat Transfer at 100 ft/sec Velocity

Figure 22

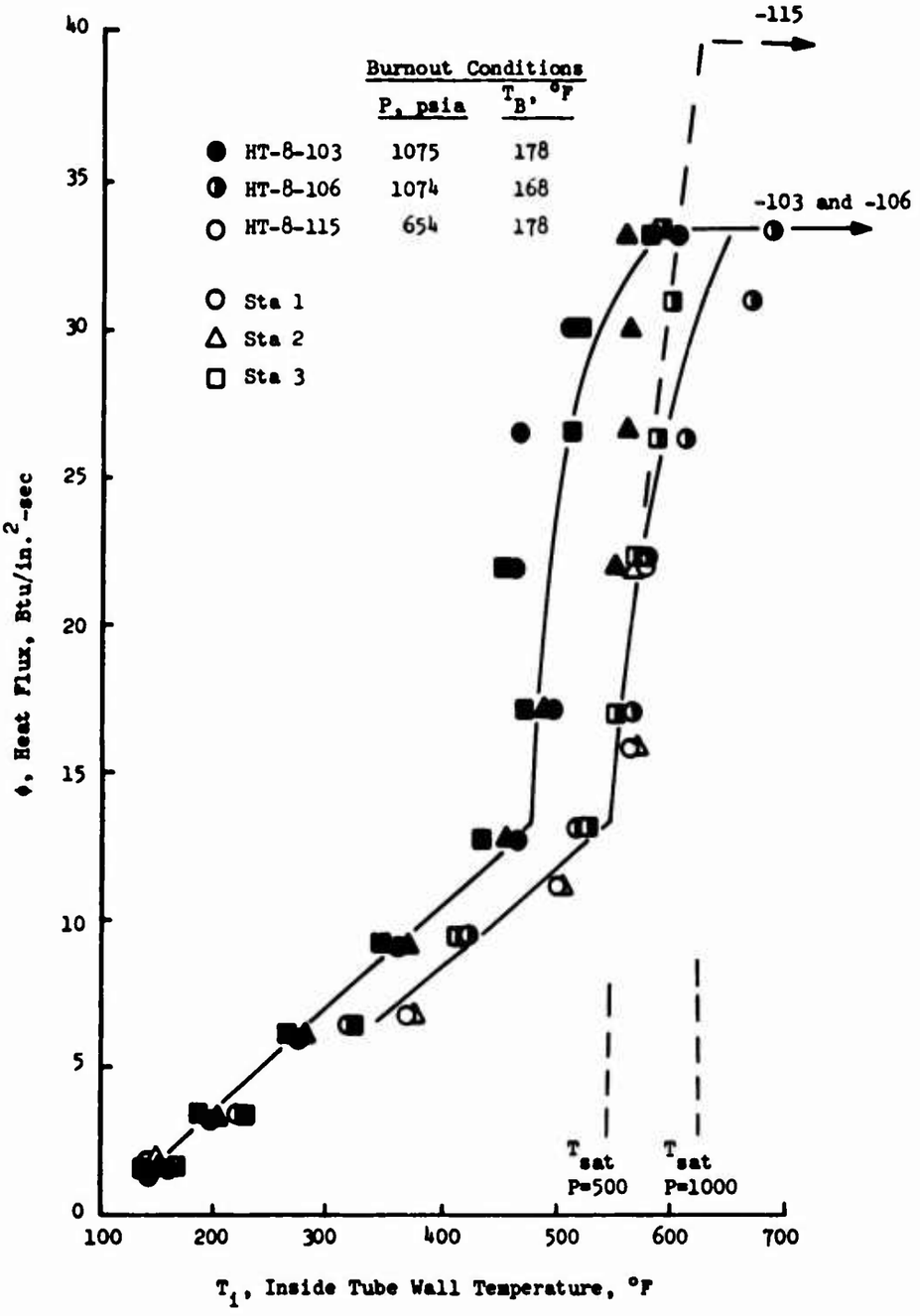

Subcritical MHF-5 Heat Transfer at 150 ft/sec Velocity

Figure 23

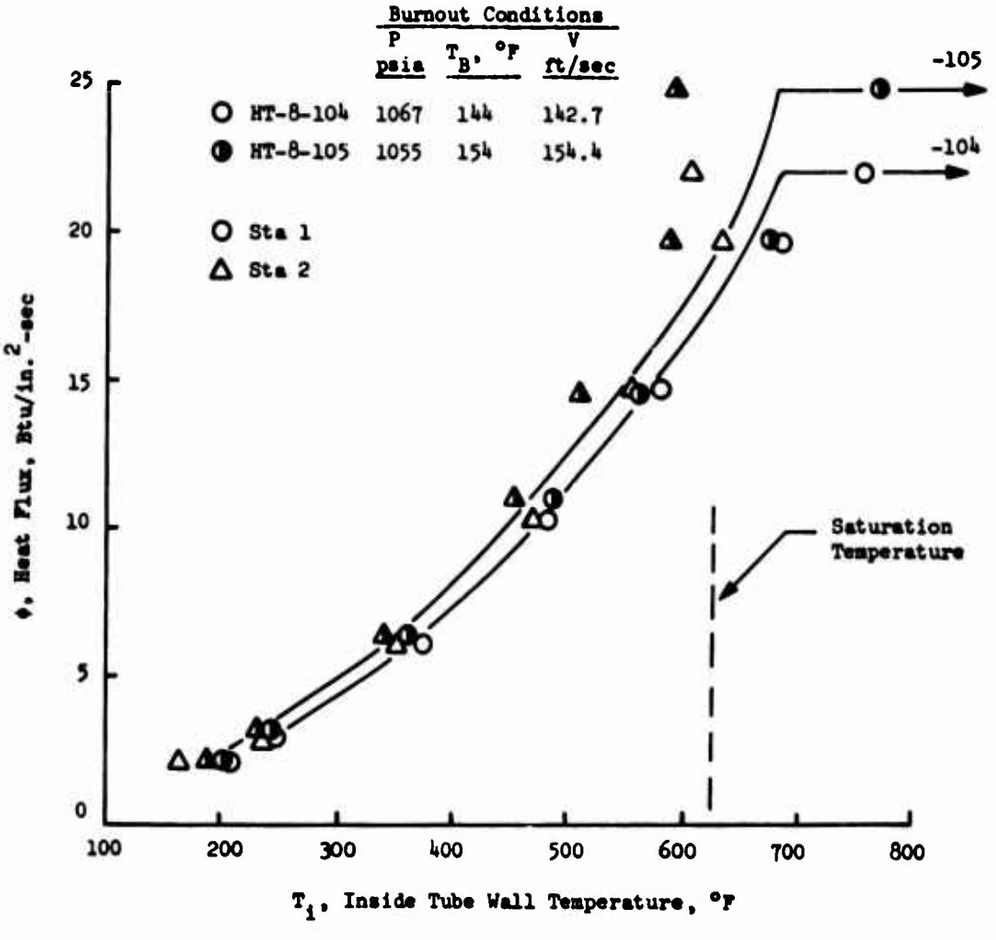

Subcritical MHF-5 Heat Transfer at 150 ft/sec Velocity
in Inconel 718 Tubes

Figure 24

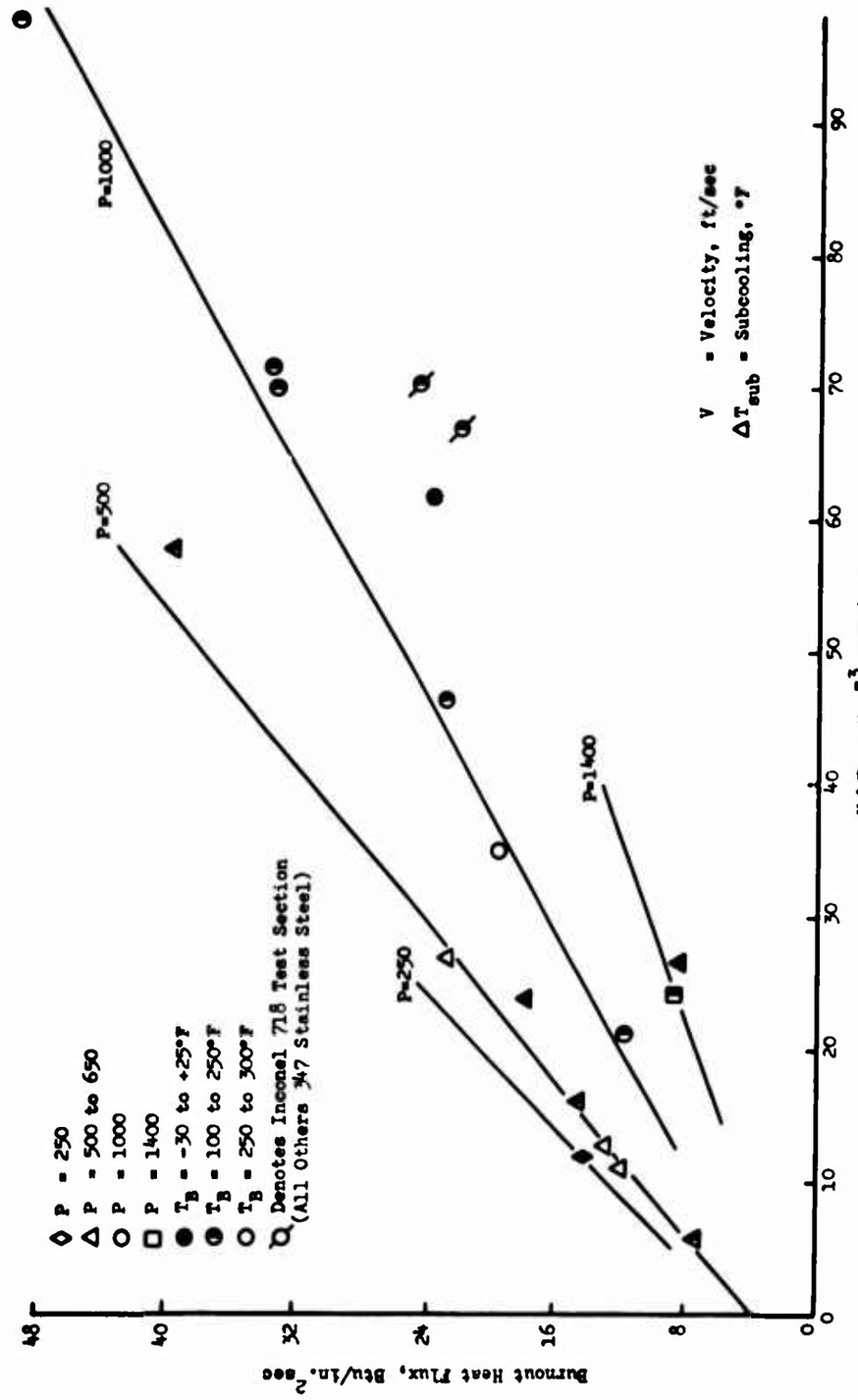

MHF-5 Burnout Heat Flux

Figure 25

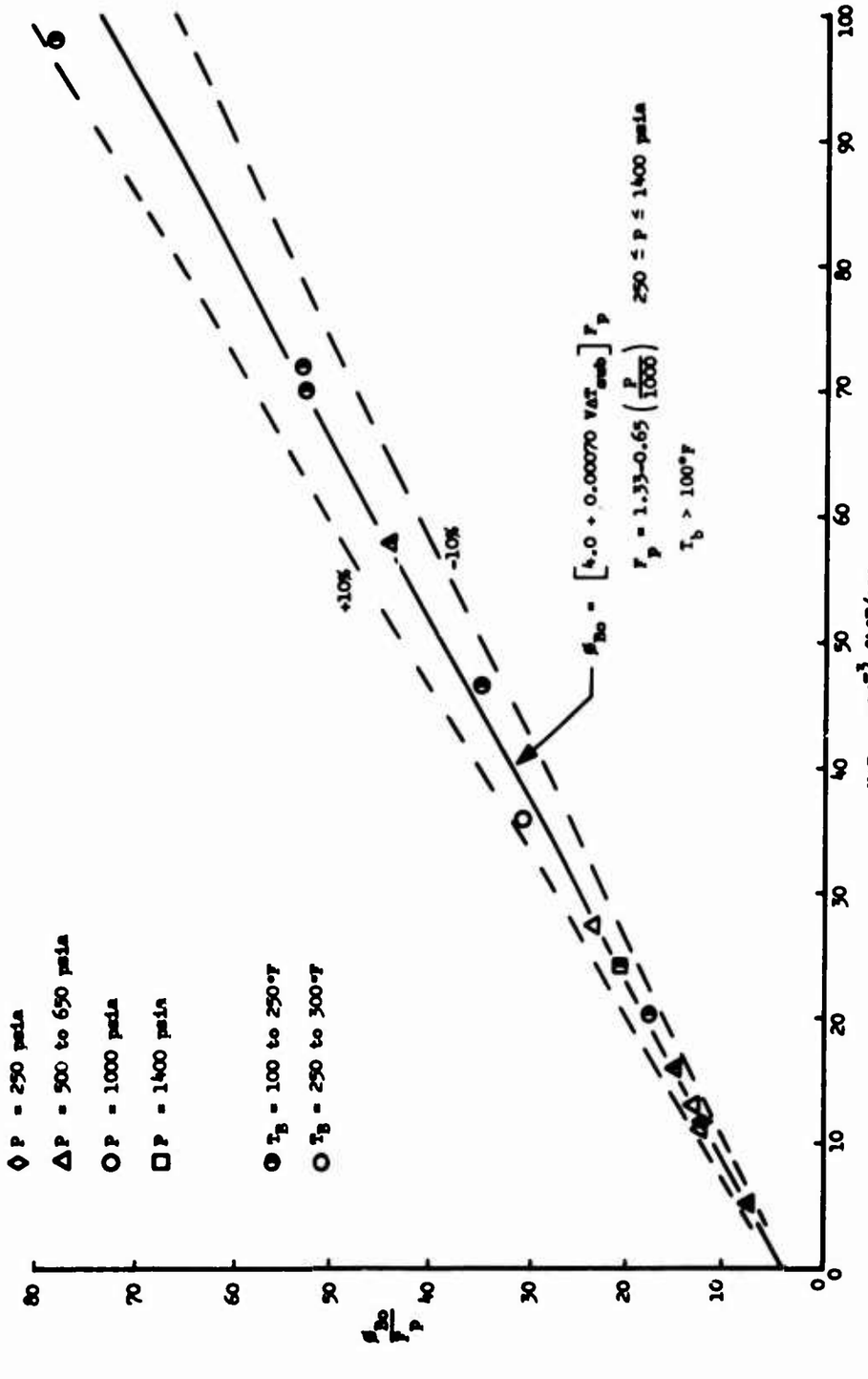

Effect of Bulk Temperature on MHF-5 Burnout Heat Flux

Figure 26

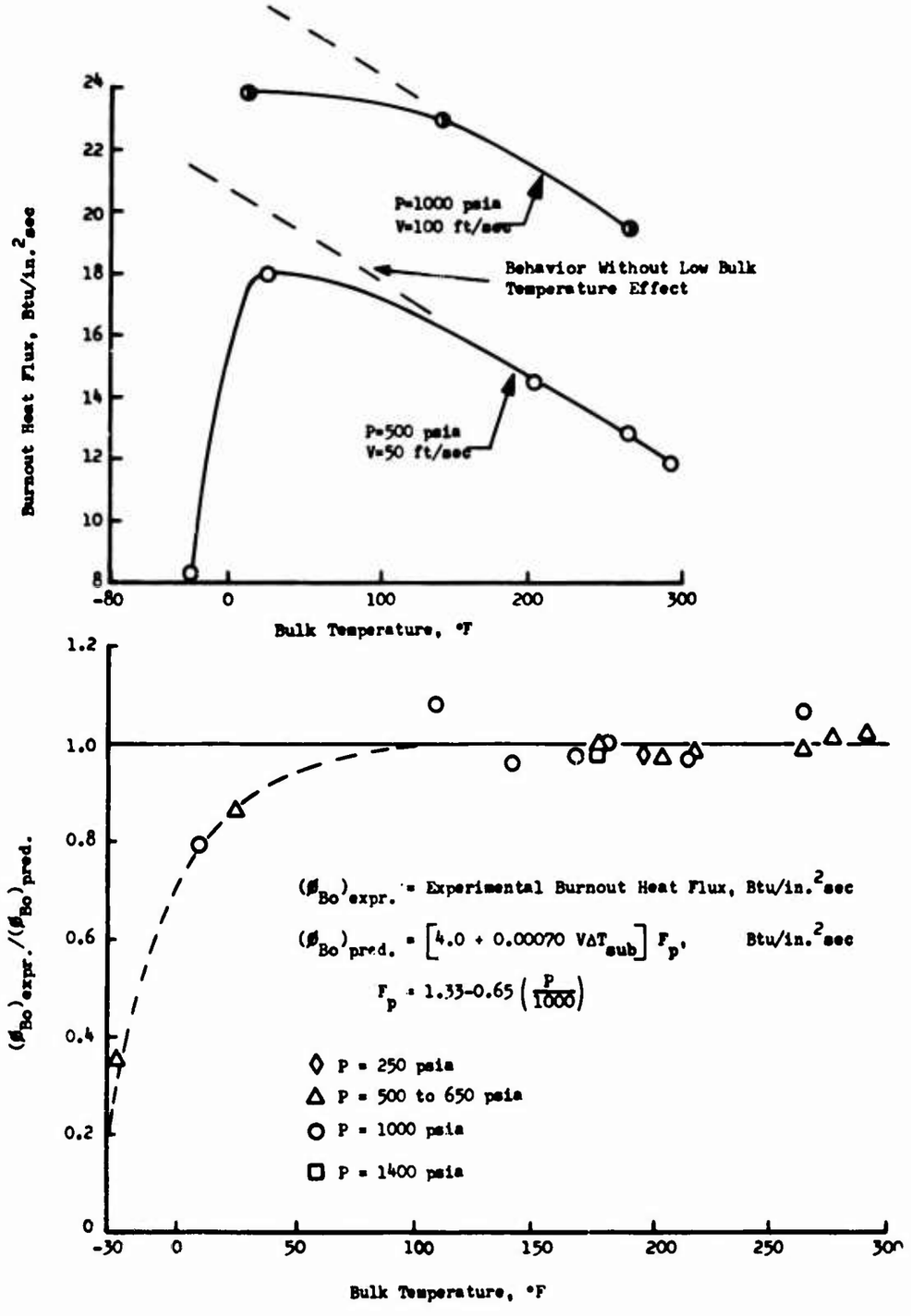

MHF-5 Burnout Heat Flux Correlation

Figure 27

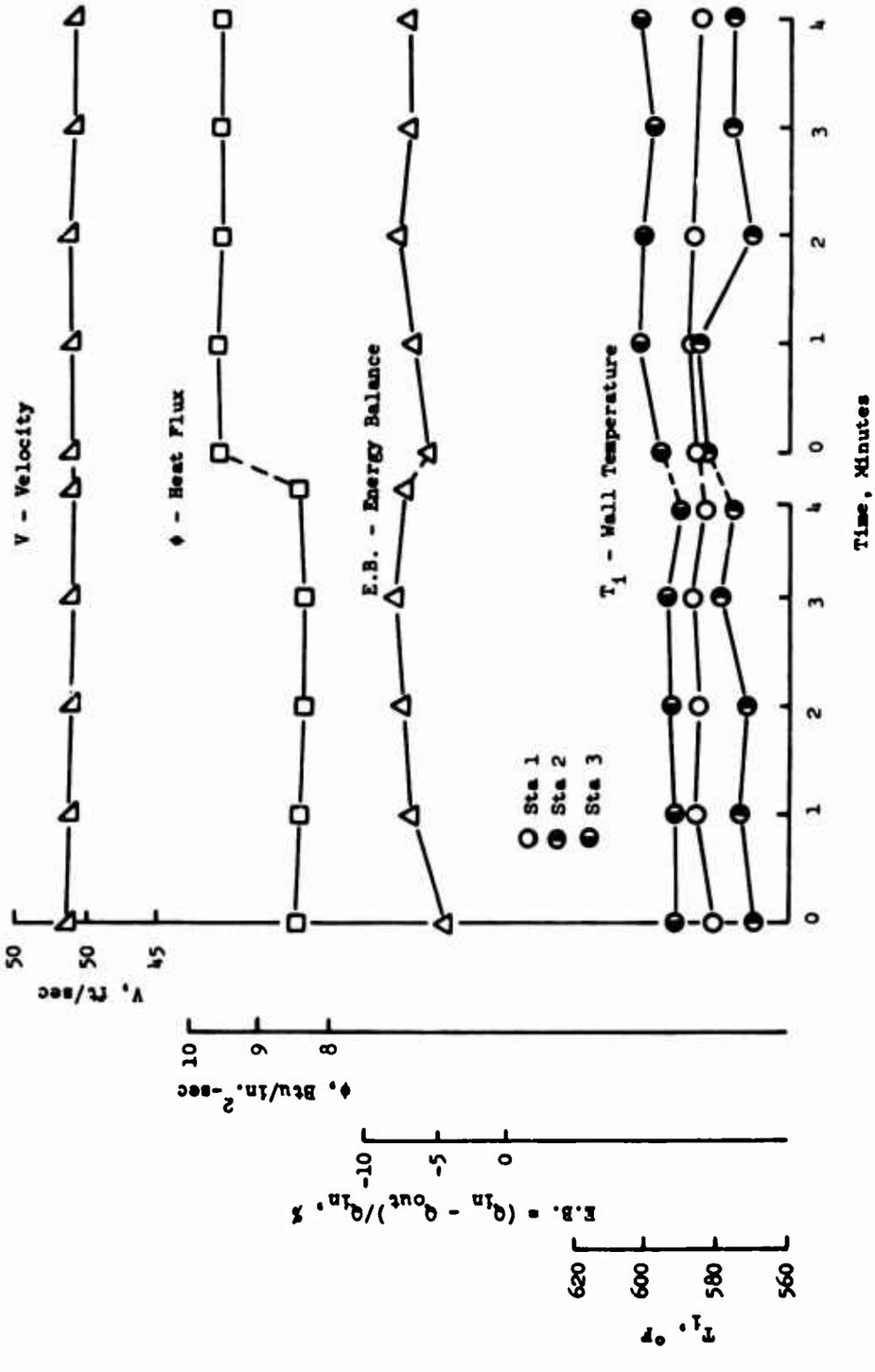

Extended Duration Test Parameters, Test HT-8-113

Figure 28

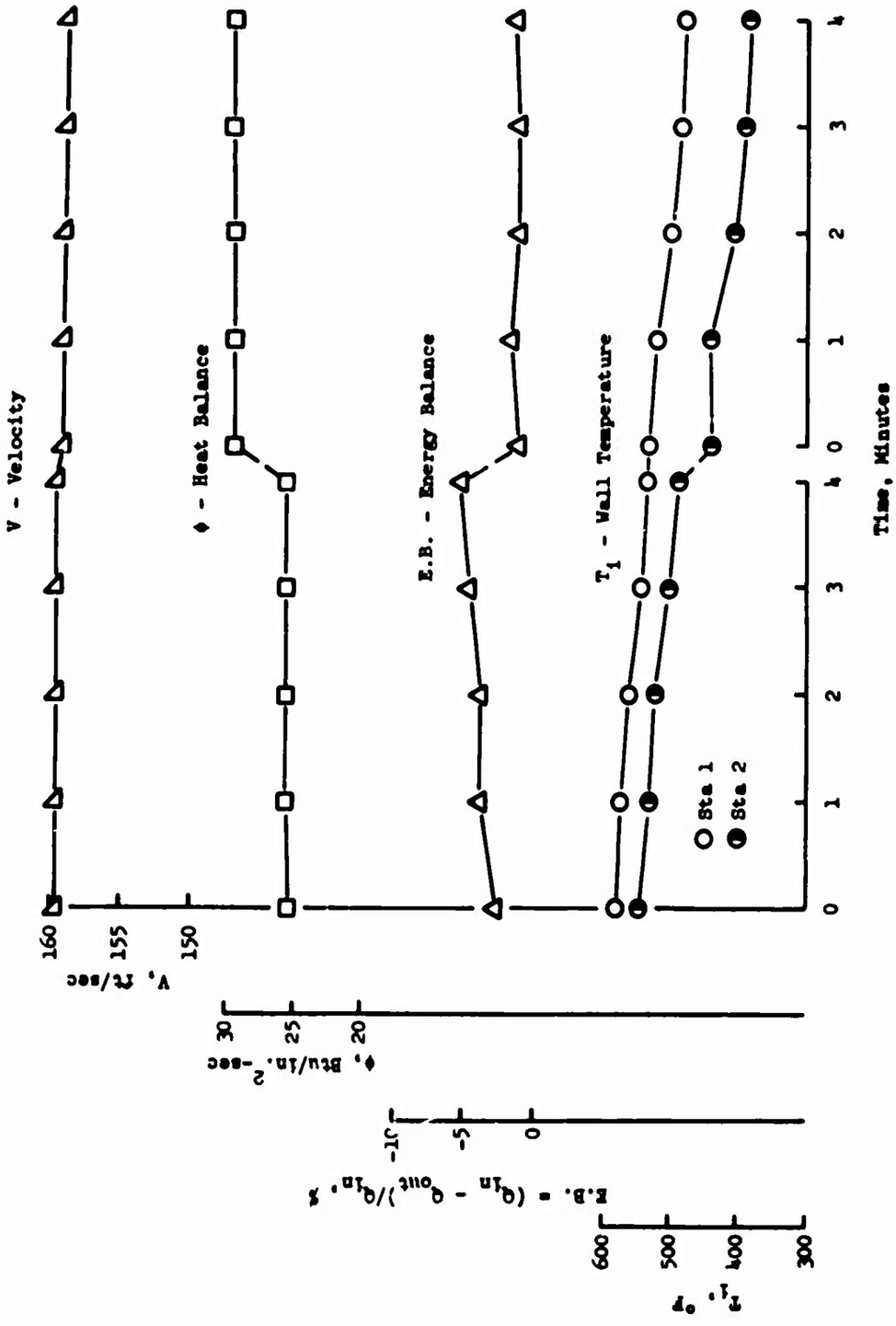

Extended Duration Test Parameters, Test HT-8-114

Figure 29

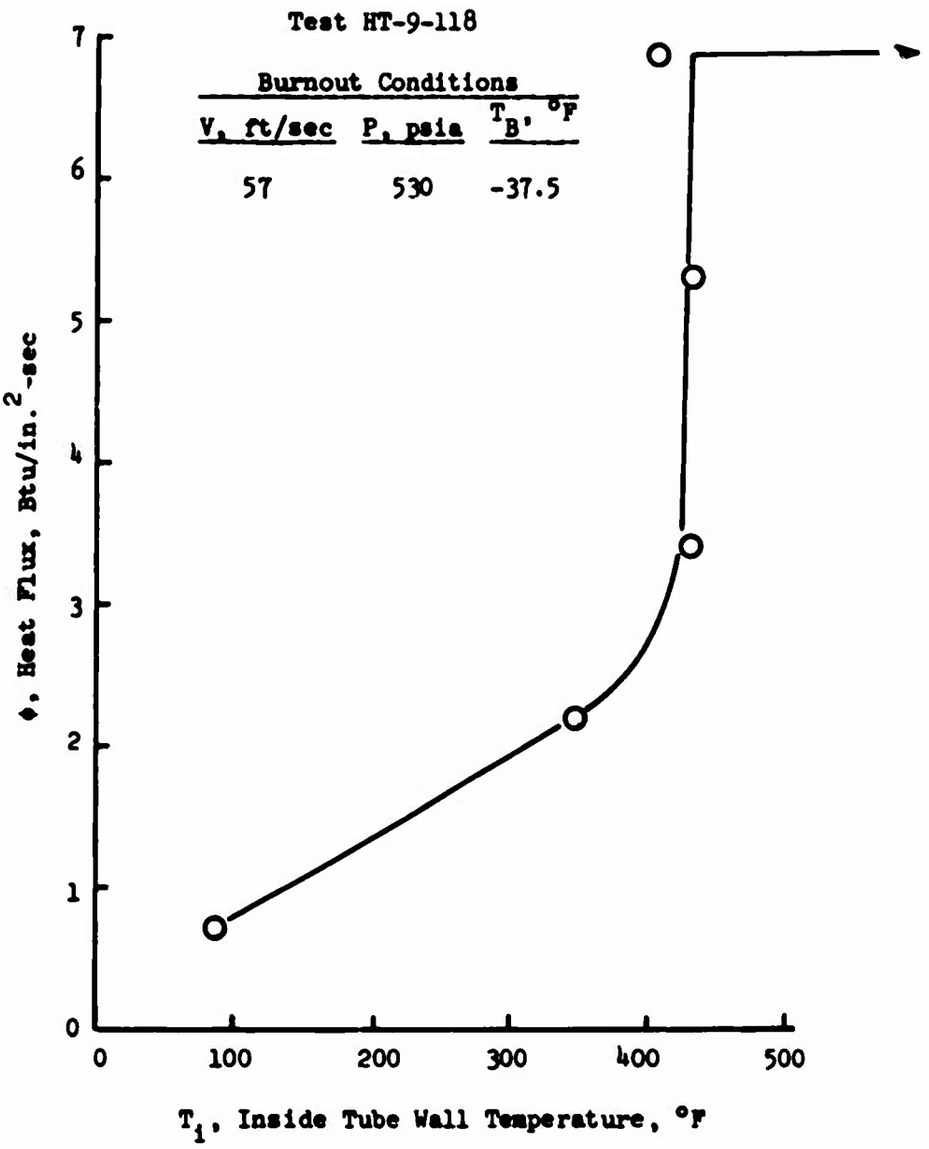

Subcritical MMH Heat Transfer at 50 ft/sec Velocity

Figure 30

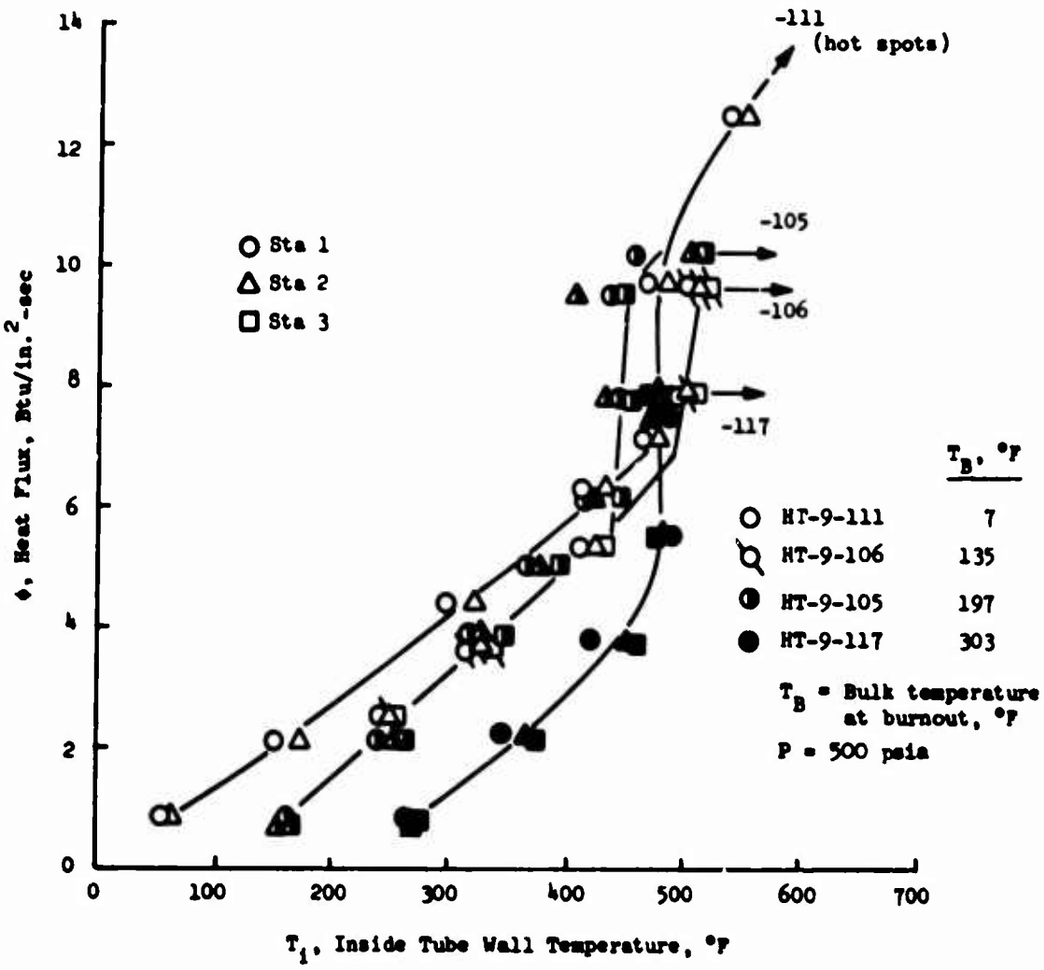

Subcritical MMH Heat Transfer at 100 ft/sec Velocity
and 500 psia Pressure

Figure 31

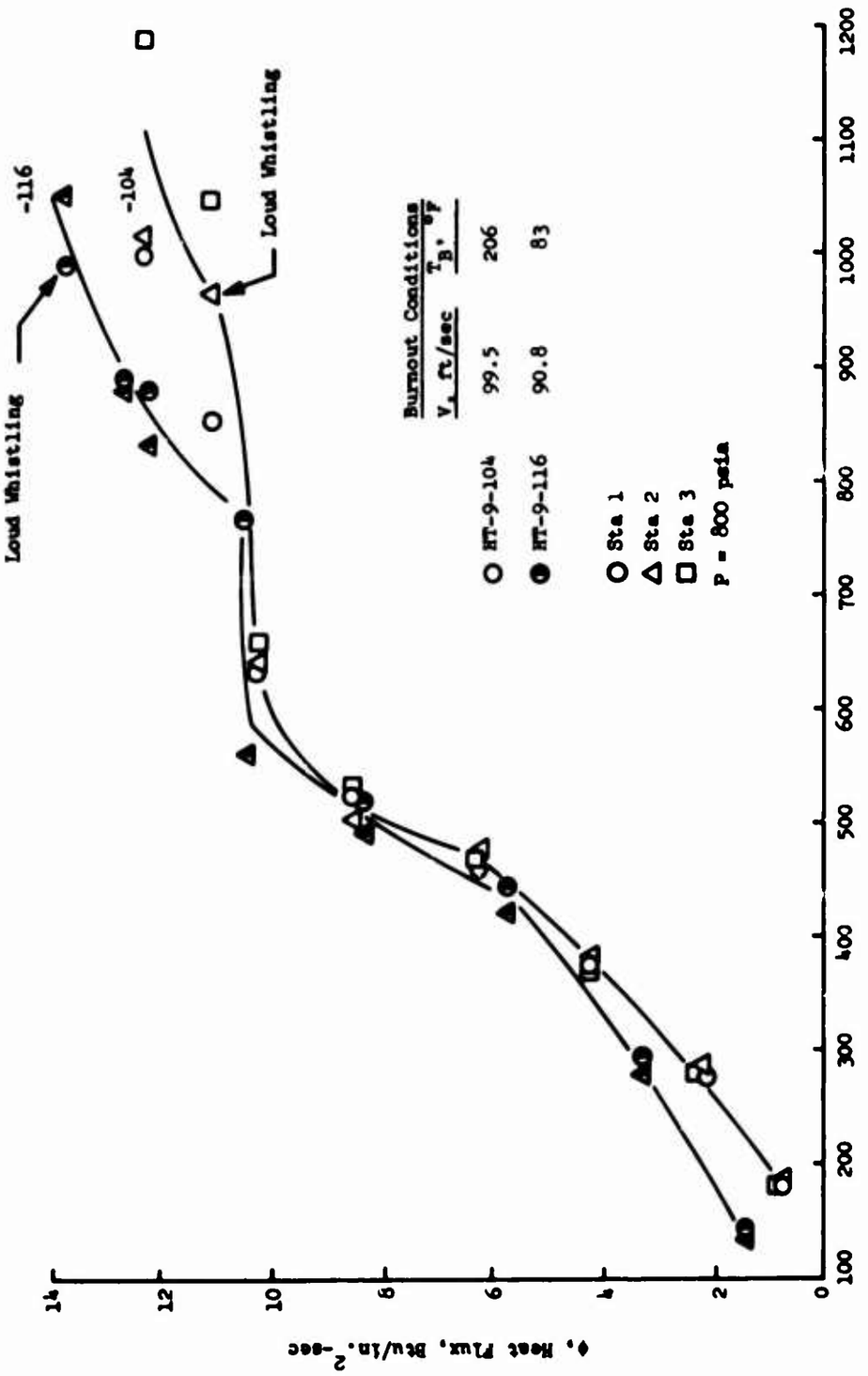

Subcritical MMH Heat Transfer at 100 ft/sec Velocity and 800 psia Pressure

Figure 32

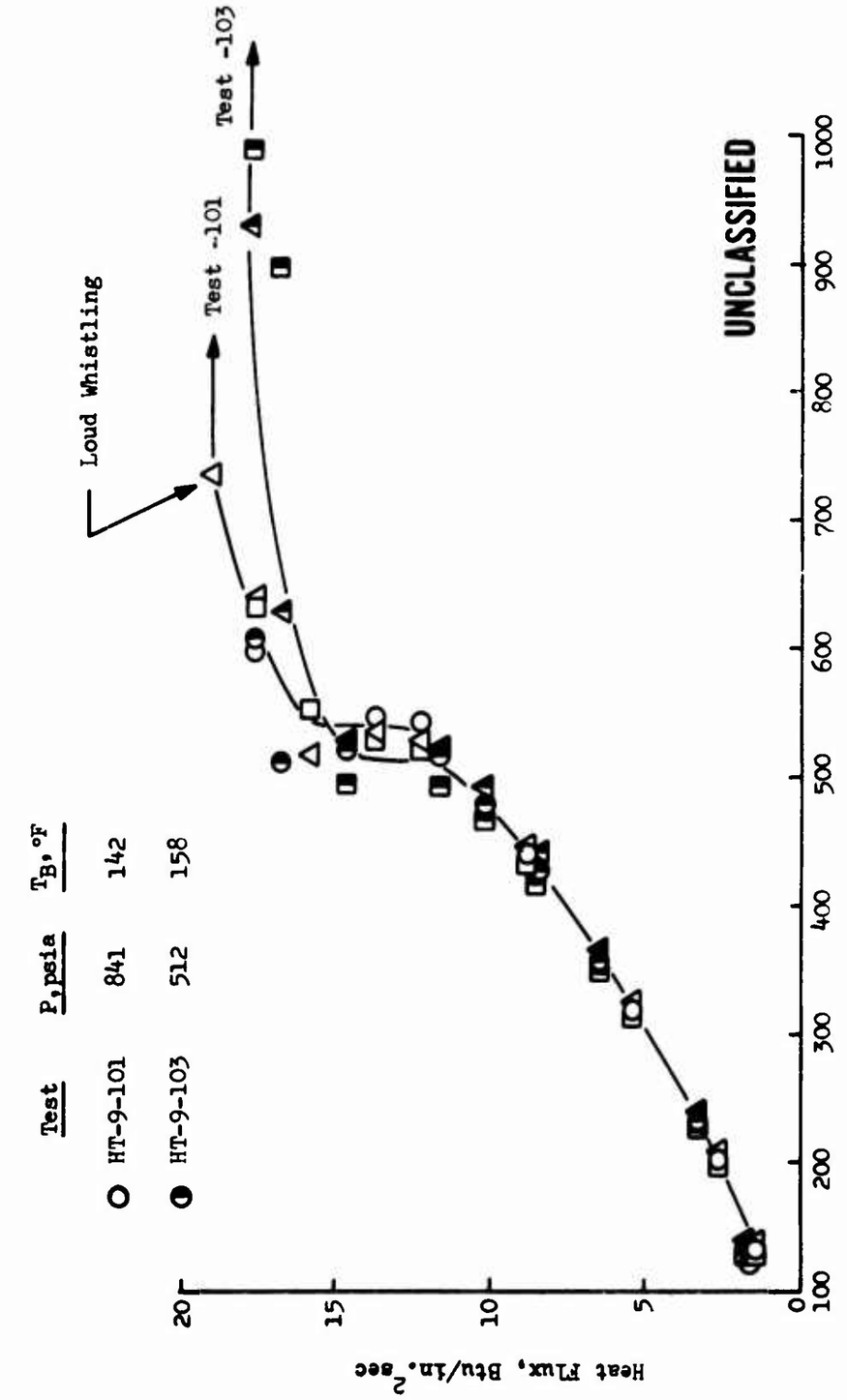

Subcritical MMH Heat Transfer at 150 ft/sec Velocity

Figure 33

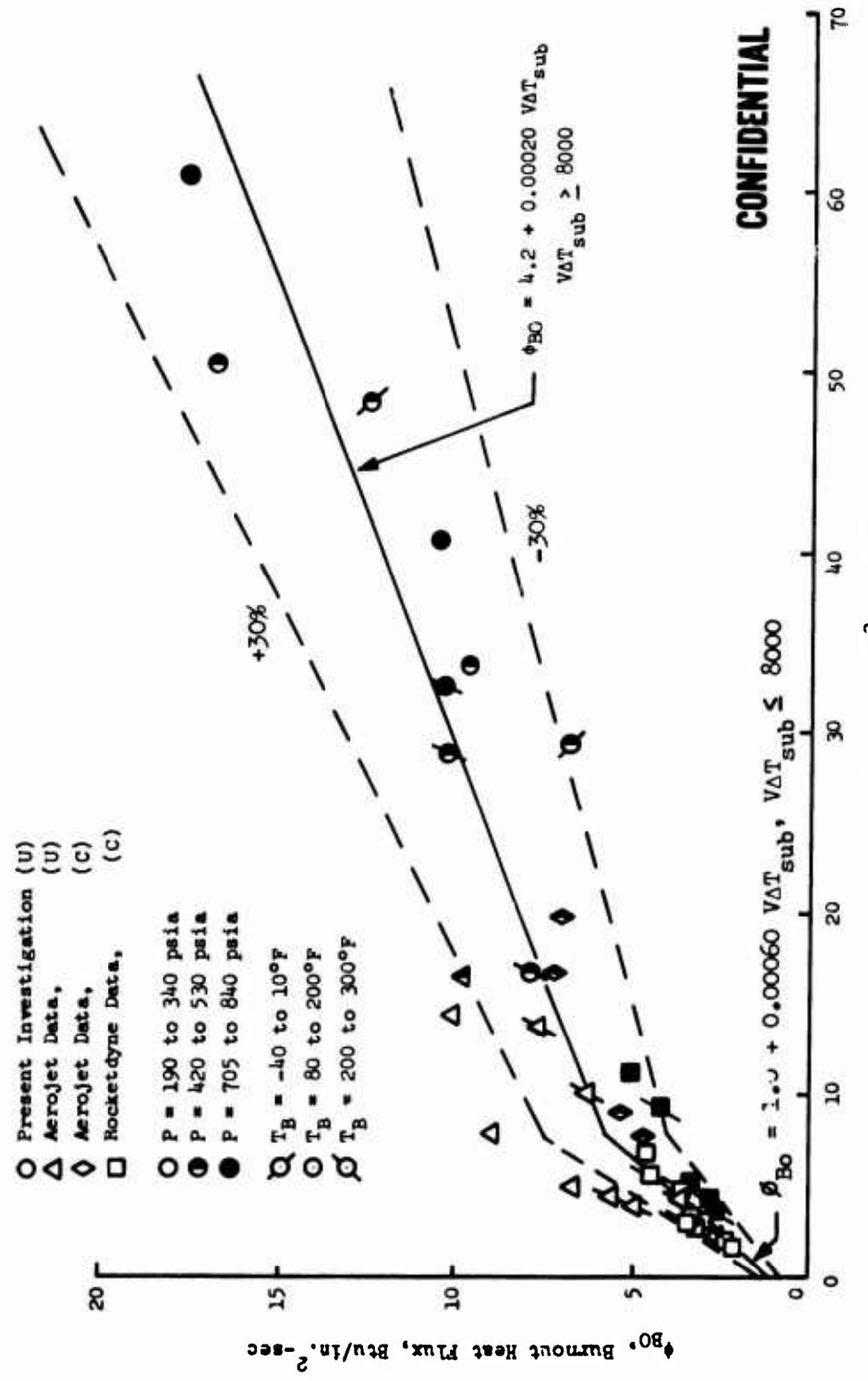

Subcritical MMH Burnout Heat Flux (U)

Figure 34

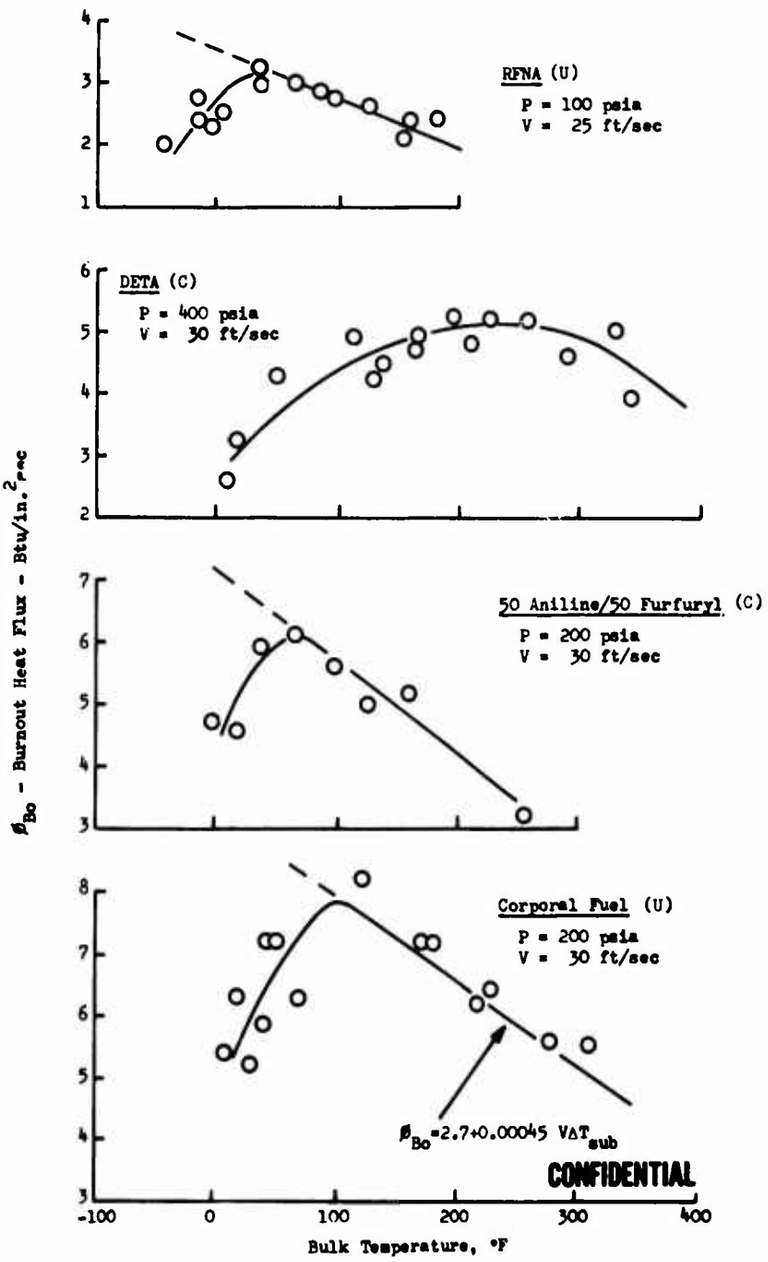

Effect of Bulk Temperat... on Burnout Heat Flux of RFNA, Diethylene Triamine, Corporal Fuel, and 50 Aniline/50 Furfuryl Alcohol (u)

Figure 35

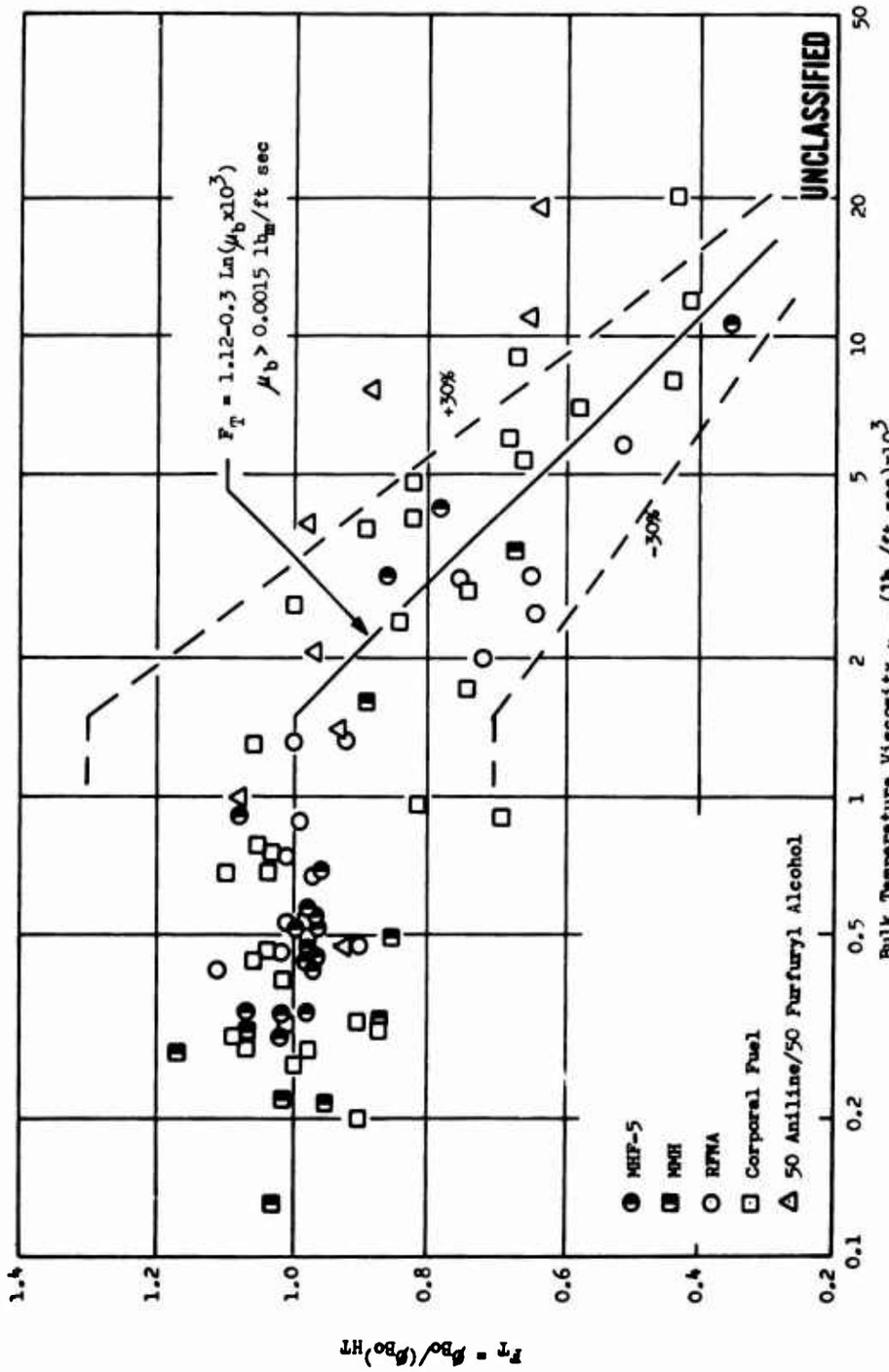

Correlation of Low Bulk Temperature Effect with Viscosity

Figure 36

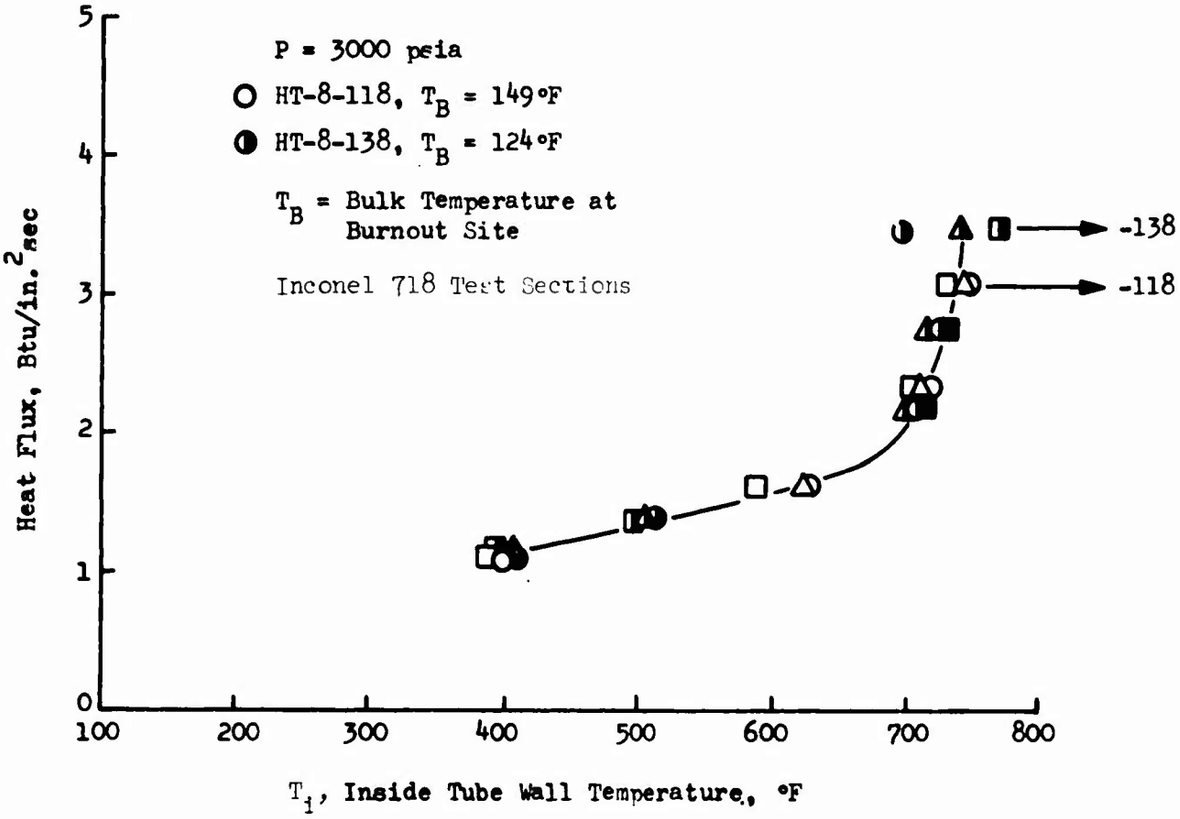

Supercritical MHF-5 Heat Transfer at 20 ft/sec Velocity

Figure 37

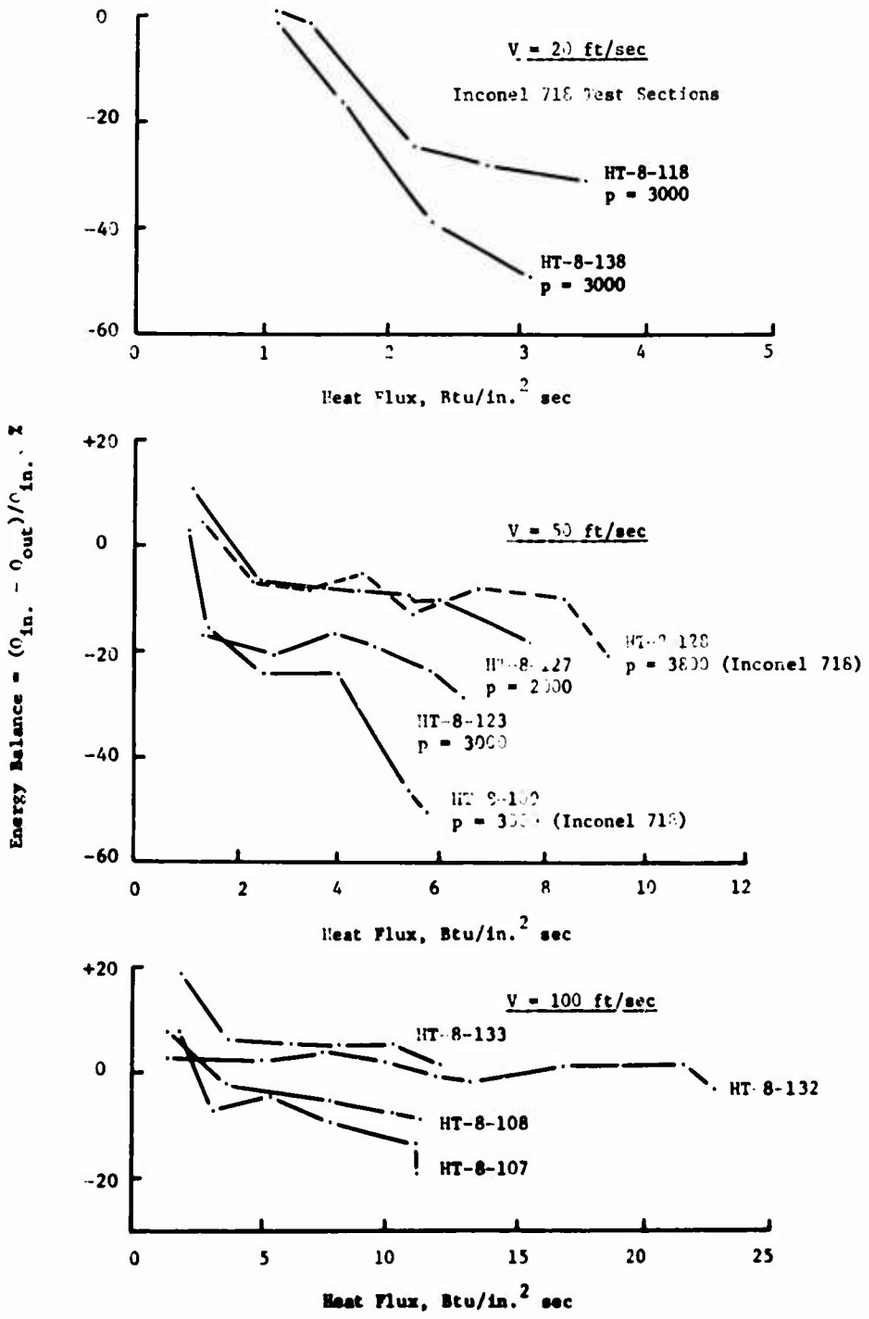

Energy Balances for Low Velocity MHF-5

Figure 38

Test	Failure Point Conditions T_B, °F	P, psia	
HT-8-127	179	2020	
HT-8-123	104	2950	
HT-8-128	180	3830	(Inconel 718)
HT-8-109	156	2990	(Inconel 718)

○ Sta. 1
△ Sta. 2
□ Sta. 3

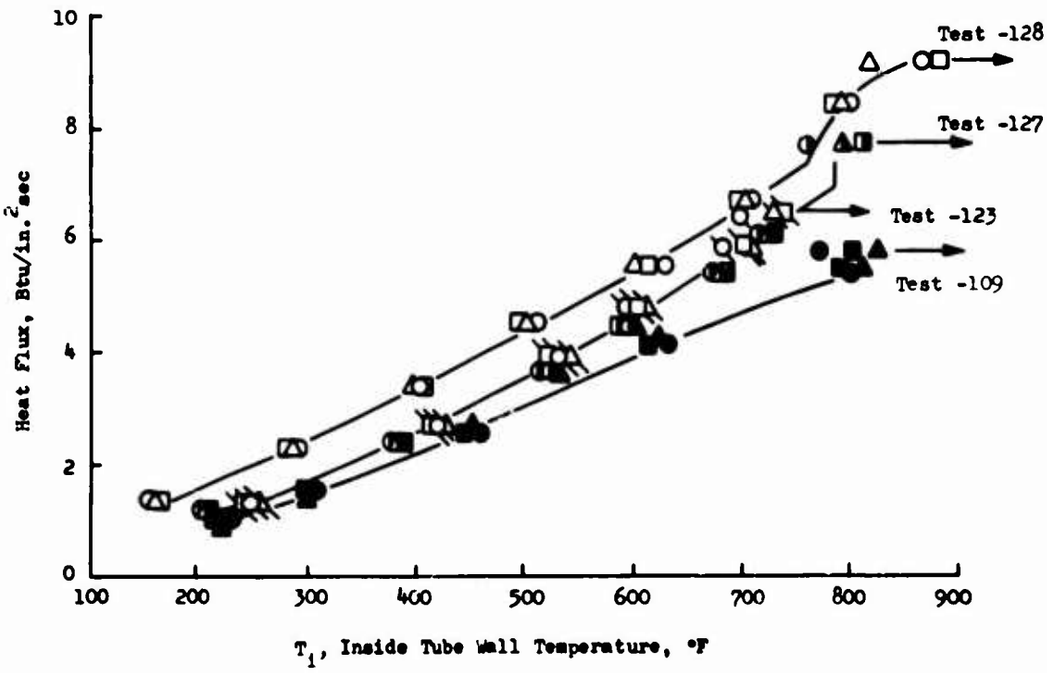

Supercritical MHF-5 Heat Transfer at 50 ft/sec Velocity

Figure 39

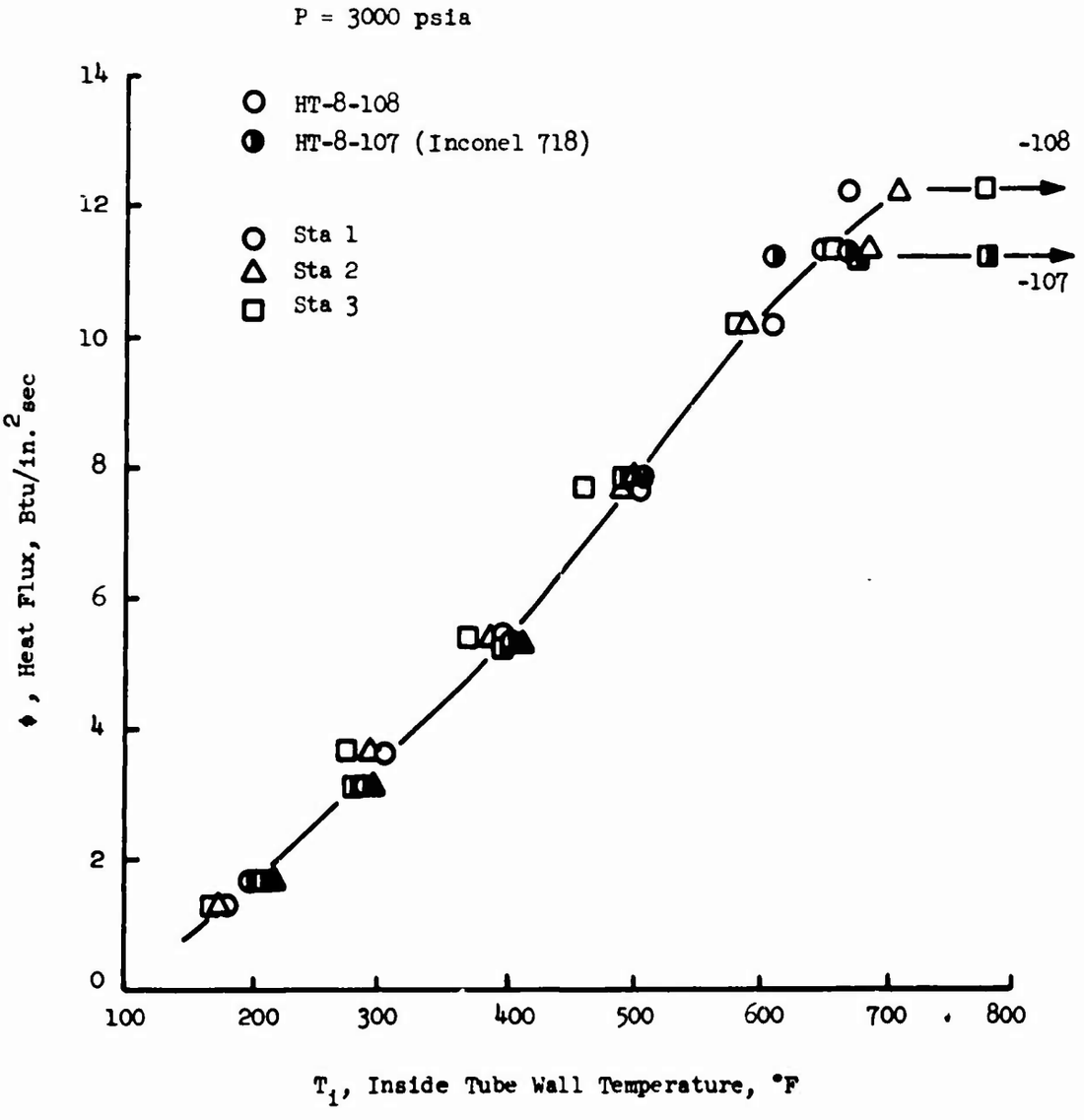

Supercritical MHF-5 Heat Transfer at 100 ft/sec Velocity and 150°F Bulk Temperature

Figure 40

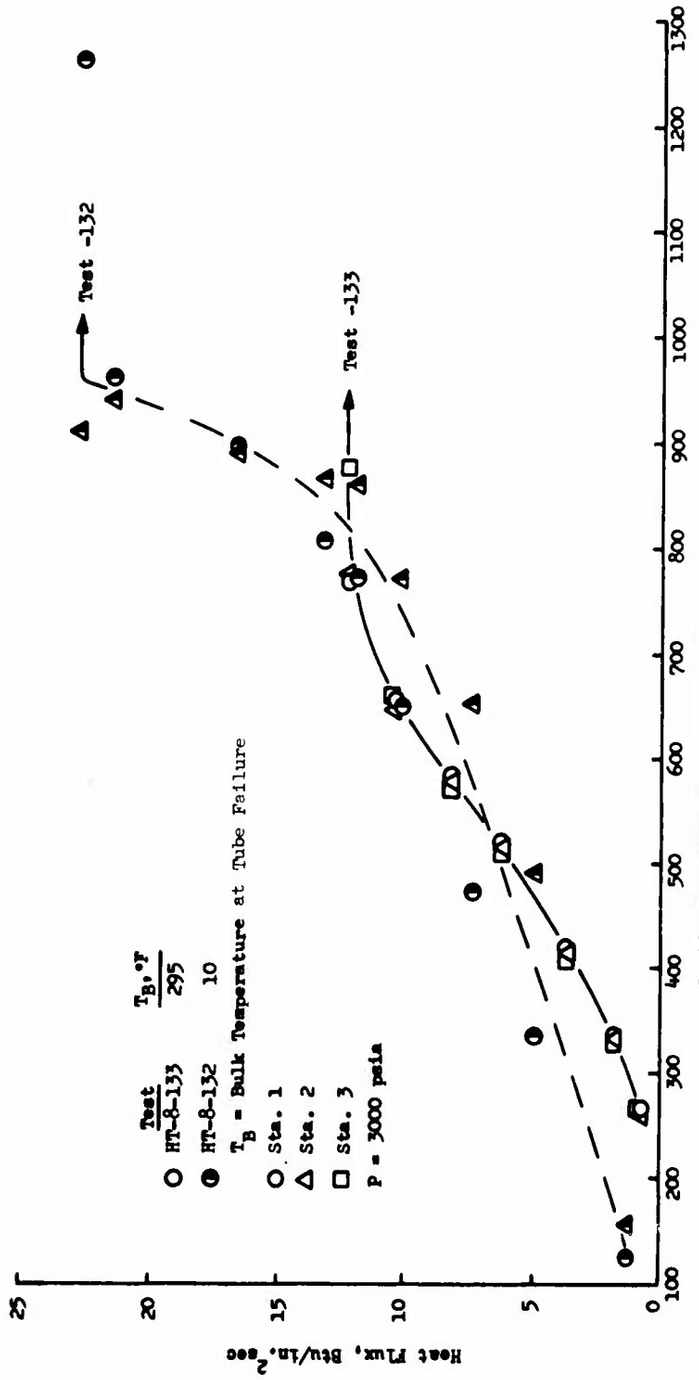

Supercritical MHF-5 Heat Transfer at 100 ft/sec Velocity

Figure 41

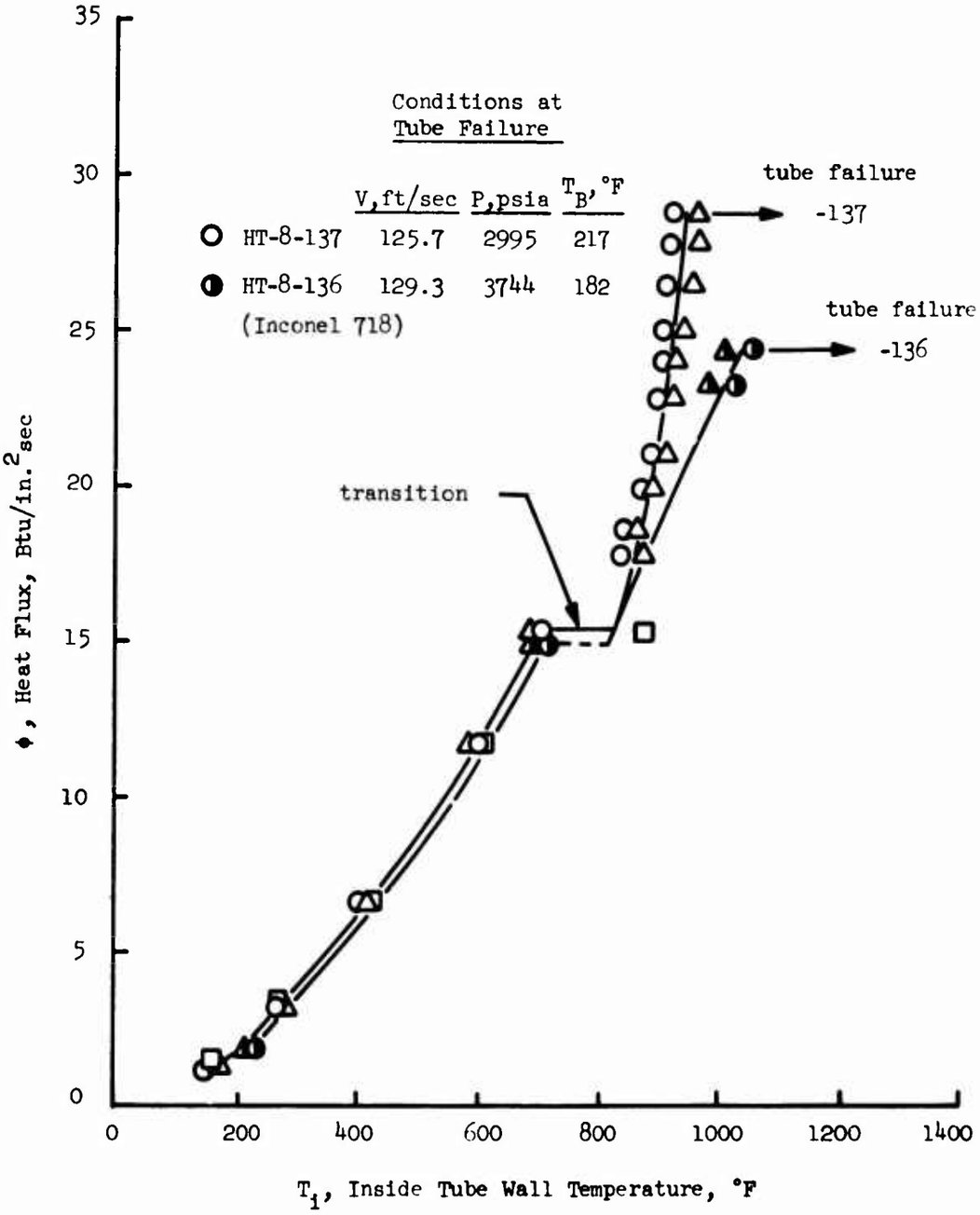

Supercritical MHF-5 Heat Transfer at 125 ft/sec Velocity

Figure 42

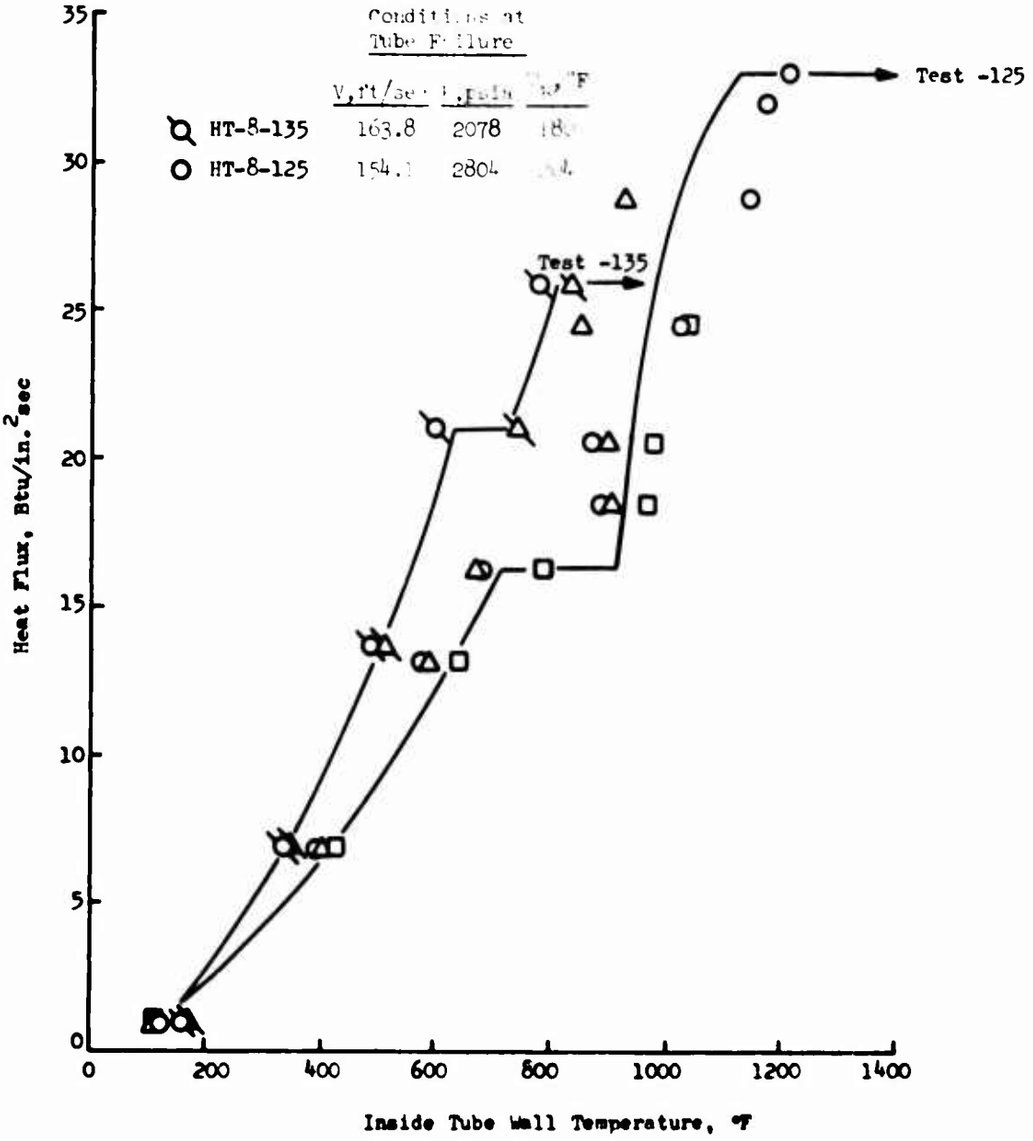

Supercritical MHF-5 Heat Transfer at 160 ft/sec Velocity

Figure 43

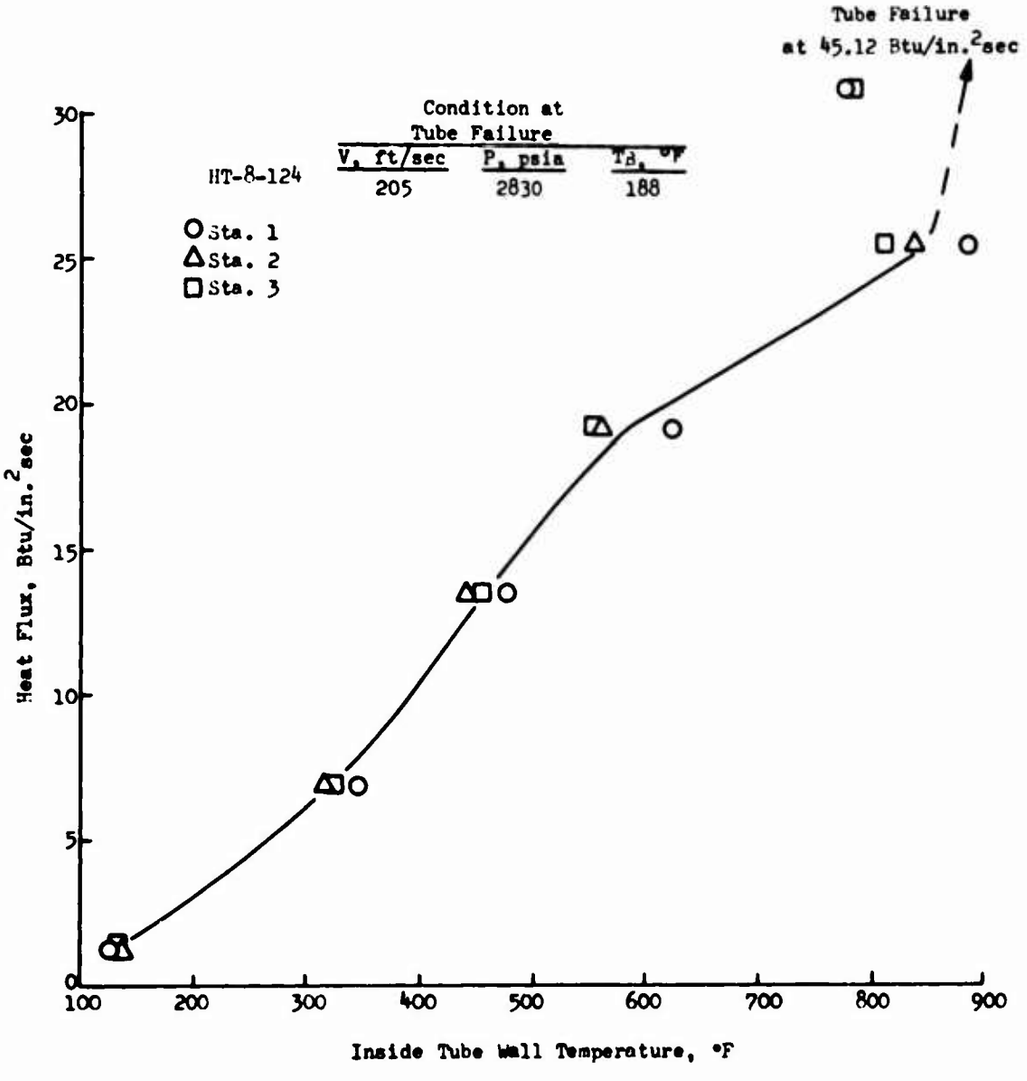

Supercritical MHF-5 Heat Transfer at 200 ft/sec Velocity

Figure 44

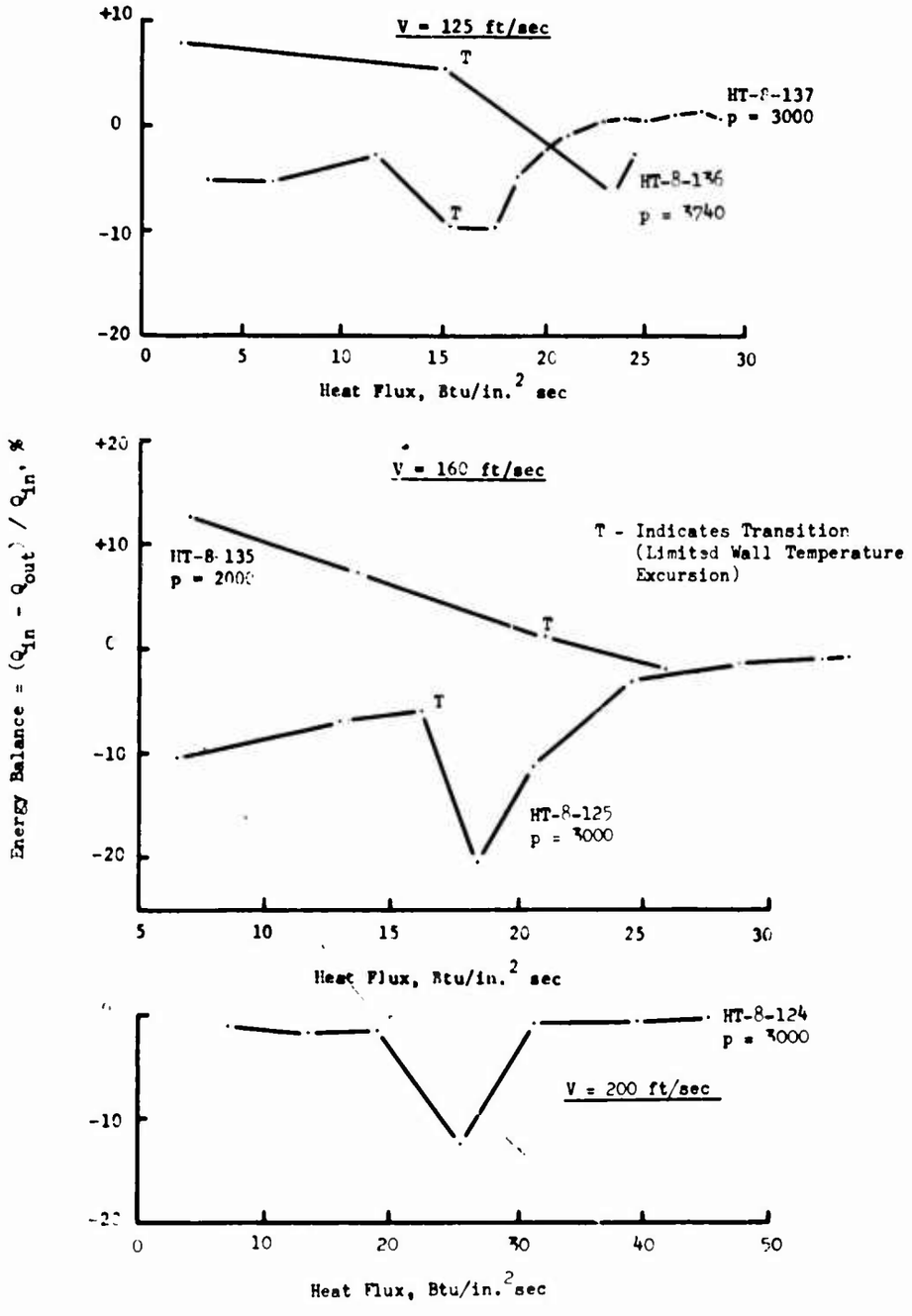

Energy Balance for High Velocity MHF-5

Figure 45

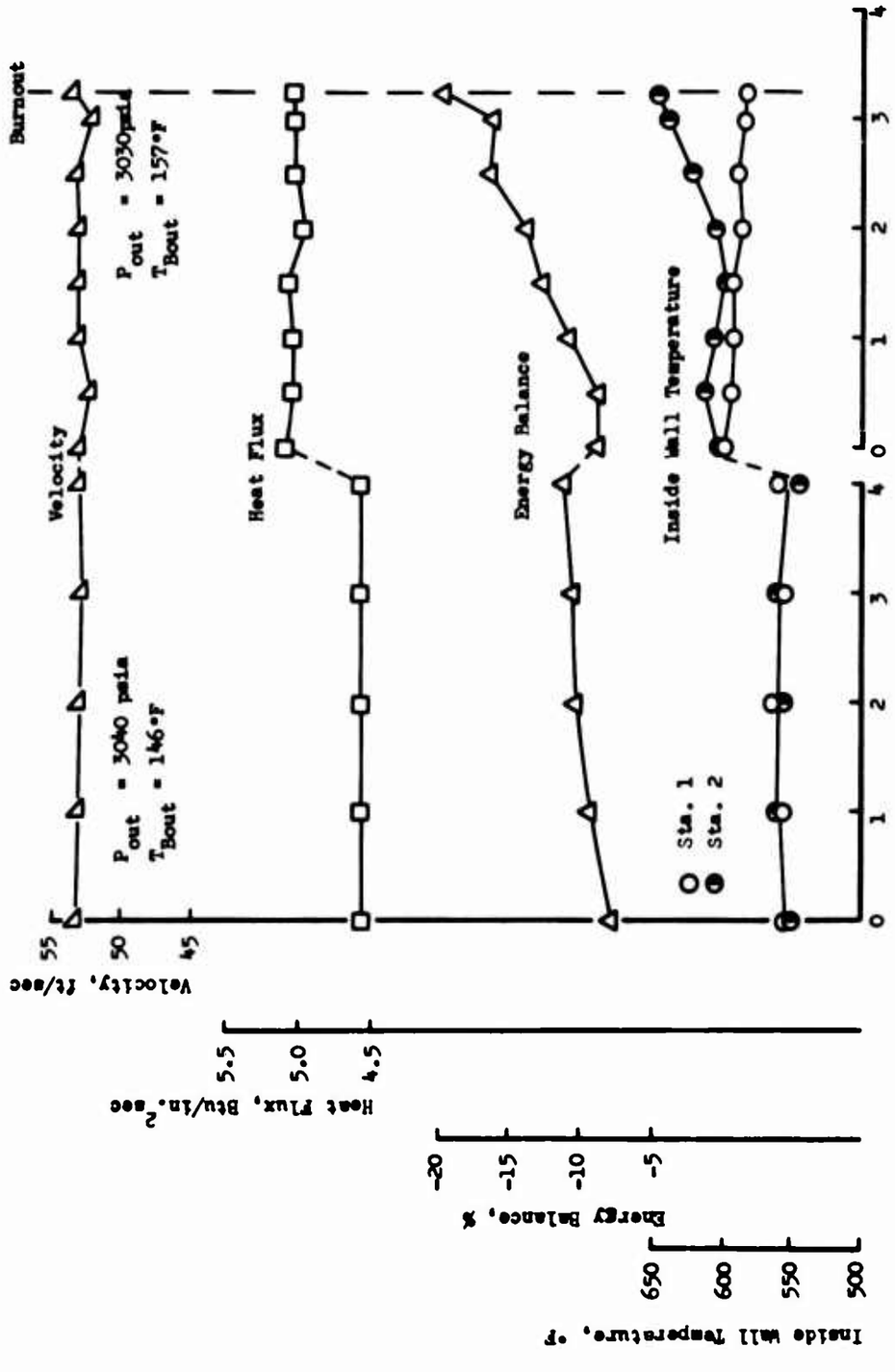

Extended Duration Test Parameters, Test HT-8-134

Figure 46

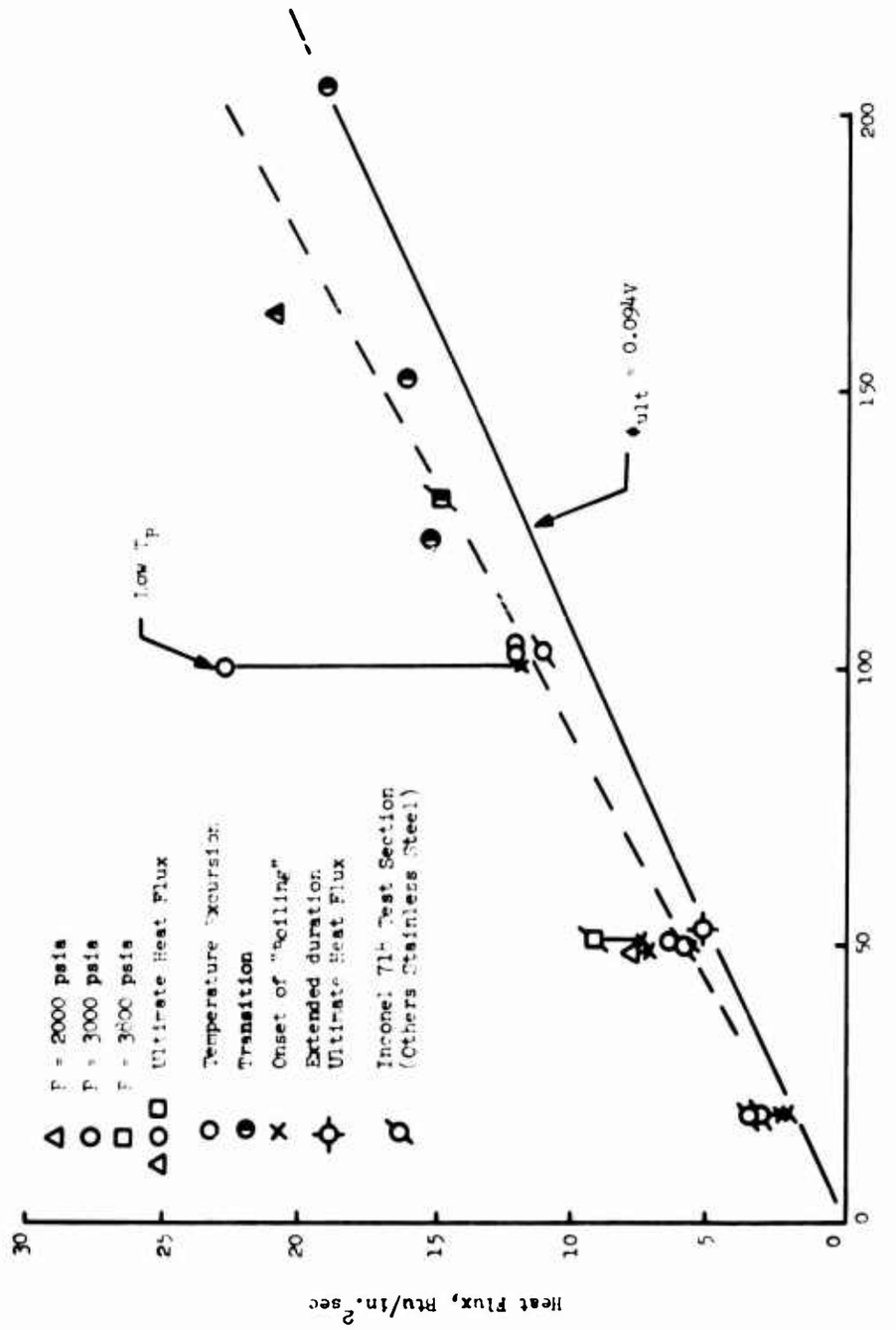

Correlation of MHF-5 Ultimate Heat Flux with Velocity

Figure 47

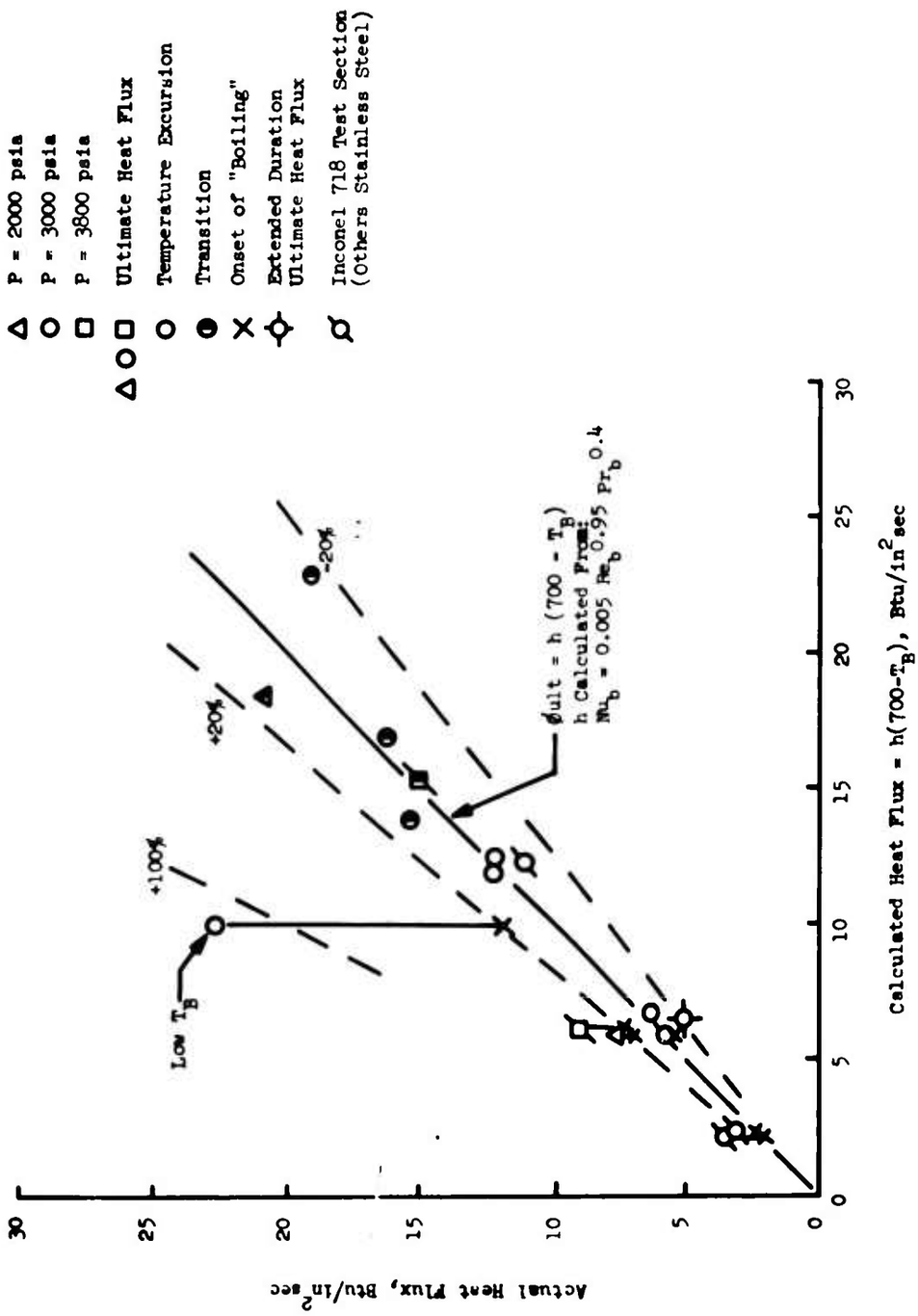

Prediction of MHF-5 Ultimate Heat Flux

Figure 48

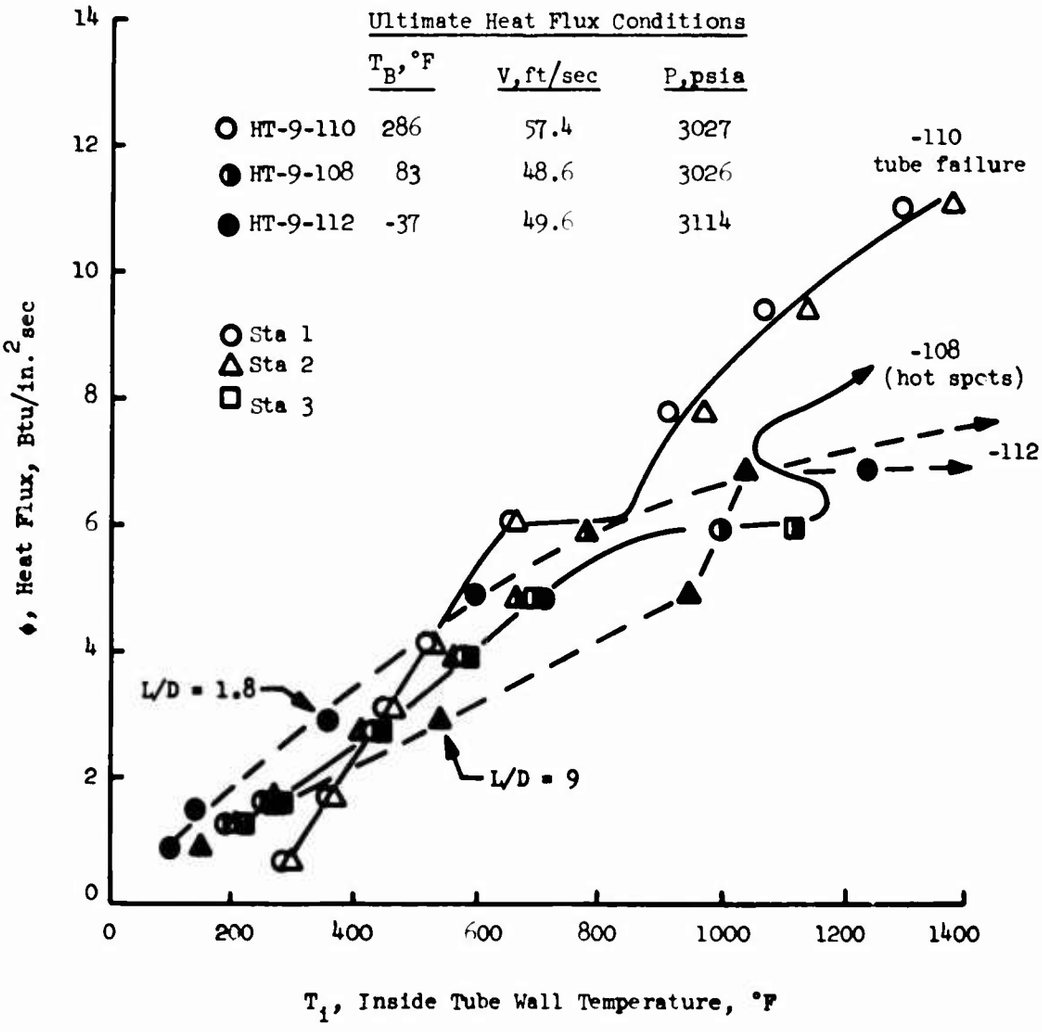

Supercritical MMH Heat Transfer at 50 ft/sec Velocity

Figure 49

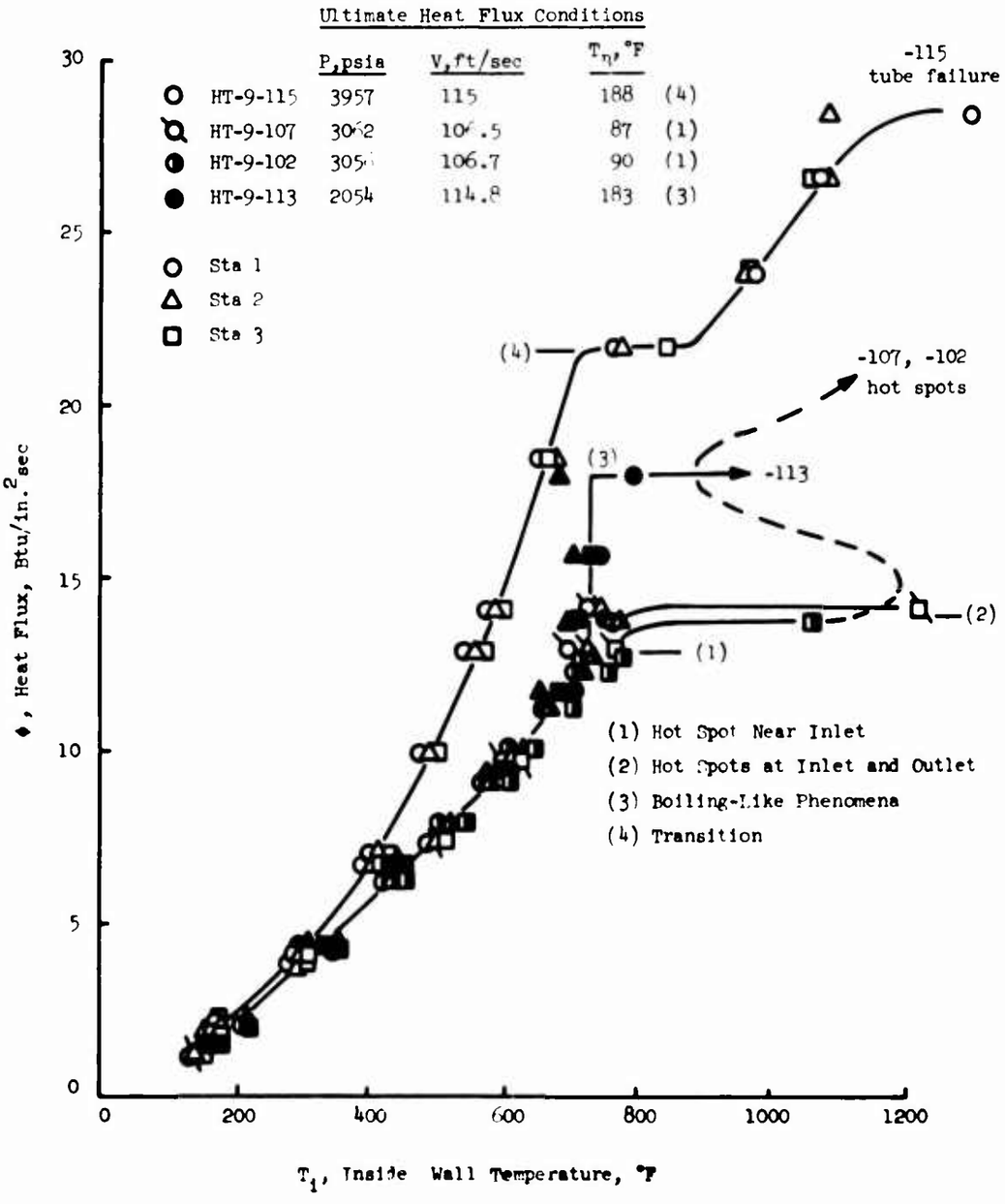

Supercritical MMH Heat Transfer at 100 ft/sec Velocity

Figure 50

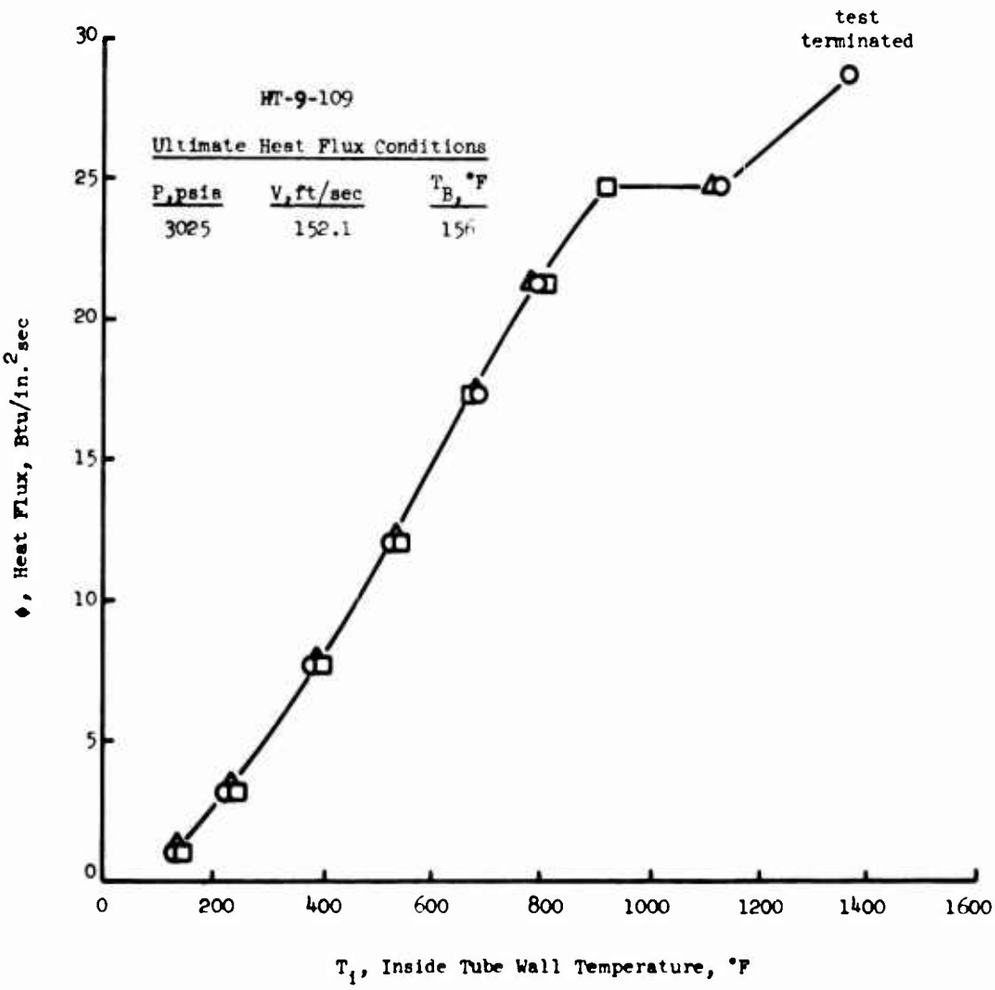

Supercritical MMH Heat Transfer at 150 ft/sec Velocity

Figure 51

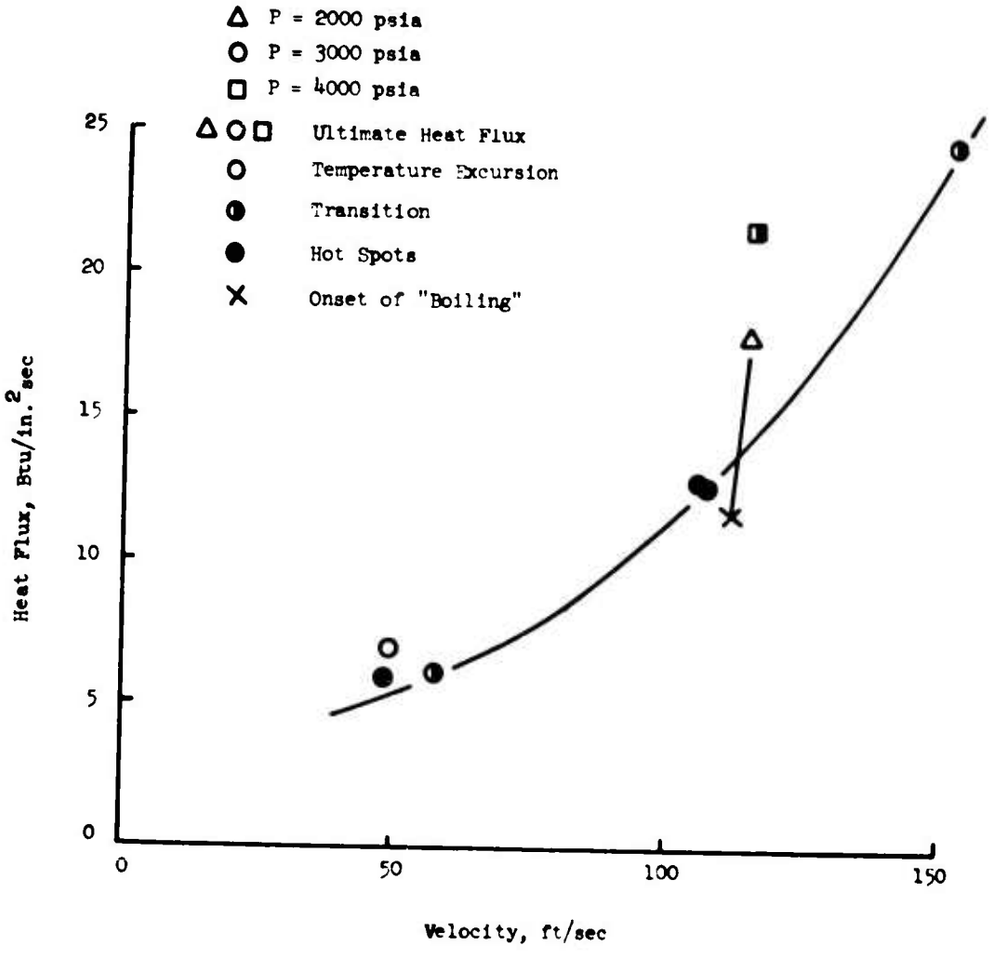

Correlation of MMH Ultimate Heat Flux with Velocity

Figure 52

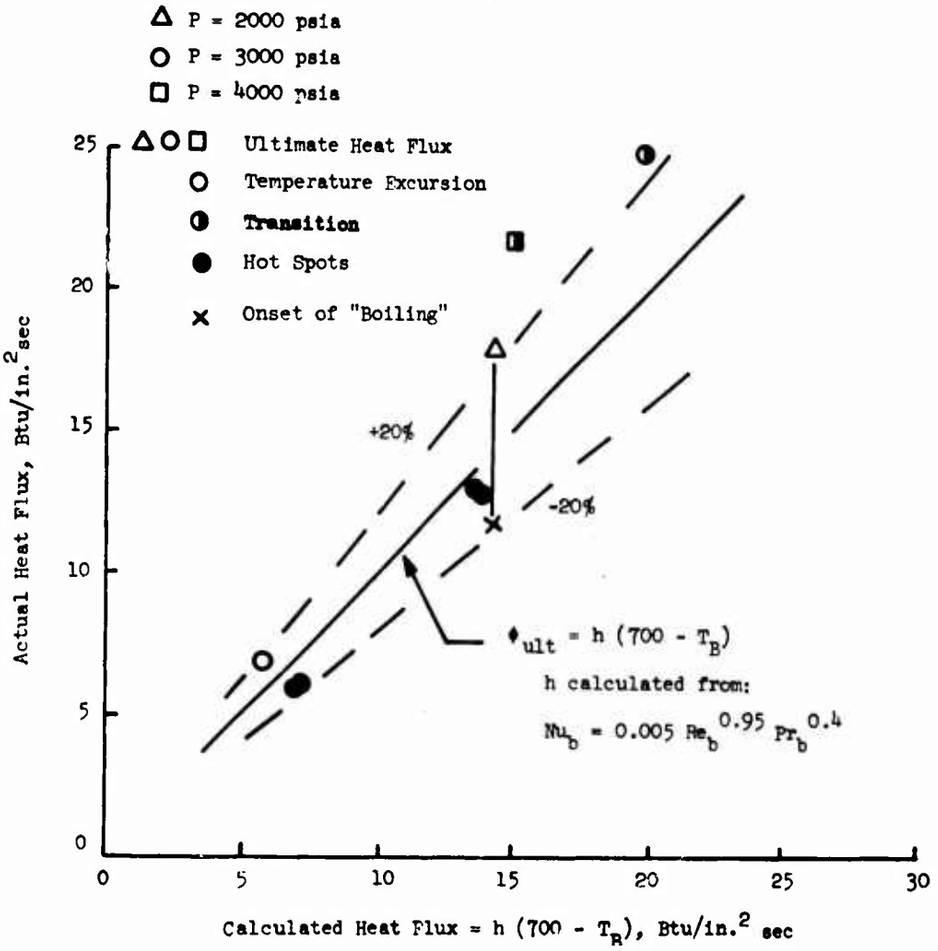

Prediction of MMH Ultimate Heat Flux

Figure 53

TUBING SECTION FROM HEAT TRANSFER TEST HT-8-114 (MHF-5)

Interior surface color varies from bronze (center) to gray (ends). The original color was metallic gray. Dark streaks are actually troughs eroded into the surface.

Magnification: 8X

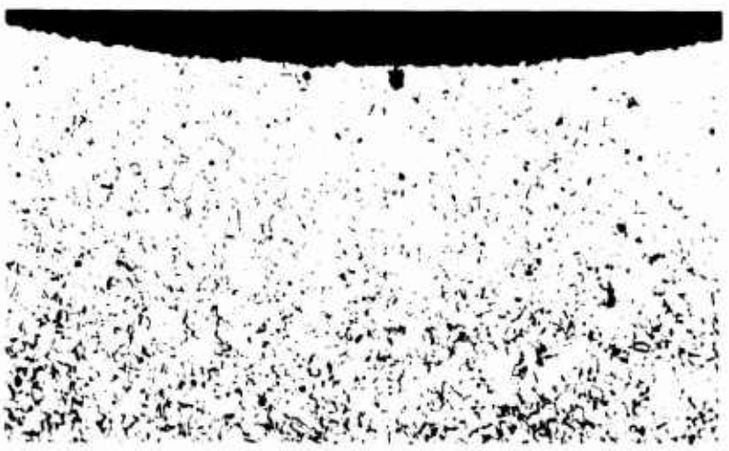

PHOTOMICROGRAPH OF TUBE I.D. SURFACE (TEST HT-8-114)

The pit in the surface is actually the end view of a trough formed by a corrosion-erosion action. A bridge of metal was left across the trough in this particular area. The pit depth is approximately 0.0008 in.

Magnification: 250X

Test Section HT-8-114

Figure 54

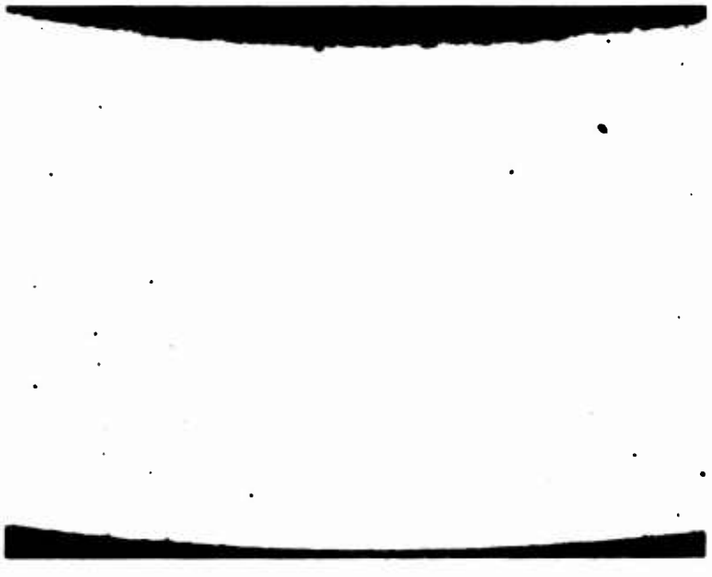

TUBE WALL CROSS-SECTION VIEW (TEST HT-8-114)

This photomicrograph gives a comparison of the tube surfaces (I.D. and O.D.). Notice the surface roughness on the I.D. A small trough is shown in the center of the I.D. Tube wall thickness is 0.0155 in.

Magnification: 250X

TUBE INTERIOR SURFACE LENGTHWISE VIEW (TEST HT-8-114)

Erosion apparently formed the pit shown above in tube interior surface (approximately 0.0008 in. deep).

Magnification: 250X

Photomicrographs of HT-8-114 Test Section

Figure 55

POSTTEST PHOTOGRAPH OF TEST SECTION HT-8-134
(Tube has been sectioned longitudinally)

[illegible] SECTION FROM JACKET

A uniform carburized layer approximately 0.0003 in. thick formed on the tube's interior surface.

Magnification: 100X, etched

TYPE 347 [illegible] CONTROL SPECIMEN

The grain structure and interior surface are shown in this photomicrograph as they appear before testing.

Magnification: 100X, etched

Test Section HT-[illegible]

Figure 56

TUBE WALL CROSS-SECTION FROM BULGE AREA (HT-8-134)

An interior surface coating and sharp notches are evident. The area indicated by lines is shown enlarged below. The hardness of the surface layer is Rockwell C 34.5 and the tube material hardness is Rockwell B 85.

Magnification: 100X

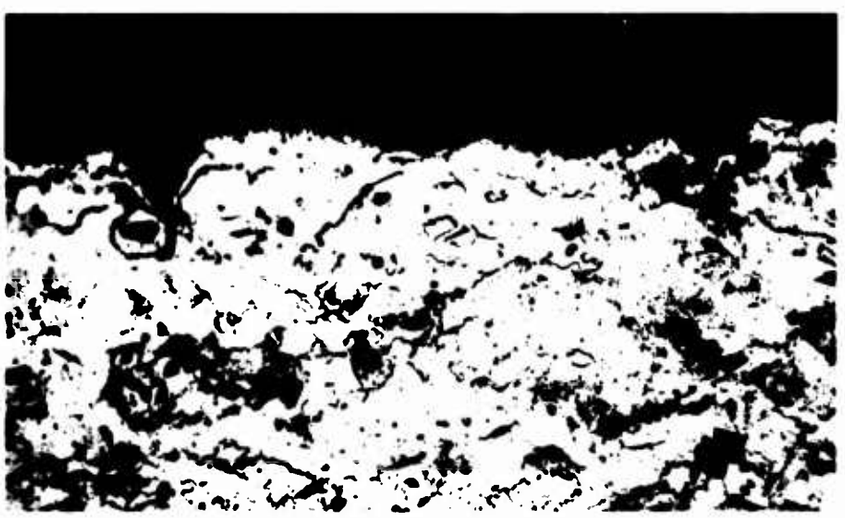

[illegible] of Bulged Area (HT-8-134)

Figure 57

Photomicrographs of Shiny Area (HT-8-134)

Figure

TEST HT-9-107 FULL SECTION (ENH)

This segment was taken from the coolant inlet end of the test section where hot spots first developed. Blackening and residues are evident. A transverse cut was made on the top half of the tube and a specimen was mounted for an end view of the tube wall (No. 1). The remaining segment of the tube half-section was mounted for longitudinal views of the tube wall (No. 2's). Coolant flow was from right to left in this tube segment. The tube ruptured just to the left of the area shown (note bulging).

Magnification: 8X

END VIEW OF TUBE I.D. SURFACE (NO. 1)

The entire interior surface is coated with a carbonaceous layer of material. Notice the crack formed in the surface layer.

Magnification: 250X, etched

LONGITUDINAL VIEWS OF TUBE INTERIOR EDGE (HT-9-107)

Two photomicrographs of the same edge with different focuses to resolve the different surface layers. A layer of black carbonaceous material (top focus) covers a white layer of carburized metal (see bottom right edge). The bottom left surface exhibits intergranular penetration by carbon. The hardness of the carburized metal is Rockwell C 44.

Magnification: 250X, etched

LONGITUDINAL VIEW OF TUBE INTERIOR EDGE

This photomicrograph was taken of the same specimen shown above, but in a different location. A carbonaceous material appears to be lifting metal particles out of the tube surface. The attack shown here is similar to that found on Test Section HT-8-134 (MHF-5).

Magnification: 250X, etched

Photomicrographs of HT-[illegible] Test Section

Figure 6)

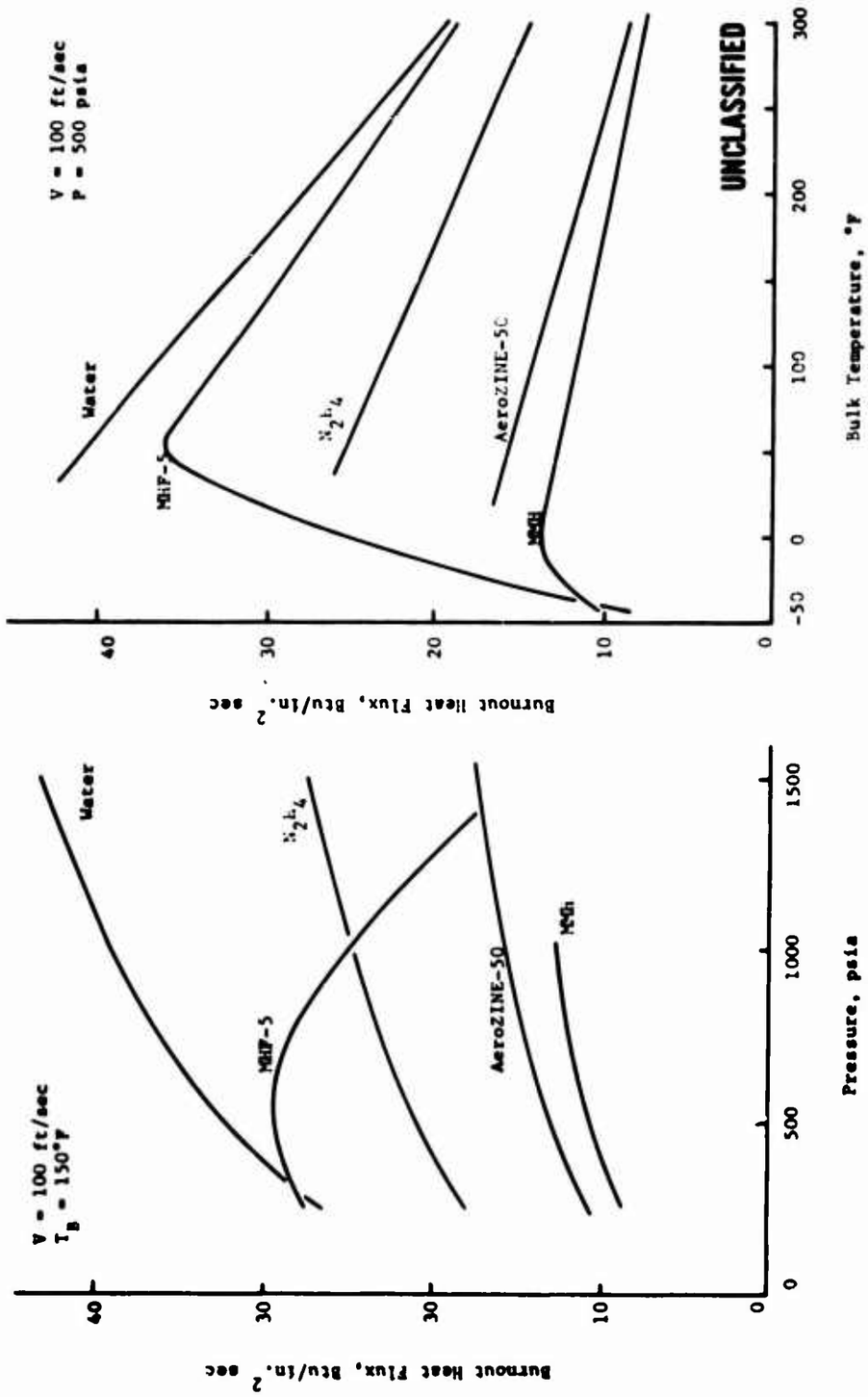

Comparison of Burnout Heat Flux Characteristics
(Subcritical Pressure)

Figure 61

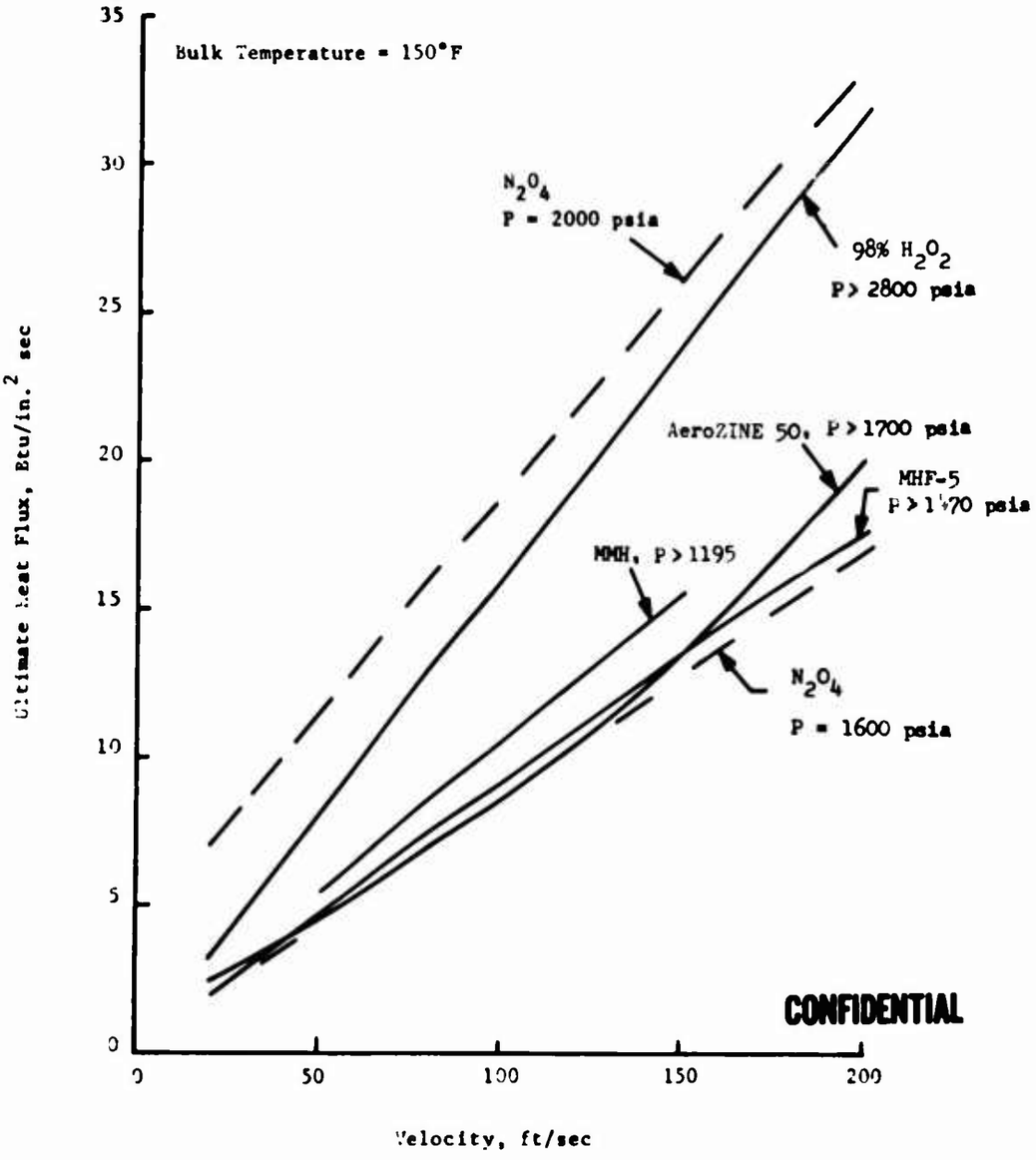

Comparison of Ultimate Heat Flux Limits
(Supercritical Pressure) (u)

Figure 62